DEVELOPMENT OF CYTOKINE ELUTING COATINGS TO MODULATE MACROPHAGE BEHAVIOUR AND MITIGATE THE FOREIGN BODY REACTION AGAINST IMPLANTABLE BIOMATERIALS

by

Daniel Jordi Hachim Diaz

Licentiate in Chemistry and Pharmaceutical Sciences, Pontifical Catholic University of Chile,

2010

Submitted to the Graduate Faculty of

Swanson School of Engineering in partial fulfillment

of the requirements for the degree of

Doctor of Philosophy

University of Pittsburgh

2017

UNIVERSITY OF PITTSBURGH

SWANSON SCHOOL OF ENGINEERING

This dissertation was presented

by

Daniel Jordi Hachim Diaz

It was defended on

November 2, 2017

and approved by

Steven David Abramowitch, Ph.D., Associate Professor, Department of Bioengineering

Pamela Ann Moalli, MD Ph.D., Associate Professor, Department of Obstetrics, Gynecology & Reproductive Sciences

Yadong Wang, Ph.D., McAdam Family Foundation Professor, Department of Biomedical Engineering, Cornell University

Dissertation Director: Bryan Nicklaus Brown, Ph.D., Assistant Professor, Department of Bioengineering

DEVELOPMENT OF CYTOKINE ELUTING COATINGS TO MODULATE MACROPHAGE BEHAVIOUR AND MITIGATE THE FOREIGN BODY REACTION AGAINST IMPLANTABLE BIOMATERIALS

Daniel Jordi Hachim Diaz, PhD

University of Pittsburgh, 2017

Recent studies have implicated that an inadequate host biomaterial response, driven predominately by pro-inflammatory (M1) macrophages and downstream formation of fibrotic capsule, is a major cause of the severe surgical mesh-related complications in pelvic prolapsed woman. We have hypothesized that shifting this macrophage response towards an anti-inflammatory (M2) phenotype will lead to a better implant integration into the host tissue. A coating for local and transient delivery of interleukin-4 (IL-4, an M2 cytokine) was developed, using layer-by-layer (LbL) deposition of chitosan and dermatan sulfate. Implantation studies revealed that the released IL-4 promoted a predominant M2-like macrophage response, associated to decreased fibrotic capsule deposition and changes in collagen composition, suggesting improved mesh integration into the host tissue and potential for reduction in downstream complications.

Immunosenescence, dysregulated macrophage function, and delayed resolution of the immune response against pathogens have been demonstrated in aged individuals. We have sought to elucidate the impacts of aging upon the host response to polypropylene mesh in aged versus young mice. The host response in aged mice resulted in delayed cell recruitment, significant differences in macrophage marker expression and a highly shifted pro-inflammatory (M1)

response at early stages, associated with an unresolved host response in the long-term, compared to young mice.

A sequential delivery of MCP-1 (macrophage chemoattractant protein-1) and IL-4 has been developed to restore the delayed cell recruitment and reverse the inflammatory macrophage response in old mice, respectively. The host response to single and sequential delivery regimens was well distinct in old versus young implanted mice. While single delivery of IL-4 was not enough to counteract the high inflammatory response in old mice, the sequential delivery of MCP-1 and IL-4 was capable of restoring recruitment and M2-like macrophage response, associated to decreased capsule deposition in the long term. Contrarily, the sequential delivery regimen in young mice was not as effective as IL-4 alone promoting an M2-like response, but still capable of reducing inflammatory macrophages and capsule deposition. These results demonstrate that a proper understanding of biological context has the potential to improve the performance of biomaterials-based approaches in aged individuals.

TABLE OF CONTENTS

LIST OF TABLES

LIST OF FIGURES

PREFACE

First of all, I would like to thank my mentor Dr. Bryan Brown for all his support and encouragement during all these years in the laboratory. Dr. Brown has been a great mentor, he always supported all my ideas with constructive criticism and provide excellent support to accomplish every goal in my research projects and career. In addition, he always motivated me to push my boundaries - thanks to him, I have had very rich professional development experiences in innovation ventures and leadership activities.

I would also like to thank all members of my committee; Drs. Abramowitch, Moalli and Wang, for their guidance and constructive feedback, as well as assistance with some of my experiments and analysis, especially to Dr. Abramowitch's students William Barone and Katrina Knight.

To all the great members of the Brown Lab, I really appreciate all your support and friendship. I will never forget the many great experiences we had together and of course, all the fun and the jokes. Thanks for that and I will really miss you all.

Special thanks to Dr. Joel Gillespie for kindly providing me access and training to multiple instruments for material characterization at the Material Characterization Laboratory at University of Pittsburgh, these have been instrumental to the success of the present dissertation.

On a personal note, I would like to thank my wife, Vanessa, for her love and for always being there for me whenever I needed support. This is also dedicated to my parents and my family, who always supported and believed in me, and were far away missing Vanessa and me during all these years. I will never forget and thank all my great old and new friends who were always watching for us and shared unforgettable moments. To everyone mentioned here, and anyone who I may have forgotten, thank you for everything.

1.0 HOST RESPONSE AGAINST SURGICAL MESH FOR PELVIC ORGAN PROLAPSE

The host response against biomaterials, also known as foreign body reaction, is an adverse process initiated by the innate immune system and ubiquitous to all implanted biomaterials, that results in chronic inflammation and fibrotic scarring around the implant, negatively impacting the performance of biomaterials and integrity of the host tissue. Recently, macrophages have been recognized as intrinsic drivers of the dysregulated events that follow material implantation, and hence restoring balanced macrophage regulation by immunomodulation will be explored. The present dissertation is focused on the controversial use of surgical mesh for pelvic organ prolapse, as the implantation of these devices is highly associated to severe complications, in which an exacerbated and persistent inflammatory host response against the mesh biomaterial is suggested as a major cause. However, the results of this work can potentially be applied to multiple other biomaterials, medical devices and tissue engineering approaches for improved integration into the host tissue.

1.1 PELVIC ORGAN PROLAPSE

Pelvic organ prolapse (POP) is a gynecologic condition commonly observed in women of advance age and who have undergone vaginal childbirth [1-6], with significant negative impact on quality of life. POP occurs when loss of support to the vagina causes the organs supported by it, to descend or fall out of their normal position in the pelvis into the vaginal canal. The vagina is supported by a series of connective tissues (often referred to as ligaments), striated muscle (levator ani muscles) and dysfunction of one or more of these structures can lead to reduced pelvic support and subsequent pelvic organ prolapse [1, 5, 7-9]. POP is also highly associated to urinary incontinence [5]. The anterior wall of the vagina is the most common tissue structure to prolapse, usually involving the descent of the bladder, also called cystocoele. Other types of prolapse include enterocoele (small intestine), colon (sigmoidocoele) and rectocoele (rectum) [6]. It is now widely accepted that POP can be considered physiological with aging when prolapse is both asymptomatic and situated in levels above the hymen [5, 6, 10].

Women with more clinically relevant vaginal prolapse can experience one or more symptoms, including but not limited to bulging sensation, vaginal pressure, urinary incontinence and dyspareunia [5, 6]. Table 1 list the symptoms in women with advanced POP.

Table 1. Symptoms in women with clinically relevant Pelvic Organ Prolapse [5, 6].

Vaginal	**Urinary**	**Gastrointestinal**	**Sexual**
Bulging	Incontinence	Incontinence	Dyspareunia
Pressure	Frequency, urgency or hesitancy	Feeling of incomplete emptying	

Table 1 (continued).

Heaviness	Weak or prolonged urinary stream	Straining during defecation	
	Feeling of incomplete emptying	Urgency	
	Manual assistance to start or complete voiding	Assisted evacuation to start or complete defecation	
		Feeling obstruction during defecation	

1.2 EPIDEMIOLOGY

Pelvic floor disorders have a disproportionate effect upon women's healthcare and its associated costs. As many as one third of premenopausal to a half of postmenopausal women are affected by pelvic floor disorders, with increased incidence in women over the age of 50, who have experience vaginal birth and/or obesity [11, 12].

More than 300,000 women per year in the United States alone will undergo surgery for pelvic organ prolapse, with direct costs totaling more than $1 billion per year, and estimated to increase a 46% in the next decades due to the increasingly aging population [13, 14]. Native tissue repair has a recurrence rate exceeding 30% in the following 2 years after surgery;

therefore, mechanical reinforcement of tissues using synthetic mesh materials became extensively used, accounting for a third of the total surgical procedures performed [11, 12]. It is projected that by the year 2050, 4.9 million women will be affected with prolapse in the U.S. alone [11, 15]. In 2010, approximately 100,000 surgeries were performed for prolapse using synthetic mesh [13, 15].

1.3 TREATMENTS FOR PELVIC ORGAN PROLAPSE

Treatment depends largely on the severity of the symptoms, including pelvic-floor muscle training, pessaries and surgery. While pelvic-floor muscle training has been shown to be an effective treatment of urinary incontinence, the effects on pelvic organ prolapse are not clear, with only a few studies suggesting it can slow its progression [5, 6].

The use of pessary is the only non-surgical treatment available, and reserved for patients that are poor surgery candidates or declined surgery [5, 6]. These devices are inserted inside of the vaginal cavity to provide mechanical support and relieve pressure on pelvic organs. Currently, there are 20 different types of pessaries available in the market, made of plastic or silicone. The most common types of pessaries include the ring, the Gelhorn and donut, all available in different sizes. The ring (with or without support) is a good first choice and the most commonly used, because it is easy to insert and remove. Manufacturers recommend that these patients do follow-up visits every 4 to 6 weeks. The most common side-effects of pessaries are vaginal discharge and odor, while other serious complications have been reported due to negligent use.

Surgery is the option for women who fail or decline pessary treatments and present advanced prolapse. Reconstructive surgery aims to correct the prolapsed vagina while preserving sexual function. Surgery techniques are classified by transabdominal and transvaginal routes (Table 2), and frequently augmented with surgical mesh implantation [5, 6, 10]. A combination of these procedures may also be performed. In the particular case of anterior wall prolapse (cystocele), the most frequent type of transabdominal procedure is the sacral colpopexy, mainly done by an open incision or keyhole incision using laparoscopic and robot approaches implantation [5, 6, 10]. On the other hand, the most common transvaginal procedure is the colporrhaphy, which in combination with synthetic mesh offers improved reproducibility and low rates of prolapse recurrence; however, highly associated to complications [10, 16-18]. For this reason, sacral colpopexy is the preferred method of surgical repair, but not exempt of mesh-related complications, and if present the severity may be greater [5, 6, 10].

Table 2. Rate Transabdominal and transvaginal surgery procedures for pelvic organ prolapse [5, 6].

Transabdominal procedures	**Transvaginal procedures**
Hysterectomy	Hysterectomy
Sacral colpopexy	Colporrhaphy
Paravaginal repair	McCall culdoplasty
Vault suspending and uterosacral ligament plication	Manchester repair (cervix amputation and uterus suspension to cardinal ligaments)
Enterocele ligation	Prespinous and sacrospinous colpopexy

Table 2 (continued).

Posterior vaginal wall repair	Enterocele ligation
	Paravaginal repair
	Le Fortes procedure
	Perineal reconstruction

1.4 SURGICAL MESH AND RELATED COMPLICATIONS

Given the high recurrence rates observed (>30% in 2 years) following native tissue repairs, synthetic surgical meshes have been increasingly used to restore mechanical and anatomical support to the vagina and pelvic organs [10, 19, 20]. Surgical meshes used in POP repair were originally designed for use in the reinforcement of hernia repairs; however, companies were able to remarket these products as 510K devices for use in prolapse. This also meant that surgical meshes for POP were released into the market without consideration of the specific biological and mechanical properties of the vagina. In contrast to abdominal tissues, the vagina has been shown to be more prone to inflammation, given the existence of an epithelium and different tissue architecture [7, 8, 21, 22]. In addition, the smooth muscle found in the vagina and its supportive connective tissues are more flexible, capable of being under continuous tensile and compressive forces, in contrast to the stiffer but also more fibrous skeletal muscle [7, 8]. Thus, there may be a mismatch between the properties of currently available mesh materials and vaginal tissue.

Not surprisingly, mesh use in POP surgeries have been shown to be associated higher complication rates (10-20%) than when mesh is used in other tissues [10, 16-18, 23]. The most common complications include pain and mesh exposure, which occurs when the mesh erodes through the vaginal tissues and becomes exposed through the vaginal epithelium, also known as mesh erosion or protrusion. Other complications include infection, organ perforation, incontinence, severe dyspareunia, scarring, neuro-muscular damage, bleeding and autoimmune problems (Table 3) [9, 24, 25]. Some studies suggest that the transvaginal route results in higher rates of mesh-related complications compared to the transabdominal route [10, 16].

In 2008, due to the high number of reported complications, the FDA issued a public health notification regarding the use of mesh in POP, which resulted in a 5-fold increase of reports in the 3 years following [26]. Also, most recently (January 2016) FDA upgraded the classification of surgical mesh for transvaginal repair procedures from class II (moderate risk) to class III (high risk), with significant clinical monitoring and reporting requirements for those companies which manufacture and sell mesh for this application [10, 16]. Currently, most mesh companies are under litigation and some of them have discontinued manufacturing these devices as a result of litigation fees.

Table 3. Rate of mesh-related complications in patients with Pelvic Organ Prolapse after surgical implantation [9, 11-13, 24, 25]

Mesh-related complication	% based on case reports	% based on clinical trials
Mesh exposure	1 - 18.8	5 - 19
Organ perforation	5.8	3.5
Severe pain	2.9 - 18.3	0 - 10

Table 3 (continued).

Dyspareunia	2.2 - 15	8 - 27.8
Overall	10	15 - 20

1.5 PATHOGENESIS OF MESH-RELATED COMPLICATIONS

The pathogenesis of these complications and poor mesh performance are still not clearly defined. A few studies have suggested a closed relationship between stress shielding (biomechanical mismatch between mesh and tissue) and an inflammatory host response against the mesh biomaterial with mesh complications [21, 22, 27-30]. Is it also recognized that other factors are contributing, including implantation route (transvaginal vs transabdominal), surgical technique and health of the patient (e.g. obesity, diabetes and tobacco use) [10, 16].

Significant attention has been placed on the structural properties of the mesh, revealing that the high stiffness of meshes shields the implanted tissue from physiological mechanical performance (stress shielding), resulting in loss of collagen, elastin and atrophy of smooth muscle [27, 28]. Stiffness has been previously linked to weight, porosity, pore size and knit pattern of the mesh; showing direct impact on the host response against the implanted mesh, leading to chronic inflammation, bridging fibrosis (capsule of two or more mesh fibers that fuse together) and poor tissue integration, which may ultimately result in mesh-related complications [28, 31]. In general, these studies have shown that meshes with higher density and pore diameters less than 1 mm were associated with poor tissue-ingrowth, higher inflammatory

response and subsequent fibrotic encapsulation [27, 29, 31]. Mesh shrinkage was also observed in these type of meshes, and highly associated with mesh-related complications [22, 27, 28].

1.6 FOREIGN BODY REACTION AGAINST SURGICAL MESH

The inflammatory host response against implanted biomaterials is also known as foreign body reaction (FBR). Once medical devices are implanted, the foreign body reaction begins with an immediate nonspecific adsorption of proteins at the bare surface of the biomaterial and development of a thrombus that will serve as a transient provisional matrix. The concentration, type and conformation of chemo-attractants, cytokines and growth factors are dependent on the surface properties of the biomaterial, and will dictate the recruitment, adhesion and activation of inflammatory cells [30]. Following transient matrix formation, the acute inflammatory phase initiates with neutrophil infiltration, followed by cytokine-mediated recruitment of macrophages. The assembly of macrophages at the tissue-biomaterial interface leads to further secretion of inflammatory cytokines, that promotes exacerbated and persistent recruitment of more macrophages [21, 22, 30]. In the long-term, the permanency of the implant leads to chronic inflammation, frustrated phagocytosis and the fusion of macrophages to generate foreign body giant cells with subsequent tissue degradation and/or formation of a stiff fibrotic capsule surrounding the implant, both of which may result in failure of the mesh to function as intended [21, 22, 30].

It is now increasingly recognized that macrophages are key mediators of tissue-biomaterial interactions and can play both positive and negative roles following the implantation of biomaterials, being critical determinants of the success of a biomaterial in-vivo [32-34].

Recent studies and claims against mesh manufacturers have implicated the foreign body reaction in mesh complications [21, 22, 28]. Macrophages represent a key cell type in determining the progression and outcome of the foreign body reaction.

1.7 MACROPHAGES IN THE HOST RESPONSE AGAINST BIOMATERIALS

It has been recently demonstrated that macrophages have an important regulatory role in the host response against biomaterials, determining the success of biomaterials in the long-term. Shortly after the initial infiltration of neutrophils a few hours after implantation, monocyte-derived macrophages are also recruited in response to inflammatory cytokines and damage associated molecular patterns (DAMPS) [34]. Monocytes are cells that express chemokine receptors and adhesion molecules that facilitate extravasation and migration from the bone marrow and blood to injured sites where they differentiate into macrophages [21, 30, 34]. In addition, each tissue has its own pool of tissue-resident macrophages, however, the relative contribution of circulating versus tissue-resident macrophage subsets in the host immune response and tissue remodeling remains mostly unknown [34].

To perform multiple regulatory functions, macrophages adopt distinct phenotypes along a continuum spectrum contained between two extremes - pro-inflammatory (M1) and anti-inflammatory/regulatory (M2) macrophages [32, 34-36]. In the host response against biomaterials, these macrophages initially adopt a predominant M1 phenotype in response to necrotic cellular debris and pro-inflammatory cytokines (e.g. IFN- γ, TNF-α). M1 macrophages are important part of the host response and other regenerative processes as they secrete pro-

inflammatory cytokines, proteases and reactive oxygen-species for pathogen control, removal of cell/tissue debris and angiogenesis [30].

In case of non-degradable biomaterials, such as polypropylene mesh, the permanency of the implant and persistent inflammatory stimuli cause chronic inflammation and failed transition to the regenerative phase, where M2 macrophages predominate [34]. In normal regenerative processes, M2 macrophages secrete anti-inflammatory cytokines (e.g. IL-10, IL-13) and growth factors (e.g. VEGF, PDGF-β, and TGF-β) facilitating the resolution of inflammation and promoting tissue repair, by recruitment of fibroblasts and deposition of new extracellular matrix (ECM) [32-34, 37]. Of note, a unique event in the host response against non-degradable biomaterials is the formation of multinucleated foreign-body giant cells, a result of frustrated phagocytosis of macrophages that instead fuse at the surface of the biomaterial, further exacerbating the inflammatory response [30]. Failure to resolve the inflammatory phase results in foreign body reaction, that leads to the formation of fibrotic scar tissue, that encapsulates the implant and prevents its integration into the host tissue [21, 22, 30, 34].

All these events have been shown to be closely related to the structural properties and mechanical performance of surgical meshes [27, 28]. In particular, the predominant M1 response against light-weight and higher porosity polypropylene mesh was found to be attenuated compared to the heavier and less porous surgical meshes [28, 31]. When comparing the response to single fibers versus knots in the mesh, a denser inflammatory response was observed in knots, but the percentage of either M1 or M2 macrophages remained similar, suggesting that the host response is proportional to the area of material in contact with the host tissue [21, 22].

In addition, M2:M1 ratios have been shown to be a predictor of the success of a biomaterial, in which higher ratios are associated to more beneficial remodeling outcomes [32,

38]. For example, multiple studies using ECM-derived materials have shown to facilitate timely transition from an M1 to an M2 phenotype, associated to better remodeling outcomes and signs of functional recovery [33, 34, 37].

1.8 CURRENT APPROACHES

Initially, the immune host response against biomaterials was perceived as a negative event that led to the development of “immune-inert” biomaterials. In the particular case of mesh implants, plastic-based (mostly polypropylene and polytetrafluoroethylene) biomaterials are still under use because many other well-known biocompatible materials have not shown superior mechanical performance. Both degradable and biologic (ECM-derived) surgical meshes have not been conclusive showing lower rates of mesh-related complications, and recurrence is similar to native tissue repairs [39-41]. As a consequence, a wide range of surface modification and coatings have been developed in order to reduce protein adsorption, cell adhesion, inflammatory cytokine secretion and FBGC formation at the tissue-biomaterial interface. Surface modification was performed to change hydrophilicity, charge and crystallinity of the biomaterial [42-45]. Several coating materials have been also used and include collagen, synthetic-hydrogels, and chitosan [46-51]. Even though these coatings have suggested reduction of the inflammatory host response in animal models, they have shown to perform similar or even worse than conventional meshes in clinical trials. For example, chitosan coated mesh was shown to perform similar to a polypropylene-polydioxane composite mesh [52], while transvaginal implantation of collagen-coated mesh was shown to have increased risk of mesh erosion [53].

Additionally, functional biomaterials that deliver immunosuppressant and anti-inflammatory agents have been developed though surface functionalization or drug-eluting coatings to mitigate the host response against the biomaterial [54, 55]. Studies using immobilized alpha-MSH, an anti-inflammatory peptide, on the surface of neural electrodes has shown to inhibit the expression of inflammatory cytokines on microglia (a brain tissue-resident macrophage) [54]. In general, eluting mesh implants with immunosuppressant agents such as hydrocortisone have shown to reduce the inflammatory host reaction and reduce encapsulation of the implant in the long term; however, presenting a negative impact on angiogenesis [55]. Other studies using titanium rod eluting coatings for the release of 7ND protein, a mutant of the macrophage chemoattractant protein-1 (MCP-1), was shown to reduce macrophage migration towards MCP-1 in a femoral rod implantation model [56], and later on showed decreased implant wear particle-induced osteolysis in a mouse calvarial model [57]. Interestingly, other studies using coatings that release nitric oxide (NO), were capable of enhancing angiogenesis of implanted biomaterials, as well as reduced inflammation and diminished capsule formation [58, 59].

Surface topography has also been recognized as an important cue influencing the host response against biomaterials. One study has shown that nano-scale topographical changes in the surface of poly(ε-caprolactone) (PCL), poly(lactic acid) (PLA) and poly(dimethyl siloxane) (PDMS) affected the adhesiveness, cell fusion and cytokine secretion in RAW 264.6 cells in vitro [60]. In particular, this study showed that diameter, surface roughness and geometry of electrospun fibers influenced macrophage activation and formation of FBGC, which is consistent studies done on the host response to surgical mesh with different architecture [21, 27, 31]. Multiple other studies on titanium implants have shown consistently that nanostructured implant

surfaces restricted macrophage migration and diminished secretion of pro-inflammatory cytokines [61, 62].

However, none of these approaches have considered both the acute inflammation and the regenerative phase as necessary elements of the host response to promote functional integration of implanted biomaterials. Recent studies on ECM coated meshes have shown a reduction in M1 macrophages and foreign body giant cells, but no changes in the number of M2 macrophages, resulting in less dense collagen tissue at 35 days post-implantation [38, 63, 64]. However, these studies introduced to this application the concept of M2/M1 macrophage ratios as predictor of the success of biomaterials, being increased ratios associated with better remodeling outcomes. Since then, latest biomaterial-based approaches are increasingly studying macrophage polarization and shown consistently that the most successful biomaterials are associated with higher M2/M1 ratios [34, 37]. Thus, a few novel approaches have emerged to purposely shift macrophage modulation using pro-M2 cytokines. Hydrogels containing IL-4 were shown to polarize macrophages to an M2 phenotype and enhance regeneration in a nerve gap injury model [65]. Another study used continuous pump infusion of IL-4 on coated rods with ND7 protein (MCP-1 inhibitor), showing increased bone formation and enhanced bone geometry, even compared to ND7 coated rods alone, suggesting that macrophage modulation is a superior strategy than reducing macrophage recruitment and inflammation [66]. Another interesting study uses sequential delivery of IFN-γ (M1 cytokine) followed by IL-4 (M2 cytokine) in a scaffold to promote angiogenesis and bone regeneration, and shown to have improved outcomes compared to IL-4 alone [67], suggesting that the functions of both M1 and M2 macrophages and optimal M1 to M2 transition are essential to obtain functional remodeling outcomes.

1.9 HYPOTHESIS, APPROACH AND SPECIFIC AIMS

Thus, these previous results led us to hypothesize that polarization of macrophages at the tissue-implant interface towards an anti-inflammatory/regulatory (M2) phenotype would promote integration of the implant into the host tissue; therefore, mitigating the foreign body reaction and potential mesh-related complications. To address this hypothesis, we developed a cytokine eluting coating for surgical mesh implants that enables localized, controlled delivery of IL-4, an M2 polarizing cytokine.

Immunosenescence, dysregulation of macrophage function, and delayed resolution of the immune response in aged individuals have all been demonstrated [68-70], suggesting that the host response against biomaterials in aged individuals may differ from those in younger individuals. However, only a few studies examining the effects of aging upon the host response have been performed, which is relevant as medical devices are often intended to treat elderly patients. Therefore, we have sought to elucidate the impacts of aging upon the host response to polypropylene mesh implanted into aged mice versus young adult mice. The results of this study will be used towards the development of contextual delivery regimens to improve the integration of surgical mesh implants on elderly patients.

To accomplish this study, we have developed a research plan consisting of three aims: 1) Development of a conformal cytokine eluting coating for surgical mesh implants, 2) Early-stage and downstream effects of IL-4 eluting coatings on the host response against surgical mesh, and 3) Elucidate the effects of aging in the host response against biomaterials to design a contextual delivery regimen.

2.0 AIM I: DEVELOPMENT OF A CONFORMAL CYTOKINE ELUTING COATING FOR SURGICAL MESH IMPLANTS

2.1 INTRODUCTION

Currently, lightweight, large pore polypropylene mesh is the gold standard for implants in both POP and hernia repair [12]. These materials are associated with a reduction in complications as well as a reduction in both tissue degradation and inflammation observed in animal testing. A number of studies investigating the use of alternative polymers [71], coatings (collagen, chitosan) [51, 63, 72] and surface modification [73, 74] have been performed; however, performance in preclinical studies has not improved, and in some cases has been worse than polypropylene alone. Other groups and companies are trying to increase biocompatibility by using biologically derived surgical meshes (e.g. materials composed of crosslinked and non-crosslinked extracellular matrix (ECM) from dermis, urinary bladder and small intestinal submucosa) [75-77]; however, studies done in hernia repair have not been conclusive and led to mesh companies to unsupported claims of superiority and safety, but also high recurrence rates likely due to the suboptimal mechanical performance and the non-permanency of the mesh over time [77, 78]. A small number of studies are underway using biologic meshes for POP, but few results regarding the efficacy of these methods are currently available. Thus, currently, there is no surgical repair (or treatment) for pelvic organ prolapse that is not either associated with

complications or with high rates of recurrence (in the case of native tissue repair); therefore, there is an urgent need for a device that has better tissue integration and fewer complications.

We aim to test the hypothesis that shifting the macrophage response towards an anti-inflammatory (M2) phenotype will lead to a better implant integration into the host tissue. To accomplish this study, a nanometer thickness coating with the ability to provide local and transient delivery of IL-4 (an in vitro M2 polarizing cytokine) has been developed, preserving the complex architecture and structural properties of the implant. This coating is based on the layer by layer (LbL) technique [79, 80], consisting of an alternate cyclic deposition of multiple polyelectrolyte layers mediated by opposite electrostatic charges on the surface of a charged substrate. This method has previously been shown to produce a tunable, uniform and conformal coating of nanometer thickness for controlled release of proteins [56, 79-85]. Therefore, the number and sequence of layers can be easily modified in order to provide the desired amount and release time of IL-4. Also, nanometer thickness of this coating was desired to preserve the architecture and pore space of the mesh, which is commonly thought to be important for adequate tissue ingrowth and mechanical performance in clinical settings [71, 86].

2.2 METHODS

2.2.1 Materials

A polypropylene mesh, Gynemesh® PS (Ethicon, Somerville, NJ) was used. Maleic anhydride, chondroitin sulfate B, chitosan (low molecular weight, deacetylation degree 85%), chondroitinase ABC, chitosanase, bovine serum albumin (BSA) and histologic staining materials

were purchased from Sigma Aldrich (St. Louis, MO). Murine IL-4, anti-murine IL-4 antibody, murine IL-4 ELISA detection kit were purchased from Peprotech (Rocky Hill, NJ). Mouse arginase-1 antibody (rabbit), anti-rabbit Alexa-fluor 488 (donkey) and anti-rabbit Alexa-fluor 594 (donkey) were purchased from Abcam (Cambridge, MA). Anti-rabbit Alexa-fluor 488 (donkey) was purchased from Thermo Fisher (Pittsburgh, PA).

2.2.2 Plasma treatment of polypropylene meshes

Polypropylene (PP) meshes were cleaned using a 1:1 acetone:isopropanol mixture and then air dried prior to irradiation with 15 seconds of argon plasma at 600W, an argon gas flow of 35 mL/min and a steady state pressure of 250 mTorr (50 mTorr initial pressure) using an Ion 40 Gas Plasma System (PVA Tepla America, Inc).

An adapted radio frequency glow discharge (RFGD) based on a previously developed microwave plasma procedure was used to obtain a negatively charged surface [87]. Briefly, maleic anhydride powder (1.5 gr) was placed into a glass plate inside of the machine chamber. 1 cm^2 pieces of PP mesh were then placed around the plate to a distance of 8.5 cm. After an initial pressure of 50 mTorr was reached, 30 seconds of maleic anhydride plasma treatment was performed at 600W, an argon gas flow of 35 mL/min and a steady state pressure of 250 mTorr. Finally, in order to remove the physisorbed maleic anhydride and to hydrolyze the anhydrides and produce carboxylic acid groups (negatively charged at physiological pH), PP meshes were rinsed for 30 minutes with milli-Q water and then boiled for 20 minutes in fresh milli-Q water.

2.2.3 Layer by layer coating of charged polypropylene meshes

In order to deposit a conformal coating of nanometer thickness onto the surface of negatively charged PP meshes, a Layer by Layer (LbL) procedure was performed (Figure 1). Chitosan was chosen as polycation and dermatan sulfate (chondroitin sulfate B) as polyanion. Chitosan was dissolved in 0.5 % acetic acid and dermatan sulfate in milli-Q water. Both polyelectrolites were prepared at a concentration of 2 mg/mL. First, meshes were dipped in chitosan for 10 minutes at room temperature, then meshes were washed 3 times (10, 20 and 30 seconds) in milli-Q water and air dried (pressurized clean air). Next, meshes were dipped in a dermatan sulfate solution for 10 minutes at room temperature. Meshes were washed again in milli-Q water and air-dried. This cycle was repeated until a core coating of 10 bilayers ($PP^{-}[CH/DS]_{10}$) was achieved. After coating, meshes were lyophilized and stored at 4°C.

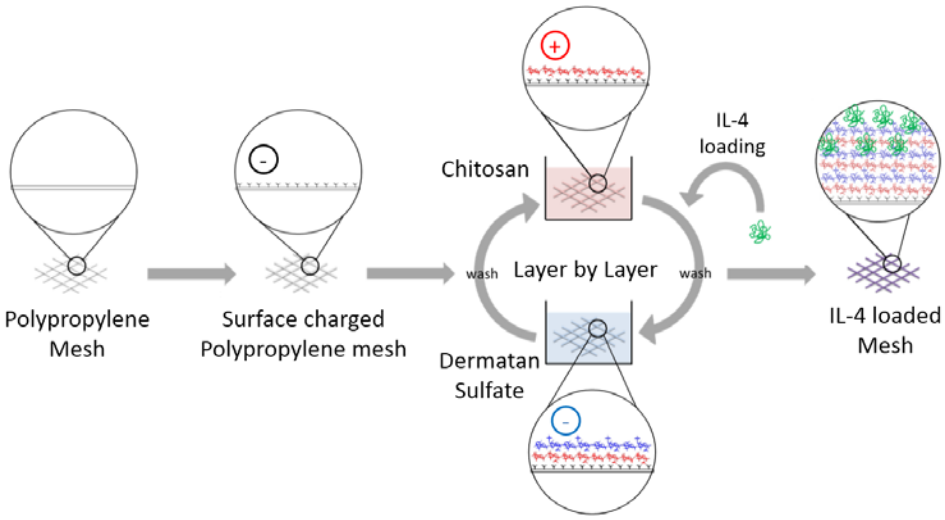

Figure 1. Schematic of layer by layer coating procedure performed on polypropylene surgical meshes

2.2.4 IL-4 loading of coated polypropylene meshes

Prior to IL-4 loading onto the meshes, an IL-4 (1.5 µg/mL) - dermatan sulfate (2 mg/mL) mixture was made and incubated overnight at 4°C in order to complex IL-4 into the polyanion. Then, polypropylene meshes with a 10-bilayer core coating were further coated with 20, 40 and 60 bilayers containing IL-4 ($PP^{-}[CH/DS]_{10}[CH/DS^{IL\text{-}4}]_{x}$, where x stands for number of bilayers, and $DS^{IL\text{-}4}$ stands for dermatan sulfate bound IL-4). After coating, IL-4 loaded meshes were lyophilized and stored at -20°C. Coated (no IL-4) meshes were used as controls, using the same numbers of bilayers used for IL-4 loaded meshes. All mesh materials were then terminally sterilized using ethylene oxide.

2.2.5 Coating characterization

An Alcian blue staining was performed on whole samples to stain the GAG components and reveal the coating. A 1% Alcian blue solution was made in 3% acetic acid and adjusted to pH 2.5. Coated meshes and controls were re-hydrated in distilled water and then immersed into the Alcian blue solution for 30 minutes at RT. Then meshes were washed in running tap water for 5 minutes and rinsed 5 minutes in distilled water. Images were taken using a standard optical camera.

Additionally, elemental composition of the coated meshes was performed using an X-ray photoelectron spectroscopy (XPS), using an ESCALAB 250Xi, Thermo Scientific (Pittsburgh, PA). To identify the elements in the coating/surface of the meshes, an initial survey of 10 scans was obtained and for detailed elemental information, spectra of 25 scans were obtained for

Carbon, Oxygen, Nitrogen and Sulfur. Spectra data was analyzed using Avantage software, Thermo Scientific.

Finally, meshes were analyzed under Fourier transform infrared spectroscopy with attenuated total reflectance (ATR-FTIR) using a Bruker Vertex 70 (Billerica, MA) equipped with a germanium ATR crystal at a resolution of 1 cm^{-1}, 2 mm of aperture, 32 scans and processed by OPUS software to adjust the baseline, to smooth spectra and to remove H_2O and CO_2 peaks due to environmental noise.

2.2.6 IL-4 loading and release assays

Immunolabeling was used to qualitatively demonstrate the loading and distribution of IL-4 throughout the coating. IL-4 loaded, coated (no IL-4) and pristine meshes were immersed in a 1% BSA solution to block non-specific adsorption of antibodies (1h, RT). Washing was performed in between each step by dipping the meshes 4 times in 0.05% Tween 20. Then meshes were immersed and incubated in a solution of anti-murine IL-4 (from rabbit) as primary antibody (1:100 in 0.1% BSA, 2 hours, RT). Meshes were then immersed in a solution of anti-rabbit-Alexa Fluor 546 as a secondary antibody (1:100 in 0.1% BSA, 30 min, RT). Mesh fluorescence was observed under confocal microscopy (Leica DMI4000 B, Buffalo Grove, IL), in which an excitation/emission of 480/520 nm was used to observe the mesh autofluorescence (green) and 561/572 nm to observe the specific fluorescence due to the loaded IL-4 (red).

Loading efficiency and release assays were performed following manufacturer instructions of the Peprotech IL-4 ELISA kit. First, 1 cm^2 pieces of IL-4 loaded (20, 40 and 60 bilayers) and coated (no IL-4) meshes were immersed into 400 µL of a solution 0.05 units/mL chondroitinase ABC and 0.05 units/mL chitosanase in 1X PBS. Incubation was performed to

multiple time points at 37°C, after which 400 µL of solution were aliquoted and stored at -80°C until the end of the experiment. After collection, replacement with fresh solution was performed to continue the release assay. To perform the ELISA assays, 100 µL aliquots were used from each sample (N = 9) at each time point.

To determine release profile kinetics; correlation and curve fitting analyses were performed using the data from cumulative release versus time, until the first-time point where the release reaches a plateau, which corresponds to the total release. To corroborate power law dependence, besides direct curve fitting tests, a linear trend was corroborated using a LOG (cumulative release) versus LOG (time) curve.

2.2.7 *In vitro* macrophage culture assay

An *in vitro* macrophage culture assay was performed in order to demonstrate preservation of bioactivity of IL-4 released from the coated meshes. Bone-marrow mononuclear cells were obtained from murine bone marrow as previously described [88], then these cells were seeded in plates and differentiated to macrophages with DMEM, 10% FBS, 10% L929 supernatant, 1% HEPES, 2% MEM NEAA, 0.1% β-2-mercaptoethanol (Sigma Aldrich, St. Louis, MO) for 7 days. 5 x 10^5 cells were plated into 24-well plates with α-MEM, 10% FBS, 0.05 units/mL of both chondroitinase ABC and chitosanase. Macrophages were exposed to 1 cm^2 pieces of pristine, coated (no IL-4) and IL-4 loaded (40 bilayers) meshes. Immunolabeling isotype (rabbit IgG) and soluble IL-4 (20 ng/mL) were used as negative and positive controls, respectively. Cells were incubated at 37°C and 5% CO_2 for 72 hours. After incubation, cells were fixed with 2% PFA and then blocked with 2 % horse serum, 1% BSA, 0.1% triton X-100, 0.1% tween-20 for 1 hour at RT. Immunolabeling was performed using anti arginase-1 as primary antibody (1:200, overnight

at 4°C) and Alexa Fluor-488 (1:300, 1 hour at RT) as secondary. A 500 nM DAPI solution was used stain nuclei. Images were taken in an array of 3 x 3 images per each well using a Carl Zeiss Observer.Z1 microscope and then the intensity of arginase-1 staining was analyzed using Cell Profiler Image Analysis Software (Broad Institute, Cambridge, MA) using the same number of cells for all tested conditions.

2.2.8 Uniaxial testing of LbL coated meshes

Pristine and coated mesh samples (15 x 3 cm) were attached to a custom set of clamps to form a clamp–mesh–clamp construct. To ensure consistence, clamp to clamp distances were adjusted so meshes were tested with 9 cm long and 3 cm wide, to keep an aspect ratio of three for all samples. The clamp-mesh-clamp construct was then installed in an Instron TM 4502 (Instron, Norwood, MA, USA) screw driven testing apparatus, as previously described [89]. A preload of 0.1 N was applied using an elongation rate of 10 mm/min, which removes all slack within the sample to measure clamp to clamp distance. Samples were loaded to failure along the longitudinal axis at a rate of 50 mm/min. The load at failure in newtons and the elongation in millimeters were obtained. The relative elongation of the samples was calculated by dividing the elongation by the initial clamp to clamp distance.

Cyclic testing was performed to test structural properties of mesh and permanent elongation under the assumption that prolapse mesh will undergo repetitive loading as consequence of intra- abdominal tensile forces during early post- operative period. Briefly, samples were preloaded to 0.1 N at a rate of 10 mm/min. Clamp to clamp distance was measured, then cycled from 0.5 to 5 N (C1), 0.5–15 N (C2), and finally 0.5–5 N (C3), each for

ten cycles. Elongation was determined after each cycle (C1 to C3) under a preload of 0.1 N, then permanent deformation was measured as percentage of the initial length of the mesh.

2.2.9 Statistical analysis

Comparisons of means were performed by either one-way or two-way analysis of variance (ANOVA), using at least $p < 0.05$ as statistical significance criteria followed by Tukey's test to compare groups and Sidak's test to compare time points. Shapiro-Wilk was used to test normality. All statistical tests were performed on GraphPad Prism V7 (La Jolla California, USA).

2.3 RESULTS AND DISCUSSION

2.3.1 Surgical mesh plasma irradiation, LbL coating and characterization

An adapted radio frequency glow discharge (RFGD) method [87] was used to form a consistent and durable negative charge on the surface of polypropylene (PP) mesh in order to facilitate the desired LbL coating. The presence of a negatively charged surface was confirmed by the appearance of two peaks at 284 eV (C-C) and 288 eV (O-C=O) on the carbon spectrum and a peak at 532 eV on the oxygen spectrum, while pristine mesh only had a peak at 284 eV (C-C) when evaluated by X-ray photoelectron spectroscopy (XPS) (Figure 2a). RFGD treated meshes were then LbL coated using chitosan as a polycation and dermatan sulfate as a polyanion. Chitosan was chosen for its known biocompatibility, antimicrobial activity, and as activated

macrophages highly express chitinase-like proteins (chitin and chitosan degrading enzymes) [90-92]. Dermatan sulfate (also known as chondroitin sulfate B) was chosen for its key role in extracellular matrix (ECM) regulation and its described ability to enhance IL-4 bioactivity *in-vivo* [93]. Thus, a chitosan-dermatan sulfate LbL complex has the potential to provide enhanced release and bioactivity of IL-4 in the context of macrophage mediated host-implant interactions.

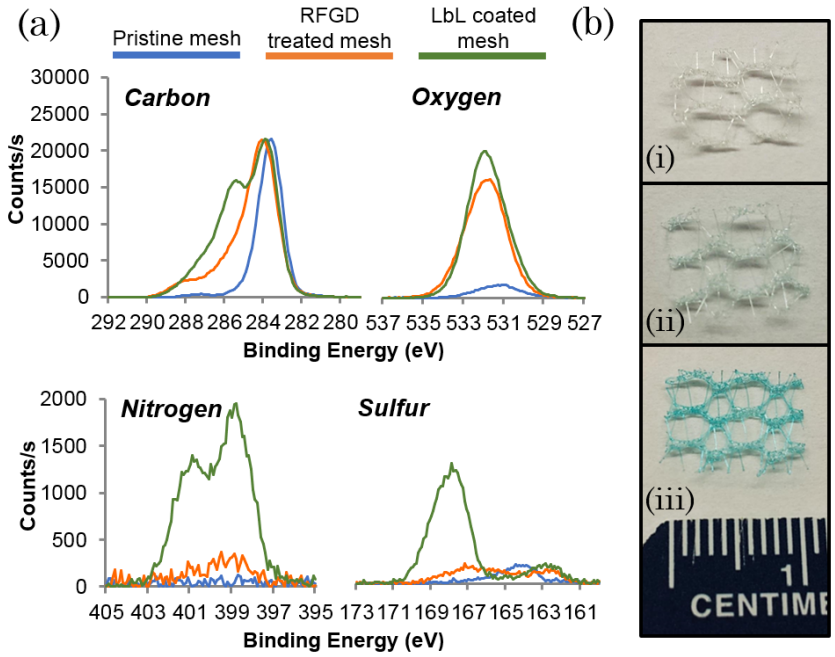

Figure 2. (a) X-ray photoelectron spectroscopy spectra (XPS) of LbL coated (green), RFGD treated (orange) and pristine (blue) mesh. (b) Images of alcian blue stained 1 cm^2 pieces of pristine (i), RFGD treated (ii) and LbL coated meshes (iii)

A coating of 10 bilayers was performed as core coating prior to IL-4 loading. Alcian blue staining was used to visualize the chitosan and dermatan sulfate components of the coating. Blue coloration and absence of precipitates along the mesh surface suggested the presence of a

conformal and uniform coating on LbL coated meshes (Figure 2b). Electron microscopy (Figure 3) was used to confirm the conformal nature of the coating and showed no apparent changes in surface topography, porosity and thickness between LbL coated, RFGD treated and pristine meshes. The presence of chitosan in the LbL coating was corroborated by the appearance of two peaks at 399 eV (C-N) and 401 eV (O-C-N) in the nitrogen spectrum and the presence of dermatan sulfate by the appearance of a peak at 168 eV (C-S-O) in the sulfur spectrum when evaluated by XPS (Figure 2a), in addition to the presence of peaks at 288 eV (O-C=O) and 286 eV (C-O) in the carbon spectrum, confirming the presence of both polyelectrolyte chains. These measurements were performed at different points on the surface of the PP mesh and spectra were identical throughout the mesh surface. These findings were consistent with ATR-FTIR measurements (Figure 4).

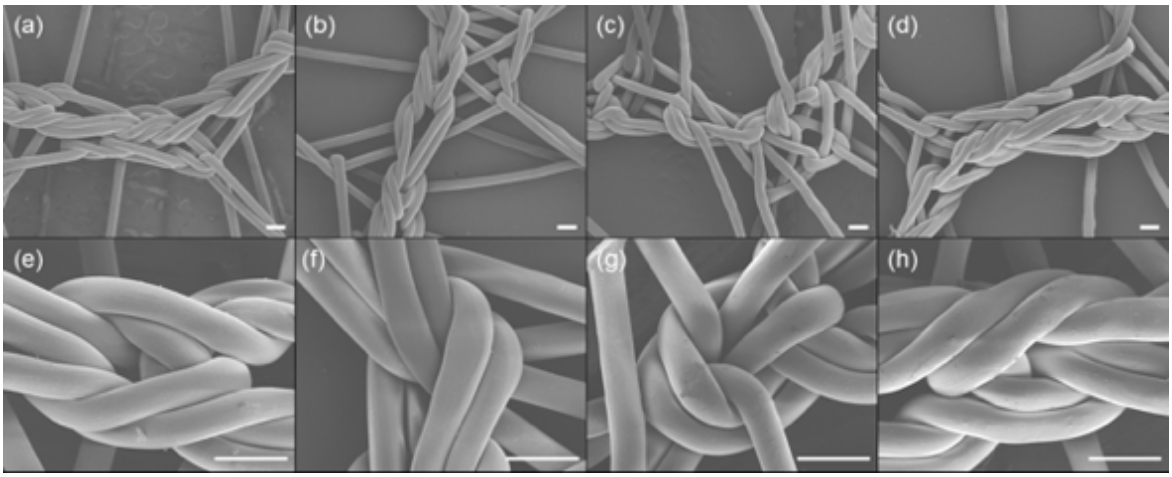

Figure 3. Scanning electron microscopy images at 40X (a-d) and 150X (e-h) of pristine (a, e), RFGD treated (b, f), LbL coated (c, g) and IL-4 loaded [40B] (d, h) meshes. Scale bars represent 200 µm

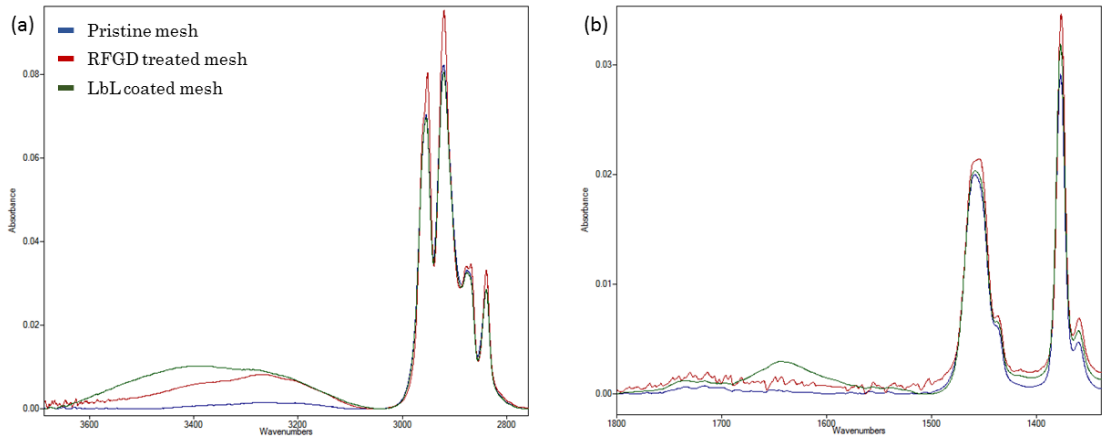

Figure 4. Attenuated total reflectance – Fourier transform infrared (ATR-FTIR) spectra of pristine (blue), RFGD treated (red) and LbL coated (green) meshes

2.3.2 Loading and release assessments of IL-4

Mesh coated with a 10-bilayer core coating was then coated with 20, 40 and 60 additional bilayers containing IL-4. IL-4 was pre-incubated with dermatan sulfate prior to LbL coating, promoting the loading of the cytokine due to the high affinity of IL-4 (net positive charge, given its isoelectric point of 9.17) for sulfated glycosaminoglycans (negatively charged). Confocal microscopy demonstrated positive IL-4 labeling distributed throughout the entire surface of IL-4 loaded meshes in contrast to the absence of positive labeling on coated (no IL-4) mesh and pristine mesh (Figure 5a). ELISA assays were performed to quantify IL-4 release over time. Results showed that both the amount of IL-4 and the length of release are dependent on the number of bilayers containing IL-4 in the LbL coating (Figure 5b). In particular, the *in vitro* release of IL-4 was observed up to 14, 22 and 30 days for coatings of 20, 40 and 60 bilayers, respectively. The release profile for all IL-4 loaded meshes followed a power law dependence,

regardless of the number of coating bilayers (Figure 5c). These findings are consistent with other studies done on LbL films as a platform to study protein release [81, 82, 85]. Based upon these results, meshes coated with 40 bilayers containing IL-4 were selected for further *in-vitro* and *in-vivo* assays, since the coating released about 90% of IL-4 only at early stages of the host response (up to 14 days). All further assays included coated (40 additional bilayers with no IL-4) and pristine mesh groups as control groups. Of note, the total amount of released IL-4 may not necessarily correlate with the total amount of IL-4 loaded into the coating, this latter being difficult to obtain due to an order of difference in the amount of IL-4 in the coating solution versus the mesh (μg versus ng), but also poor reliability due to variations in the concentration of the coating solutions by dipping substrates.

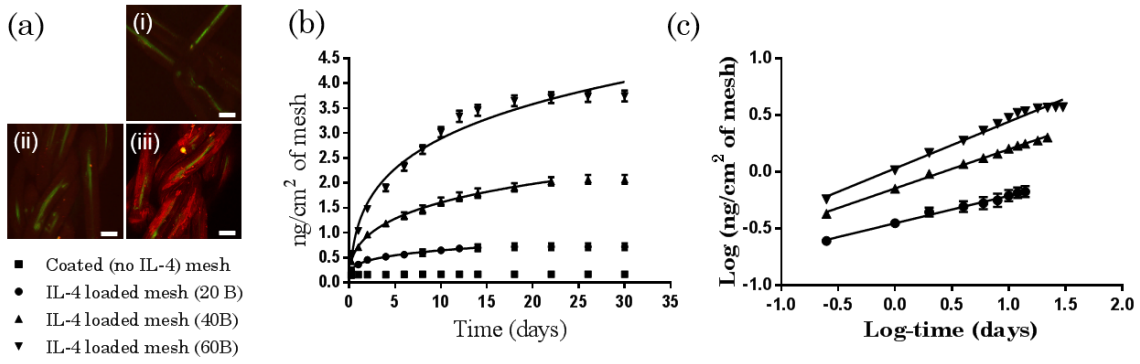

Figure 5. (a) Confocal microscopy images of IL-4 immunolabeled (red) polypropylene fibers (green) of pristine (i), coated [no IL-4] (ii) and IL-4 loaded [40B] (iii) mesh. Scale bars represent 100 μm. (b) Cumulative release of IL-4 (nanograms) versus time (days) from 1 cm^2 pieces of IL-4 loaded mesh (20, 40 and 60 bilayers). Coated (no IL-4) mesh was used as a control. Power law dependence curves are $y = 0.363x^{0.262}$ ($r^2 = 0.995$), $y = 0.718x^{0.437}$ ($r^2 = 0.997$) and $y = 1.078x^{0.412}$ ($r^2 = 0.983$) for 20, 40 and 60 bilayers, respectively. (c) Log - log linear fittings of IL-4 cumulative release versus time. Linear equations are $y = 0.242x - 0.440$ ($r^2 = 0.995$), $y = 0.347x - 0.144$ ($r^2 = 0.997$), $y = 0.412x + 0.033$ ($r^2 = 0.983$) for 20, 40 and 60 bilayers, respectively. Points represent the mean ± SEM

2.3.3 Bioactivity assessment of released IL-4

In order to show that IL-4 bioactivity remained after the coating procedure and terminal sterilization by ethylene oxide, an *in-vitro* macrophage polarization assay was performed using mouse bone marrow-derived macrophages. Macrophages exposed to IL-4 loaded meshes for 72 hours were fixed and immunolabeled against arginase-1, an M2 macrophage specific marker. Image analysis (CellProfiler, Broad Institute, Cambridge, MA) of arginase-1 positive cells revealed that the IL-4 released from the IL-4 loaded mesh remained bioactive and able to polarize macrophages towards an M2 phenotype (Figure 6). No significant increase of arginase-1 was observed for coated mesh compared to pristine mesh. Of note, the pattern of arginase-1 expression following exposure to IL-4 coated meshes was similar to the IL-4 positive control (20 ng/mL) despite the lower levels of IL-4 (2.25 ng/mL) released from the mesh surface at 72h (Figure 6d), suggesting that the coating components may enhance IL-4 bioactivity or that IL-4 is protected by the coating and released gradually.

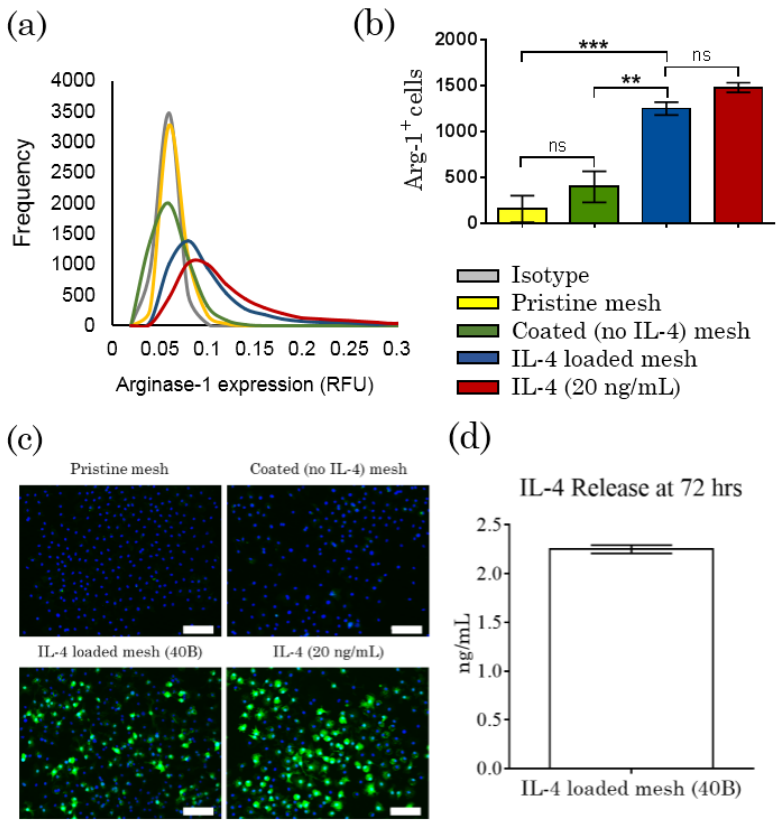

Figure 6. (a) CellProfiler image analysis from arginase-1 immunolabeled murine macrophages in an in-vitro culture exposed to 1 cm^2 pieces of pristine (yellow), coated [no IL-4] (green) and IL-4 loaded [40B] (blue) mesh. Isotype (gray) and IL-4 [20 ng/mL] (red) were used as negative and positive controls, respectively. (b) Number of arginase-1 positive macrophages determined from the CellProfiler analysis. Bars represent the mean ± SEM. Statistical significance as (**) $p < 0.01$ and (***) $p < 0.001$, using one-way ANOVA with Tukey's test. (ns) Non-significant. (c) Arginase-1 immunolabelled bone marrow-derived macrophage cultures exposed to 1 cm^2 pieces of pristine, coated (no IL-4) and IL-4 loaded (40B) meshes for 72 hrs. IL-4 (20 ng/mL) was used as positive control. Scale bars represent 100 µm. (d) Concentration of IL-4 released by IL-4 loaded meshes (40 bilayers) for 72 hours. Bar represents the mean ± SEM

2.3.4 Uniaxial testing of LbL coated meshes

To demonstrate that the nanometer thickness coating does not alter the structural properties of the mesh, we have performed uniaxial tests to determine the stiffness of coated and pristine mesh under tensile forces to failure, or under cyclic tensile forces. In a load to failure testing, load versus relative elongation was plotted and analyzed for both coated and pristine mesh (Figure 7). Two distinct regions in the curve where identified as low and high stiffness, separated by the point of inflection (intercept where the two tangent lines fit) and defined by their maximum slope over the second 30% interval of relative elongation. Results reveal that both load (N) and percentage of elongation at failure of the coated meshed were similar to those of pristine meshes. However, coated meshes presented an increased stiffness under low tensile forces, compared to pristine mesh, then present similar stiffness under high tensile forces.

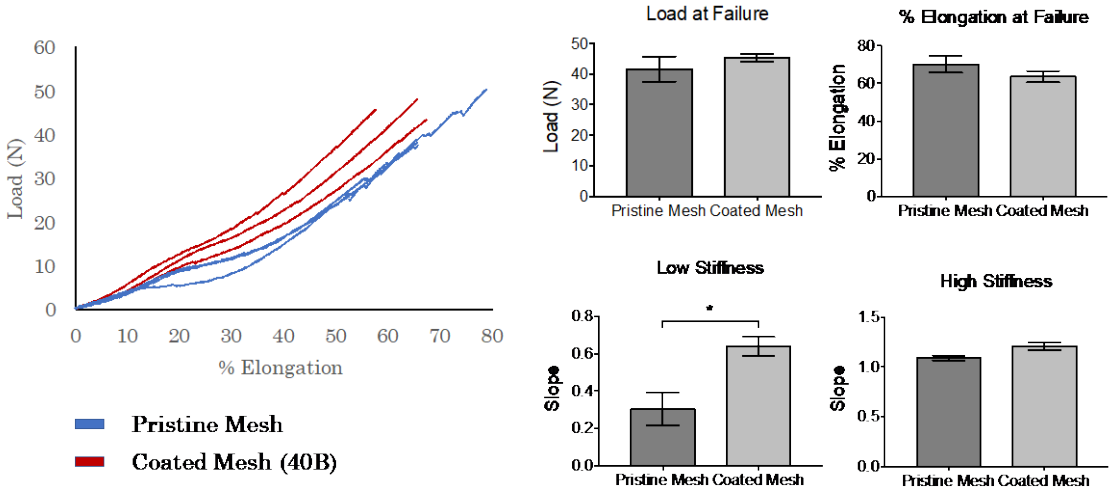

Figure 7. Load to failure test. Load (N) versus relative percentage of elongation curves of pristine (blue) and coated (red) surgical meshes (Gynemesh), load and % elongation at failure, as well as low and high stiffness. Bars represent the mean ± SEM. Statistical significance as (*) $p < 0.05$, using two-tailed t-tests. All other differences are non-significant

Cyclic testing was done to determine the permanent elongation under the assumption that prolapse mesh will undergo repetitive loading as consequence of intra- abdominal tensile forces during early post- operative period. Results show that under cyclic tensile forces, the deformation of both coated and pristine meshes after each cycle are similar (Figure 8), although there is a more consistent behavior on coated meshes, opposed to the high variability of pristine mesh. Therefore, both mechanical tests have demonstrated that the presence of the layer by layer coating has not altered the mechanical properties of the surgical meshes.

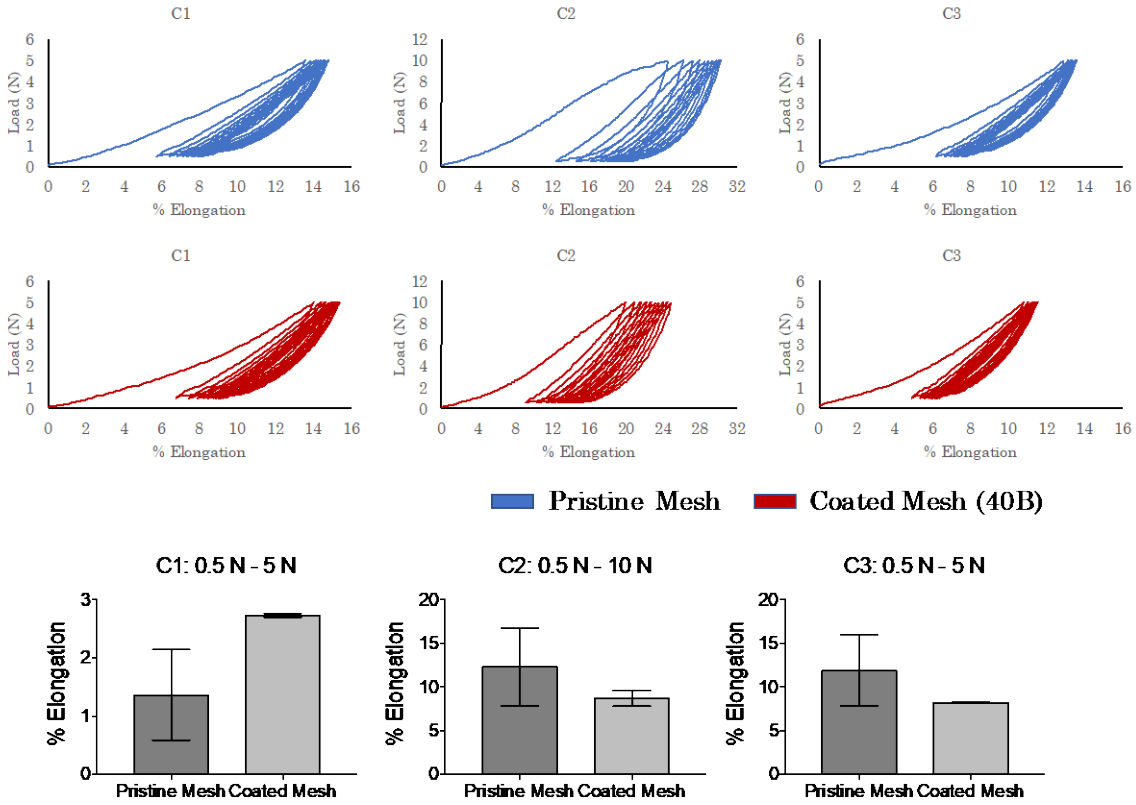

Figure 8. Cyclic testing. Load (N) versus relative percentage of elongation curves of pristine (blue) and coated (red) surgical meshes (Gynemesh) under three consecutive cycles of tensile forces (C1: 0.5-5N, C2: 0.5-10N, C3: 0.5-5N). Percent of permanent deformation is shown on the graphs in the bottom after each cycle. Bars represent the mean ± SEM. Statistical significance as (*) $p < 0.05$, using two-tailed t-tests. All other differences are non-significant

These results suggest that more than changes in structural properties, the coating provides friction at the surface of the mesh fibers, making more difficult for these fibers to rotate when deforming, opposing to movement and deformation. Once fibers are reoriented, stiffness of the mesh is the similar to pristine mesh. This is also consistent to cyclic testing, as mesh deformation of coated after the first cycle is slightly increased (but not significantly), likely due to the coating

impeding mesh fibers to rotate and come back to their original length. Then meshes behave similarly after subsequent cycles.

2.4 CONCLUSIONS

The presence of a uniform and conformal coating composed of both chitosan and dermatan sulfate is demonstrated. This coating can be loaded with IL-4 in a uniform manner through the entire surface of the mesh, and the amount and length of release can be tuned by simply changing the number and sequence of coating bilayers. The released IL-4 from LbL coated meshes is bioactive and can promote macrophage polarization towards an M2 phenotype *in-vitro*. Finally, the presence of the nanometer thickness coating preserved both the architecture and mechanical properties of the polypropylene surgical mesh, which is important to maintain the functionality of the implant as intended.

3.0 AIM II: EARLY-STAGE AND DOWNSTREAM EFFECTS OF IL-4 ELUTING COATINGS ON THE HOST RESPONSE AGAINST SURGICAL MESH

3.1 INTRODUCTION

The host response to implanted materials begins immediately upon introduction of the material into the host tissue and encompasses multiple overlapping phases including injury, protein adsorption, acute inflammation, chronic inflammation, foreign body reaction, granulation tissue formation and eventual encapsulation [30]. It is well recognized that the early interactions which occur at the material-tissue interface represent the initiating events which drive subsequent paracrine and autocrine processes of the host response and subsequent tissue remodeling with significant implications for downstream performance. Recently, macrophage-implant interactions in particular have received considerable attention as a primary determinant of the outcome of biomaterials placement [33, 37, 94-97]. A spectrum of macrophage phenotypes contained between two extremes has been identified, ranging from pro-inflammatory (M1) to anti-inflammatory/regulatory (M2) phenotypes, with significant implications in disease, tissue remodeling following injury, and biomaterial performance [33-36, 98, 99].

The findings of studies in multiple tissue and organ systems have now demonstrated that materials which elicit improved or regenerative remodeling outcomes are often associated with a shift from an initially M1 to a more M2-like profile during the early stages of the inflammatory

response which follows implantation [32, 100-104]. However, many of these studies have been performed as retrospective analyses of macrophage phenotypes associated with successful biomaterials. As a consequence, recent studies have now begun to evaluate improvements in regenerative outcomes following purposeful modulation of macrophage polarization induced by cytokine delivery from degradable materials [65, 67, 105]. These studies have demonstrated that outcomes are improved when M2-polarizing cytokines (IL-4, IL-10) are delivered and that, conversely, outcomes are negatively affected by the delivery of M1-polarizing cytokines (IFN-γ) [65, 67, 106]. A recent study, however, showed that sequential delivery of an M1 (IFN-γ) and then an M2 (IL-4) polarizing cytokine enhanced the vascularity and subsequent healing response associated with the implantation of degradable bone scaffolds [67], demonstrating the importance of both the M1 and M2 responses in the remodeling process. Others have demonstrated that the host macrophage response is also important to the performance of permanent implants. For example, it has been demonstrated that wear particle-induced polarization of macrophages towards an M1 phenotype is associated with periprosthetic osteolysis, possibly resulting in the need for surgical revision following total joint replacement [107-110]. Subsequent studies demonstrated that methods including the delivery of inhibitors of macrophage recruitment, inhibitors of M1 polarization, and promoters of M2 polarization have the ability to mitigate wear particle induced osteolysis, potentially improving the long-term performance of total joint replacements [56, 66, 106, 111].

The present study sought to examine the effects of surface-localized cytokine delivery in the early macrophage response upon the integration of a non-degradable polypropylene mesh material commonly utilized in the repair of pelvic organ prolapse. These materials have recently been shown to elicit a predominantly M1 type response which is associated with the potential for

tissue degradation and downstream complications when unresolved [21, 22]. Macrophage modulation only in early-stages of the host response, but also localized to the tissue-implant interface was sought in the present study, representing an advantage over strategies promoting non-local and/or extended shifts in the host response as it limits the potential for adverse long-term interactions and exacerbation of conditions which may exist at distant sites.

3.2 METHODS

3.2.1 Materials

A polypropylene mesh, Gynemesh® PS (Ethicon, Somerville, NJ) was used. Maleic anhydride, chondroitin sulfate B, chitosan (low molecular weight, deacetylation degree 85%), chondroitinase ABC, chitosanase, bovine serum albumin (BSA) and histologic staining materials were purchased from Sigma Aldrich (St. Louis, MO). Murine IL-4, anti-murine IL-4 antibody, murine IL-4 ELISA detection kit were purchased from Peprotech (Rocky Hill, NJ). Mouse arginase-1 antibody (rabbit), anti-rabbit Alexa-fluor 488 (donkey) and anti-rabbit Alexa-fluor 594 (donkey) were purchased from Abcam (Cambridge, MA). Mouse iNOS antibody (rabbit) was purchased from Santa Cruz (Dallas, TX). Mouse F4/80 antibody (rat) was purchased from AbD Serotec/Bio Rad (Raleigh, NC). Anti-rat Alexa-fluor 488 (donkey) and anti-rabbit Alexa-fluor 546 (donkey) were purchased from Thermo Fisher (Pittsburgh, PA).

3.2.2 In-vivo mouse mesh implantation

An implantation model using C57BL/6J female mice, 8 – 10 weeks old was used, following proper housing and treatment procedures approved by the Institutional Animal Care and Use Committee (IACUC) of the University of Pittsburgh and the National Institutes of Health Guide for the Care and Use of Laboratory Animals. A power analysis was performed to determine that 7 animals per group was required to maintain a statistical power of 80 %.

Briefly, a midline incision was made and a subcutaneous pocket was created in the abdomen of each mouse in order to implant a 1 cm^2 piece of pristine, coated (no IL-4) and IL-4 loaded (40 bilayers) meshes. PCL sutures were used to close the incision, then 0.5 mg/kg of Baytril and 0.2 mg/kg of Buprenex were administered for 3 days as antibiotic and analgesic, respectively. Buprenorphine (Buprenex), an opioid analgesic, has been studied and shown not to exert any effects nor alterations in the immunological response, both acutely and chronically administered [112, 113]. After 7, 14 or 90 days, mice were euthanized and skin/mesh/muscle tissue complex were harvested and fixed for 72 hours in neutral buffered formalin. Finally, fixed tissues were paraffin embedded and cross-sections of 7 µm were used for histological studies.

3.2.3 Immunolabeling of histological sections

Paraffin embedded tissue sections were deparaffinized and hydrated in a series of xylene/alcohol/water. Incubation with proteinase K (1X) for 10 minutes at 37ºC was performed to retrieve antigens. After 3 washes in water, samples were incubated at 37ºC in 50 mM of $CuSO_4$ in 10 mM NH_4Ac buffer pH = 5, to reduce tissue background fluorescence. Slides were washed twice in TBST (25 mM Tris buffer + 0.1% tween 20). Then, a 5% donkey serum + 2%

BSA + 0.1% tween 20 + 0.1% triton X-100 solution was used as blocking agent (2 hours, RT). To immunolabel M2 macrophages, arginase-1 (1:100) and F4/80 (1:50) primary antibodies were used (overnight at 4°C), followed by anti-rabbit Alexa Fluor 594 (1:200) and anti-rat Alexa Fluor 488 (1:100) secondary antibodies (40 min at RT) in blocking buffer. To immunolabel M1 macrophages, iNOS (1:100) and F4/80 (1:50) primary antibodies were used (overnight at 4°C), followed by anti-rabbit Alexa Fluor 594 (1:100) and anti-rat Alexa Fluor 488 (1:100) secondary antibodies (40 min at RT) in blocking buffer. Vectashield with DAPI mounting media (Vector laboratories, Burlingame, CA) was used to stain nuclei and mount. Images of centered single fibers (3 different single fibers per sample, N = 8 each group) were taken on a Nikon Eclipse E600 microscope equipped with epi-fluorescence at 40X and cell counts were analyzed using ImageJ (version 1.51a, NIH).

Image analysis algorithms were used to quantify the results obtained by imaging of histological tissue sections. First, a custom-designed algorithm (Wolfram Mathematica, version 10.0. Champaign, IL) was used to quantify both arginase-1 and iNOS expression at 7 and 14 days by means of arginase-1/DAPI and iNOS/DAPI pixel ratio versus the distance from the surface of single centered mesh fiber (3 different single fibers, N = 8 each group) images taken from histological tissue sections per sample. Next image analysis was performed using ImageJ (version 1.51a, NIH) in order to quantify the number of pro-inflammatory (iNOS, M1) and regulatory (arginase-1, M2) macrophages (F4/80) surrounding single mesh fibers in each group.

3.2.4 Histological stainings

Paraffin embedded tissue cross-sections were used for H&E, Masson’s trichrome and Picro Sirius Red staining. H&E and Masson’s trichrome stained tissue sections were imaged on a

Nikon Eclipse E600 microscope (Tokyo, Japan) at 10X and 20X, respectively. Picro Sirius Red stained tissue sections were imaged at 20X on a Nikon Eclipse TE2000-E (Tokyo, Japan), equipped with circularly polarized light.

ImageJ (version 1.51a, NIH) equipped with a color deconvolution plug-in (version 1.5) was used to quantify the area and mean thickness (calculated as the mean of apical, basal, and lateral measurements taken perpendicular to the surface of the mesh fiber, Figure 9) of capsule surrounding mesh fibers at 90 days (3 different single fibers per sample, N = 8 each group) in images taken from histological tissue sections stained with Masson's Trichrome.

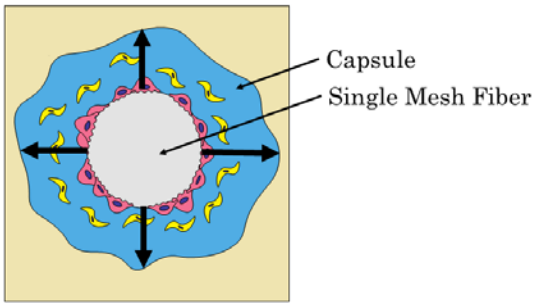

Figure 9. Quantification of the mean thickness (calculated as the mean of apical, basal, and lateral measurements taken perpendicular to the surface of the mesh fiber) of capsule surrounding mesh fibers at 90 days (3 different single fibers per sample, N = 8 each group) in images taken from histological tissue sections stained with Masson's Trichrome

A custom-designed algorithm (Mathworks MathLab, version R2015a. Natick, MA) was used to evaluate quantitatively the distribution of collagen fiber sizes surrounding mesh fibers at 90 days (3 different single fibers per sample, N = 8 each group) in images taken from histological tissue sections stained with Picro Sirius Red.

3.2.5 Gene expression analysis

Transient inflammatory tissue from mesh explants was isolated to extract RNA using Qiagen RNeasy MiniPrep RNA Isolation Columns following standard kit protocol. RNA was quantified using a NanoDrop Spectrophotometer. cDNA templates were created using Invitrogen High Capacity RNA-to-cDNA kits. Taqman Gene Expression Assays were performed for the following markers: Arg-1, IL-10, YM-1, Fizz-1, iNOS, IL-6, TNF-α, IL-12β, TGF-β1, IL-1β, MCP-1, PPARγ, MMP-9, MMP-10, MMP-13, Col1A1, CTGF, VEGFα and PDGFα, using B2M as endogenous control. Gene expression was normalized against the SHAM group.

3.2.6 Statistical analysis

Comparisons of means were performed by either one-way or two-way analysis of variance (ANOVA), using at least $p < 0.05$ as statistical significance criteria followed by Tukey's test to compare groups and Sidak's test to compare time points. Shapiro-Wilk was used to test normality. All statistical tests were performed on GraphPad Prism V7 (La Jolla California, USA).

3.3 RESULTS AND DISCUSSION

3.3.1 Studies on macrophage polarization and the early-stage host response against implanted meshes

A mouse implantation model was used to test the ability of IL-4 loaded mesh to promote an early shift (7 and 14 days) in the polarization of macrophages towards an M2 phenotype *in-vivo* and to examine the effects of such shifts in macrophage polarization upon downstream tissue remodeling (90 days). 1 cm^2 of pristine mesh, coated (no IL-4) mesh and IL-4 loaded mesh (40B) were implanted into a subcutaneous pocket in the abdomen of 8-10 week old female C57BL/6J mice. Mesh and surrounding tissue (muscle and skin) were then harvested at 7 and 14 days post-implantation and used to study macrophage polarization. Sham surgeries (no mesh implantation) were also performed. In sham animals, a normal wound healing process observed (Figure 10, top panel) and was characterized by a transient inflammatory response including significant immune cell infiltration at 7 days which was largely resolved by 14 days post-inflammation with restoration of normal tissue architecture resembling healthy tissue controls. The histologic appearance in mice implanted with mesh was also characterized by the presence of inflammatory cell infiltration in the surgical site at 7 days; however, this reaction was not resolved at 14 days and was largely localized to the area surrounding mesh fibers, regardless of mesh type (Figure 10, bottom panel), thereafter. The presence of foreign body giant cells was noted beginning at 14 days post implantation and at the 90 day time point, regardless of mesh type. While the number and distribution of foreign body giant cells was qualitatively similar across all groups, no attempt was made in the present study to quantify the number of foreign body giant cells.

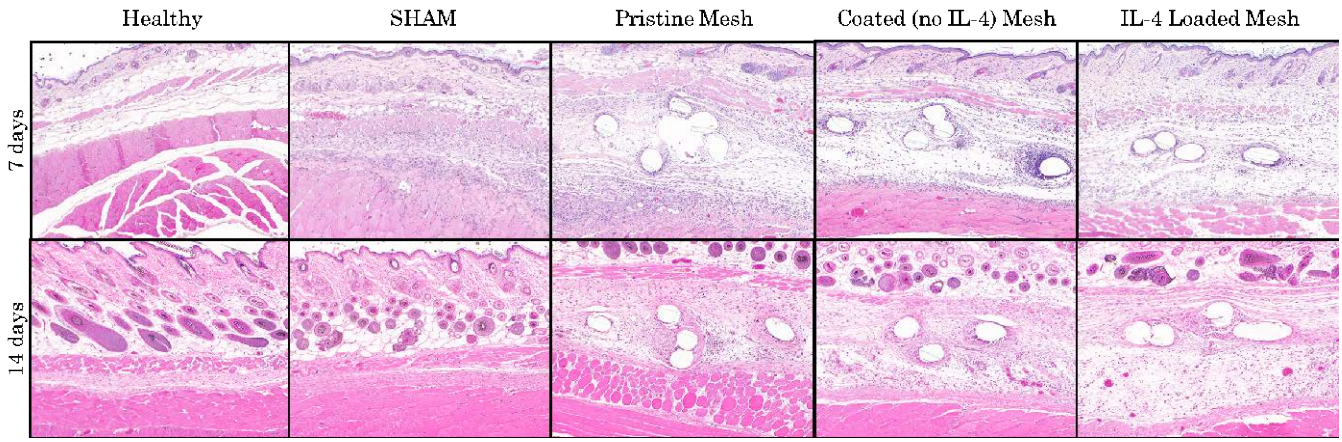

Figure 10. H&E stained tissue sections at 10X from mice implanted with a 1 cm^2 piece of pristine, coated (no IL-4) and IL-4 loaded (40B) mesh at 7 days (top panel) and 14 days (bottom panel). Healthy and SHAM (no mesh surgery) were used as controls. Scale bars represent 200 µm

Immunolabeling of F4/80 (pan macrophage marker), arginase-1 (an M2 marker) and inducible nitric oxide synthase (iNOS, an M1 marker) was performed to assess the number, location, and phenotypic profiles of the macrophages within the site of implantation at 7 and 14 days (Figure 11 a, c). In all mesh groups, the number of both arginase-1 and iNOS positive cells was observed to peak within the first 50 µm from the mesh surface (Figure 11 b, d). Therefore, this distance was considered as the tissue-biomaterial interface, where the most important interactions of the biomaterial with the surrounding tissue occur and determine the implant success in the long term.

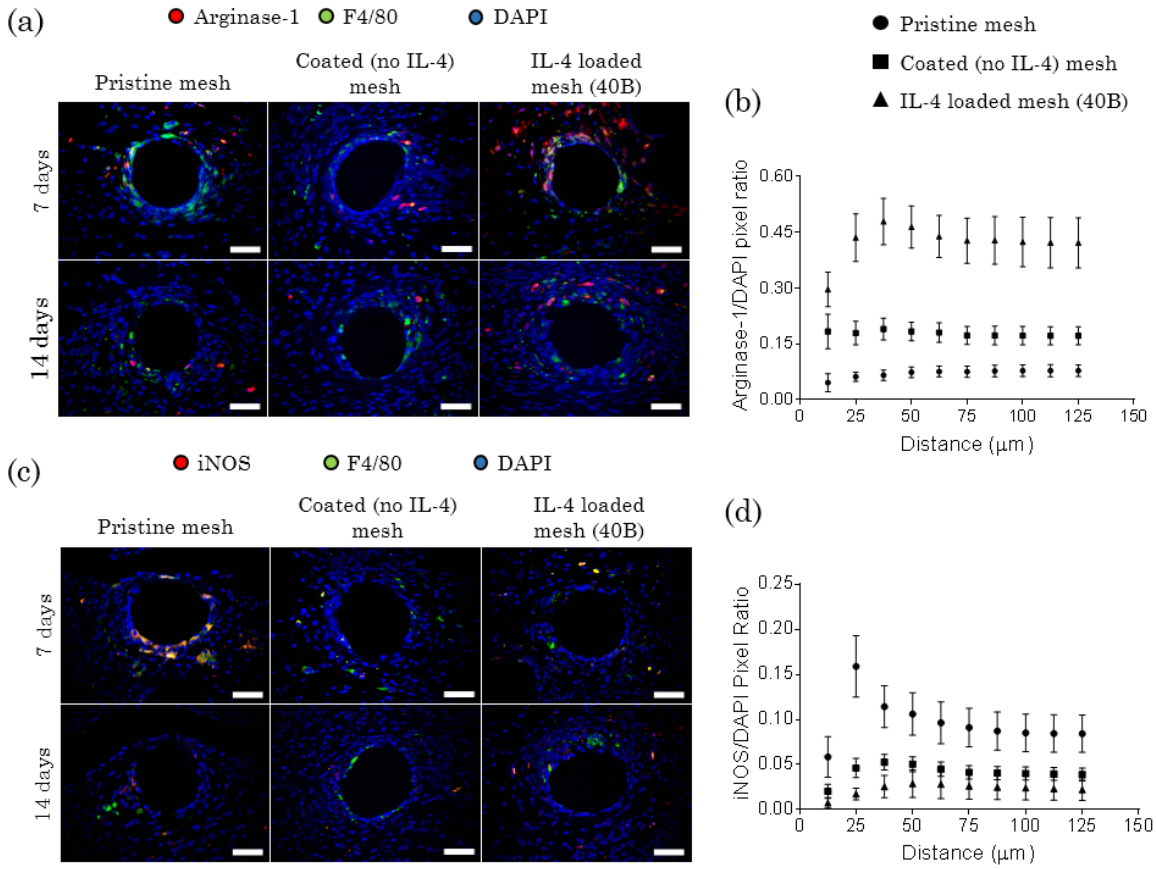

Figure 11. Fluorescence microscopy images of (a) Arginase-1 (red) and F4/80 (green) co-immunolabeling, and (c) iNOS (red) and F4/80 (green) co-immunolabeling at a single mesh fiber of tissue cross sections of mice implanted with a 1 cm^2 piece of pristine, coated (no IL-4) and IL-4 loaded (40B) mesh for 7 days (top panel) and 14 days (bottom panel). DAPI was used to stain cell nuclei. Scale bars represent 50 μm. (b) Arginase-1/DAPI pixel ratio and (d) iNOS/DAPI pixel ratio versus distance of arginase-1 and iNOS immunolabeled tissue sections at 7 days, respectively. Points represent the mean ± SEM (N = 8)

Total cell infiltration around single mesh fibers was assessed by DAPI staining, revealing no differences between groups at 7 or 14 days (Figure 12a). However, the small increases in the number of cells within the remodeling site were observed from 7 to 14 days in the pristine and IL-4 loaded mesh implantation groups. Analysis of $F4/80^+$ macrophage populations revealed a

significantly higher presence of $F4/80^+$ cells as a percentage of the total cell population in mice implanted with pristine mesh, compared to both coated (no IL-4) and IL-4 loaded mesh groups at 7 days (Figure 12b). At 14 days, the percentage of $F4/80^+$ cells in the pristine mesh group was significantly reduced and was similar to levels similar to those found in both coated (no IL-4) and IL-4 loaded meshes. The percentage of $F4/80^+$ cells in the implantation site of IL-4 loaded meshes were also significantly decreased compared to 7 days, but these decreases were smaller than those observed for the pristine mesh group. There were no differences in the percentage of $F4/80^+$ cells between coated (no IL-4) and IL-4 loaded mesh groups at 7 or 14 days. These results suggest that the coating may have had an inhibitory effect upon the recruitment of macrophages into the implantation site at early time points.

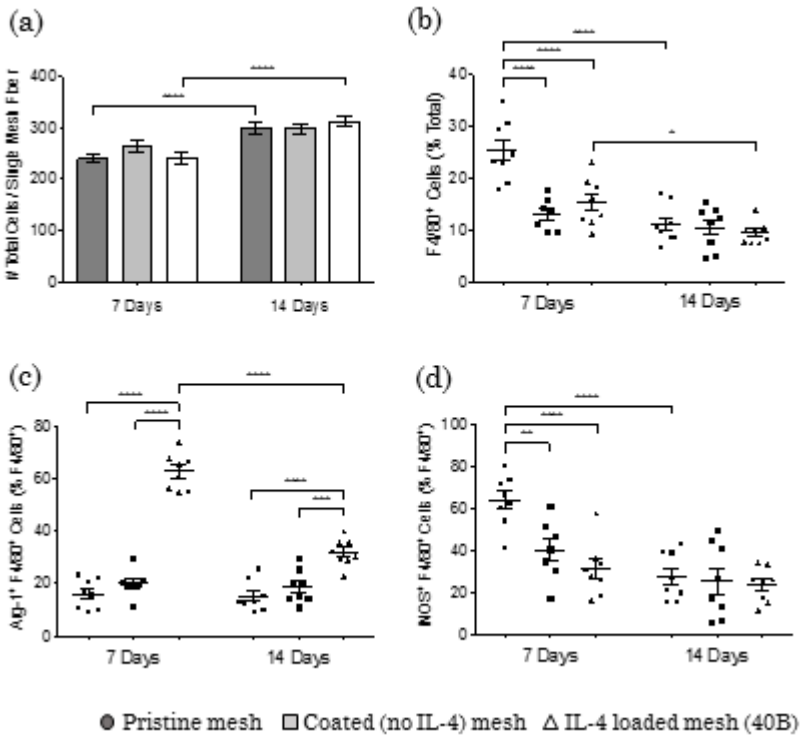

Figure 12. Image analysis of (a) total cells (DAPI) and (b) F4/80$^+$ cells as percentages of total cells (DAPI) surrounding single mesh fibers of tissue cross sections of mice implanted with a 1 cm^2 piece of pristine, coated (no IL-4) and IL-4 loaded (40B) mesh for 7 days and 14 days. Image analysis of (c) Arg-1$^+$ F4/80$^+$ cells and (d) iNOS$^+$ F4/80$^+$ cells as percentages of total F4/80$^+$ cells surrounding single mesh fibers of tissue cross sections of mice implanted with a 1 cm^2 piece of pristine, coated (no IL-4) and IL-4 loaded (40B) mesh for 7 days and 14 days. Bars and points represent the mean ± SEM (N = 8). Statistical significance as (*) $p < 0.05$, (**) $p < 0.01$, (***) $p < 0.001$ and (****) $p < 0.0001$, using two-way ANOVA with Tukey's (groups) and Sidak's (days) tests. All other differences are non-significant

Additional co-labeling was performed for arginase-1 and iNOS to assess the M1/M2 polarization profile of the cells within the implantation site. Results at 7 days post-implantation revealed that mice implanted with IL-4 loaded mesh were associated with an increased percentage of Arg-1$^+$ macrophages (F4/80$^+$) as compared to both coated mesh and pristine mesh

groups (Figure 12c). The difference in arginase-1 labeling in the IL-4 loaded mesh group was greatest in the first 40 to 50 μm from the mesh surface (Figure 11b) as compared to both coated and pristine mesh, suggesting that the effects of IL-4 released from the LbL coating are limited to distances up to 50 μm from the surface of the implanted mesh. Coated mesh did not elicit an increase in Arg-1^+ macrophages as compared to pristine mesh (Figure 12c). These results are consistent with the *in-vitro* findings showing significant increases in M2 macrophage polarization only in the IL-4 loaded mesh group (Figure 6). Results at 7 days post-implantation also showed a reduction of $iNOS^+$ macrophages in mice implanted with IL-4 loaded meshes compared to mice implanted with pristine meshes (Figure 12d). Mice implanted with coated mesh also showed a reduction in $iNOS^+$ macrophages compared to the pristine mesh implanted group; however, no significant differences were observed between the coated mesh and IL-4 loaded groups (Figure 12d). These results suggest that the coating material may have impacted the polarization of macrophages towards an M1 profile. Differences in iNOS labeling were observed to peak at 25 μm from the mesh surface of the pristine mesh implanted group at 7 days (Figure 11d), again suggesting that the effects of the coating were limited to the first 50 μm from the mesh surface.

Results at 14 days post-implantation revealed a decrease in Arg-1^+ macrophages in mice implanted with IL-4 mesh as compared to the 7 day time point; however, the percentage of Arg-1^+ macrophages was still higher than both coated (no IL-4) and pristine mesh groups (Figure 12c). The percentage of $iNOS^+$ macrophages at 14 days was found to decline in mice implanted with pristine mesh as compared to 7 days; however, there were no significant differences observed between any groups at the 14 day time point (Figure 12d). When the effects of IL-4 coating upon the percentage of Arg-1^+ macrophages at 7 and 14 days were compared (Figure

12c) it can be appreciated that arginase-1 expression in the IL-4 coated group at 14 days returned to levels similar to those observed for pristine mesh at both 7 and 14 days. This suggests that the length of IL-4 release from the LbL coated meshes occurs mostly at early stages of the host response (< 14 days) and that its effects on macrophage polarization *in-vivo* are declining by 14 days. Figure 13 shows the percentage of total cells expressing Arg-1 and iNOS co-labeled with F4/80.

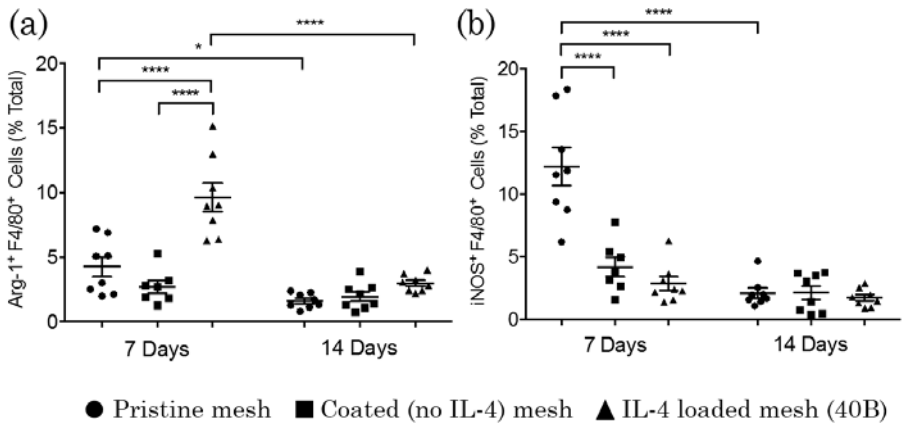

Figure 13. Image analysis of (a) Arg-1$^+$ F4/80$^+$ cells and (b) iNOS$^+$ F4/80$^+$ cells as percentages of total cells (DAPI) surrounding single mesh fibers of tissue cross sections of mice implanted with a 1 cm^2 piece of pristine, coated (no IL-4) and IL-4 loaded (40B) mesh for 7 days and 14 days. Bars represent the mean ± SEM (N = 8). Statistical significance as (*) $p < 0.05$ and (****) $p < 0.0001$, using two-way ANOVA with Tukey's (groups) and Sidak's (days) tests. All other differences are non-significant

While increases in the M2 macrophage population can likely be attributed to the release of IL-4 from loaded mesh as demonstrated *in vitro*, there are two potential rationales for the observed reduction in the number of iNOS$^+$ macrophages in the IL-4 loaded mesh group. First,

iNOS expression may be reduced as a consequence of the polarization of the macrophages at the tissue implant interface towards an M2 phenotype, given the known competitive nature of pathways leading to iNOS and arginase-1 expression in mice [114-116]. Second, decreased percentage of $iNOS^+$ macrophages may be due to the effects of the coating components and/or surface plasma treatment upon macrophage polarization. This second mechanism is supported by the significant reduction in the percentage of $iNOS^+$ macrophages (Figure 12d) but also a reduction in $F4/80^+$ cells (Figure 12b) observed in the coated mesh group at 7 days. Therefore, the coating components and/or modified mesh surface themselves appear to have effects in the reduction of M1 macrophages but not in promoting M2 macrophage polarization. Thus, the observed results are likely a combination of mechanisms driving the reduction of M1 macrophages with IL-4 mediated increases in the M2 population.

3.3.2 Effects of IL-4 and components of the coating in multiple macrophage populations

We noted that some $Arg\text{-}1^+$ and $iNOS^+$ cells did not express F4/80 (Figure 14). This suggests that cells other than macrophages may produce Arg-1 and iNOS in the area of implantation, or that one or more populations of macrophages which express other markers such as CD11b or CD68 but not F4/80 are present within the remodeling site. It is also unknown what other effects both IL-4 and coating components drive in other macrophage populations. To answer these questions, Arg-1 and iNOS were used in co-labeling with CD68 and CD11b. CD68 (Cluster of Differentiation 68) is a protein highly expressed by cells in the monocyte lineage (e.g., monocytic phagocytes, osteoclasts), circulating macrophages and tissue resident macrophages (e.g., Kupffer cells, microglia) [117-119]. CD68 is also known as ED1 in rats, the most commonly used “pan-macrophage” marker. CD11b is expressed on the surface of many

leukocytes including monocytes, neutrophils, natural killer cells, granulocytes and macrophages, as well as on 8% of spleen cells and 44% of bone marrow cells [120]. Functionally, CD11b regulates leukocyte adhesion and migration to mediate the inflammatory response.

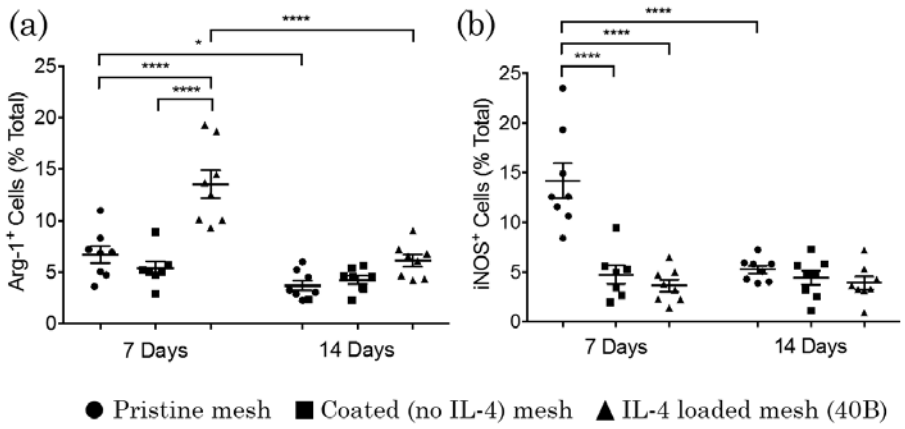

Figure 14. Image analysis of (a) Arg-1$^+$ cells and (b) iNOS$^+$ cells as percentages of total cells (DAPI) surrounding single mesh fibers of tissue cross sections of mice implanted with a 1 cm^2 piece of pristine, coated (no IL-4) and IL-4 loaded (40B) mesh for 7 days and 14 days. Bars represent the mean ± SEM (N = 8). Statistical significance as (*) $p < 0.05$ and (****) $p < 0.0001$, using two-way ANOVA with Tukey's (groups) and Sidak's (days) tests. All other differences are non-significant

Co-labeling of Arg-1 with these three macrophage populations (F4/80, CD68 and CD11b) was done at 7 days post-implantation to identify and quantify M2 macrophages is shown in Figure 15. Of note, 7 days was chosen due to the higher expression of macrophage markers compared to all other time-points. Results revealed that mice implanted with coated (no IL-4) and IL-4 eluting mesh were associated to a reduction in F4/80$^+$ macrophages, compared to the pristine mesh group. On the other hand, there were no differences in the percentage of cells for

both CD68 and CD11b in any of the implanted groups. Therefore, these results suggest that the coating may prevent any recruitment effects on F4/80$^+$ macrophages mediated by interactions of the microenvironment with the polypropylene surface, or that one or more components of the coating may exert distinct effects in the F4/80$^+$ macrophage population but not in the CD68 and CD11b populations, in particular to recruitment activity.

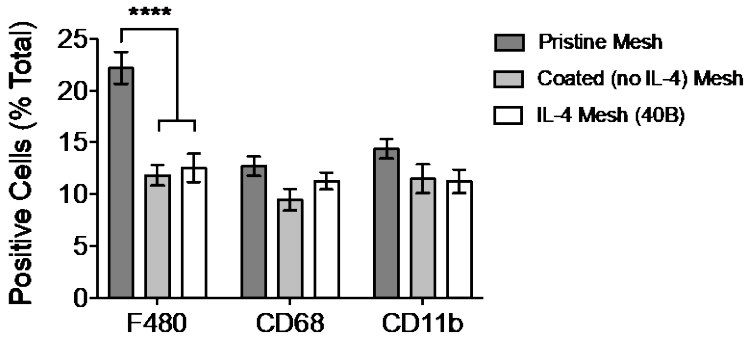

Figure 15. Image analysis of F4/80$^+$, CD68$^+$ and CD11b$^+$ macrophages as percentages of total cells (DAPI) surrounding single mesh fibers of tissue cross sections of mice implanted with a 1 cm^2 piece of pristine, coated (no IL-4) and IL-4 loaded (40B) mesh for 7 days. Bars represent the mean ± SEM (N = 6). Statistical significance as (*) $p < 0.05$ and (****) $p < 0.0001$, using two-way ANOVA with Tukey's test. All other differences are non-significant

The percentage of M2 macrophages on each of these populations has also been quantified, revealing that mice implanted with IL-4 eluting mesh presented a consistent higher percentage of M2 macrophages in all macrophage populations, compared to all other groups (Figure 16). The percentage of M2 macrophages in both coated (no-IL4) mesh and pristine groups was similar in all groups, which is consistent to previous results demonstrating that the observed shift towards an M2 phenotype is due to local delivery of IL-4.

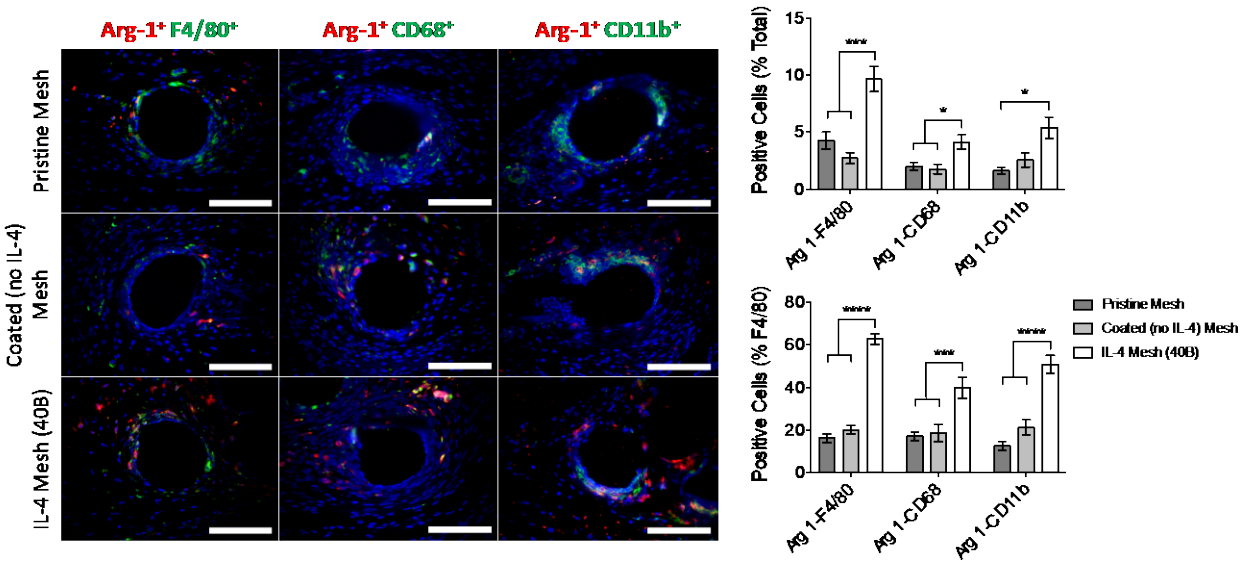

Figure 16. Image analysis of F4/80$^+$, CD68$^+$ and CD11b$^+$ macrophages co-labeled with Arg-1 (M2 macrophages), as percentages of total cells (DAPI) surrounding single mesh fibers of tissue cross sections of mice implanted with a 1 cm^2 piece of pristine, coated (no IL-4) and IL-4 loaded (40B) mesh for 7 days. Bars represent the mean ± SEM (N = 6). Statistical significance as (*) $p < 0.05$ and (****) $p < 0.0001$, using two-way ANOVA with Tukey's test. All other differences are non-significant

Similarly, the percentage of M1 macrophages has been quantified by iNOS co-labeling in all F4/80, CD68 and CD11b macrophage populations. Results show that both coated (no IL-4) and IL-4 mesh groups presented diminished percentages of M1 macrophages in the F4/80$^+$ and CD68$^+$ populations, compared to the pristine mesh group (Figure 17). There were no differences among groups in the CD11b population, that could be also consequence of the low co-localization degree between iNOS and CD11b. These results suggest that the components of the coating reduce the polarization of M1 macrophages or that the coating hides the surface of polypropylene, interrupting the interactions with F4/80$^+$, CD68$^+$ macrophages and subsequent M1 polarization.

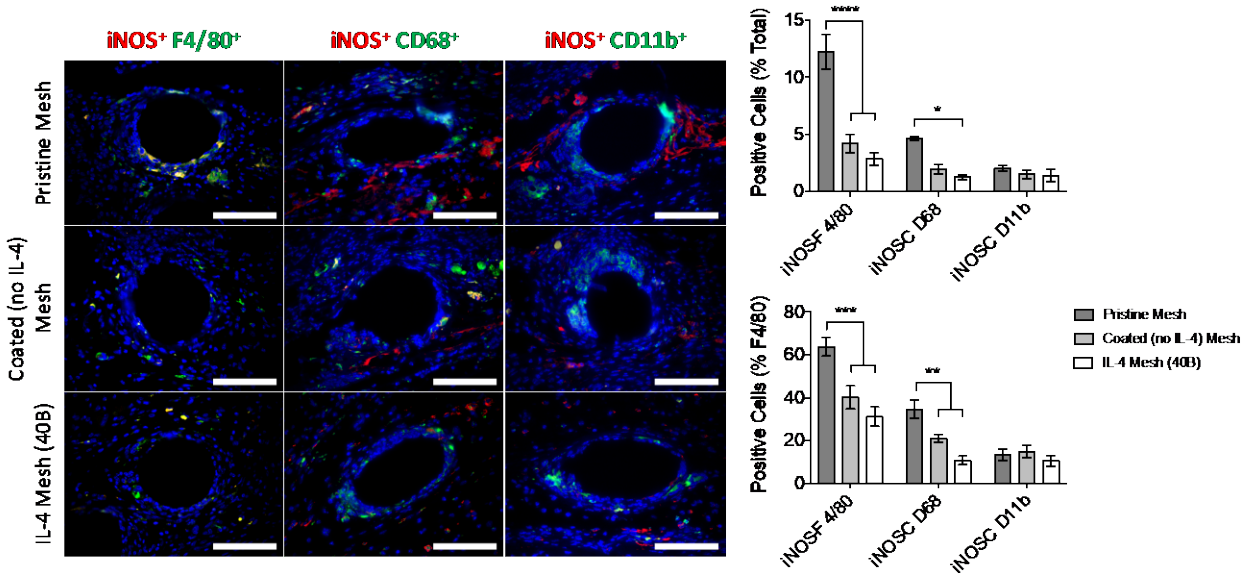

Figure 17. Image analysis of F4/80$^+$, CD68$^+$ and CD11b$^+$ macrophages co-labeled with iNOS (M1 macrophages), as percentages of total cells (DAPI) surrounding single mesh fibers of tissue cross sections of mice implanted with a 1 cm^2 piece of pristine, coated (no IL-4) and IL-4 loaded (40B) mesh for 7 days. Bars represent the mean ± SEM (N = 6). Statistical significance as (*) $p < 0.05$ and (****) $p < 0.0001$, using two-way ANOVA with Tukey's test. All other differences are non-significant

3.3.3 Gene expression analysis of the host response to IL-4 eluting meshes

Results revealed that mice implanted with IL-4 eluting mesh were associated to upregulation of M2-like macrophage genes such as Arg-1 (7 days), IL-10 (14 days) and YM-1 (7 and 14 days), compared to both coated (no IL-4) and pristine meshes (Figure 18). However, a downregulation in Fizz-1 (7 days) was observed in both IL-4 and coated (no IL-4) groups. IL-4 eluting mesh group was also associated to downregulation of M1-like macrophage genes such as IL-6 (7 days) and IL-12β (7 and 14 days), compared to both coated (no IL-4) and pristine mesh groups. In addition, upregulation of MMP-9, MMP-10 and MMP-13 was found in the IL-4 mesh group

compared to all other groups. Downregulation in CTGF was observed for both IL-4 and coated (no IL-4) mesh groups. These results are consistent with surface marker expression and demonstrate that the presence of IL-4 promotes an M2-like macrophage response, upregulating M2-macrophage genes such as Arg-1, IL-10, and YM-1; increasing MMP activity, but downregulating M1-macrophage genes IL-6 and IL-12β. Downregulation in Fizz-1 and CTGF in both IL-4 and coated (no-IL4) mesh groups suggests that downregulation in these genes are mediated by the effects of the components of the coating. Of note, it can be observed some differences in the level of gene expression between 7 and 14 days for each of the genes evaluated, which is related to the sequence and mechanisms in which these genes are activated to perform multiple biological processes involved in the host response against biomaterials. Additional time points will be studied at both early stages and in the long-term to reveal this information.

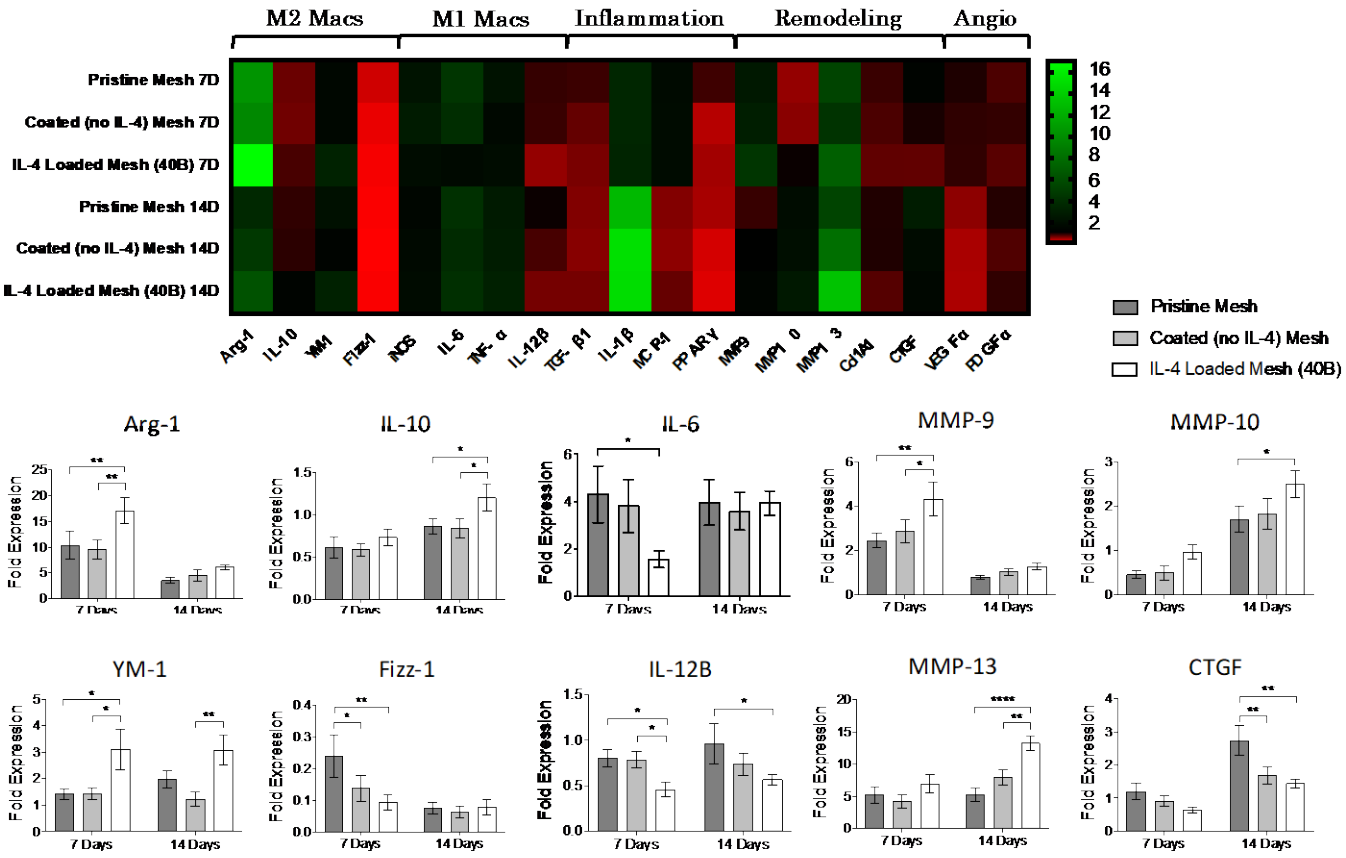

Figure 18. Taqman gene expression heat map assessing the expression of gene targets relevant to early stages of the host response against biomaterials (7 and 14 days), using tissue extracted from explanted meshes. SHAM group was used to normalize gene expression levels. Significant differences in upregulated or downregulated genes are shown separate graphs below. Bars represent the mean ± SEM (N = 6). Statistical significance as (*) $p < 0.05$, (**) $p < 0.01$ and (****) $p < 0.0001$, using two-way ANOVA with Tukey's test. All other differences are non-significant

3.3.4 Downstream effects in the host response upon macrophage polarization promoted by implanted meshes

Mesh and the surrounding tissue complex were harvested at 90 days post-implantation to evaluate the effects of mesh coating and IL-4 loading upon long-term tissue remodeling outcomes. Image analysis of Masson's trichrome stained histological sections was performed to identify and quantify capsule formation. Results revealed capsule formation around mesh fibers for all groups (Figure 19a); however, IL-4 loaded mesh elicited reduced capsule area and thickness compared to the prominent and dense capsules surrounding fibers of both coated and pristine meshes (Figure 19 b, c). Subsequent analysis of collagen fiber distribution in picrosirius red stained sections was performed using a custom-designed algorithm (Mathworks MatLab R2015a). Circularly polarized light microscopy was able to reveal the relative thickness of the collagen fibers as a function of the color hue from thin green fibers to increasingly thick yellow, orange and red fibers [121]. Results revealed that mice implanted with IL-4 loaded meshes had reduced content of both thick orange and thicker red collagen fibers, compared to both pristine and coated meshes (Figure 20). A concurrent increase in thin yellow and thinner green collagen fibers was found for IL-4 loaded mesh compared to both pristine and coated mesh. While we note that the tissue remodeling process is incomplete at the 90 day time point, these outcomes indicate a change in the quantity and type of the collagen fibers composing the fibrotic capsule. These findings may be relevant to potential improvements in mechanical performance of the implanted mesh *in-vivo*, and are the subject of future studies.

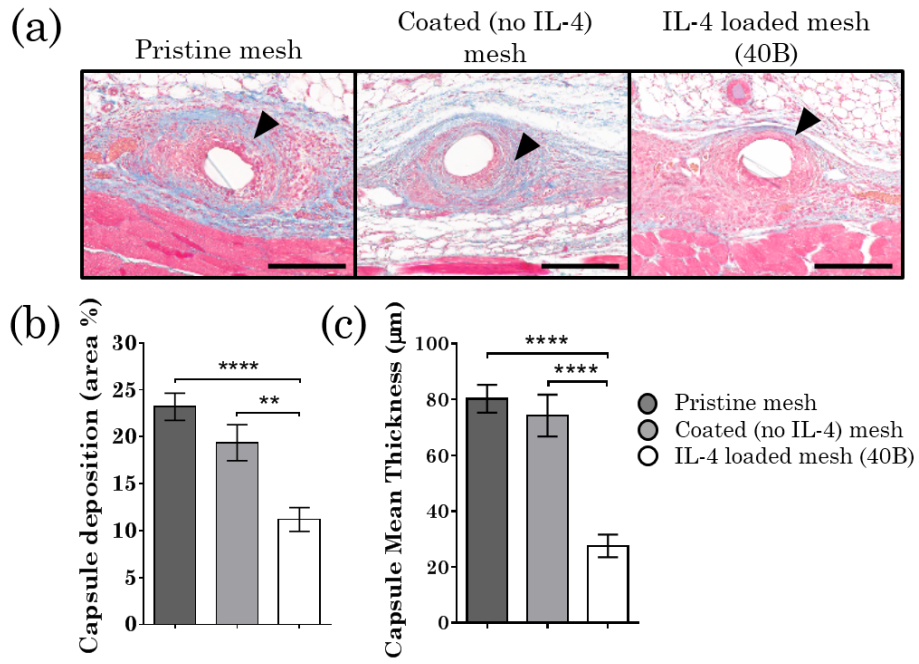

Figure 19. (a) Masson's Trichrome stained tissue sections of mice implanted with a 1 cm^2 piece of pristine, coated (no IL-4) and IL-4 loaded (40B) mesh at 90 days. Arrowheads indicate the capsule surrounding single mesh fibers. Scale bars represent 200 µm. (b) Image analysis of capsule deposition (area %) and (c) Mean thickness surrounding mesh fibers (3 images of a single fiber at 20X per sample, N = 8 samples). Bars represent the mean ± SEM. Statistical significance as (**) $p < 0.01$ and (****) $p < 0.0001$, using two-way ANOVA with Tukey's test. All other differences are non-significant

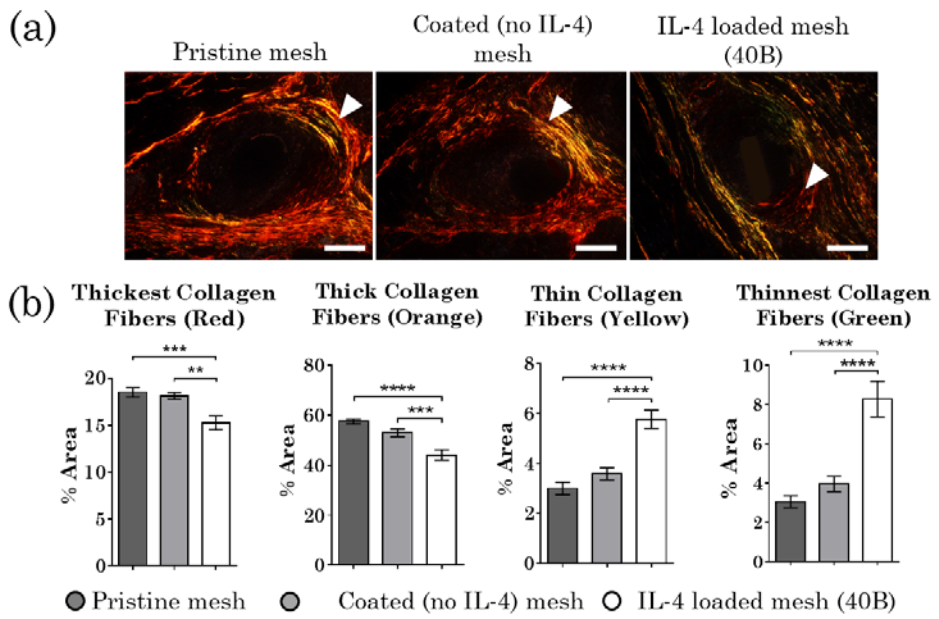

Figure 20. (a) Picro Sirius Red stained tissue sections (20X) of mice implanted with a 1 cm^2 piece of pristine, coated (no IL-4) and IL-4 loaded (40B) mesh at 90 days. Arrowheads indicate the capsule surrounding single mesh fibers. Scale bars represent 100 µm. (b) Image analysis of collagen capsule quality, surrounding mesh fibers (3 images of a single fiber at 20X per sample, N = 8). Bars represent the mean ± SEM. Statistical significance as (**) $p < 0.01$, (***) $p < 0.001$ and (****) $p < 0.0001$, using two-way ANOVA with Tukey's test. All other differences are non-significant

The results of the present study demonstrate that the release of IL-4 from LbL coated mesh promotes shifts in early-stage macrophage polarization that are associated with positive long-term effects such as minimized capsule formation and improved tissue quality and composition compared to coated and pristine meshes. These results also suggest that long-term positive outcomes are due to an early-stage increase in the proportion of M2 macrophages, rather than a decrease in the presence of M1 macrophages or total $F4/80^+$ macrophages, given that coated meshes were also capable of significantly decreasing the proportion of M1 macrophages and $F4/80^+$ macrophages (Figure 12[b, d], 13b, 14b, 15, 17) as compared with pristine mesh, but

were not associated with improved tissue remodeling outcomes (Figure 19, 20). The present study also clearly demonstrates that it is possible to transiently shift the early phases of the host response to implants which otherwise elicit a chronic pro-inflammatory response with significant impact upon the tissue remodeling outcome downstream while leaving key implant characteristics such as material properties and porosity intact.

It has been previously suggested that excessive long-term polarization towards either an M1 or an M2 phenotypes may have negative effects on remodeling outcomes [32, 33, 122]. Additionally, an increasing number studies have described pathologies associated with an imbalance and long-term presence of M1 or M2 macrophages, including but not limited to cancer, diabetes and atherosclerosis [99, 123, 124]. Therefore, localized and temporal delivery of bioactive agents represents an advantage over strategies promoting systemic and or permanent shifts in the host response as it limits the potential for adverse long-term interactions and exacerbation of conditions which may exist at distant sites. Similarly, promoting transient shifts in macrophage polarization in the early host response represents an improved approach as compared to strategies which seek to evade the host immune response. Previous studies using surface modification of biomaterials and coatings to escape the innate immune system have shown only modest improvements at early stages of the host response against biomaterials and few improvements in long-term performance [51, 73, 125-127]. Finally, the present delivery system represents an advantage over previous delivery approaches, given that significant effects on macrophage polarization are observed at lower, controllable and safer doses (picograms to nanograms), compared to the high doses (nanograms to micrograms) of IL-4 used in previous studies [65, 67, 106]. The systemic release of larger amounts IL-4 may lead to effects upon distal

tissues and/or exacerbated and contradictory outcomes associated with a fibrotic process or potential enhancement of the foreign body reaction [43, 128].

At present, the stability of the coating and release profile of IL-4 *in vivo* is unknown. Alcian blue labeling, which as used to identify the coating *in vitro*, was used to attempt to identify the coating in histologic sections. The presence of the coating was indistinguishable at any time point which we evaluated in the present study. The lack of Alcian Blue staining around the fibers, however, does not necessarily indicate that the coating is degraded. As the coating is on the nanometer scale, it may not be possible to distinguish the staining using routine histologic methods. *In-vivo*, both the chitosan and dermatan sulfate components of the coating are mostly degraded by macrophages and other cells participating in the host response. Layer by layer films have shown multiple release mechanism, depending the nature of the polyelectrolytes composing the films, being surface degradation the most predominant mechanism that gradually releases the entrapped bioactive agents by degradation of the most external layer films, followed by more internal layers [129, 130]. Therefore, IL-4 is most likely released by gradual surface degradation of the coating multilayers, mainly triggered by macrophages and other cells of the immune system with enzymatic capacity. However, release by diffusion of IL-4 may also occur to a lesser extent. Additional follow up studies should be performed to specifically address *in-vivo* release profiles.

There were several limitations to the present study. First, while the present study demonstrated positive results from the use of IL-4 as a macrophage polarizing molecule, it should be noted that multiple IL-4 isoforms do exist with potentially different functional effects [131, 132]. The IL-4δ2 isoform of IL-4, for example, has been shown to promote the expression of multiple pro-inflammatory cytokines and the chemotaxis of T and B cells [132]. Thus, careful

consideration of the exact formulation and potential adverse effects of the IL-4 containing coating is necessary. Further, it is well known that these pathways and others, including IL-4, are regulated differently in humans and mice [131, 133, 134]. Thus, additional testing must be performed to demonstrate potential relevance to human conditions. The LbL method described in the present manuscript is amenable to the use of other macrophage polarization inducing molecules and alternative molecules can likely be substituted for IL-4 if needed for further development.

Second, further investigation is needed to clearly define the resultant phenotype and the potential paracrine mechanisms by which the observed shifts in macrophage phenotype affect the remodeling process. Increases in total cellularity were observed between the 7 and 14 day time points. While these increases were moderate, they were often also accompanied by a decrease in the F4/80^{+} cell population, suggesting a replacement of the macrophages by other cells. These changes could be associated with recruitment of fibroblasts and other cells involved in late phases of the host response.

Studies in both the biomaterials and wound healing literature have shown complex and reciprocal cell-cell crosstalk between macrophages and fibroblasts during the processes of healing and fibrosis [135-138]. In the context of the foreign body reaction, these interactions have been shown to result in increased expression of MCP-1 (a potent recruiter of macrophages and a mitogen for fibroblasts), the inhibition of macrophage secretion of cytokines, and the promotion of fibroblast production of cytokines, among others [137]. Thus, the potential effects of IL-4 upon fibroblasts and subsequent effects upon macrophages and other immune cells are important and should also be considered. Further, it has been shown that macrophages can also drive fibroblasts to form multinucleated cells *in-vitro*, resembling some characteristics of the

foreign body giant cells [138]. The exact implications of such findings and their role in the present study are unknown, but warrant further examination to determine the specific effects of IL-4 coatings upon both macrophages and other cells participating in the remodeling process.

Third, in the present study, the evaluation of macrophage phenotype was performed in the area of single fibers in order to simplify quantification of macrophage numbers as well as downstream histologic outcomes around a complex shape. However, we note that recent published studies have demonstrated that density of the mesh is a local driver of the host macrophage response, where increased local mesh density is associated with an increased local pro-inflammatory response [21, 22]. While investigation of the differences in the host response between fibers and knots was beyond the scope of the present study, it will be important to evaluate the effects of IL-4 coated mesh knots in order to illustrate the effects in the host response of the released IL-4 and the coating in the presence of high density and complex geometry of the implant.

Fourth, the host inflammatory response is also known to be variable by tissue location and context. Of particular relevance to the present study, the host response to polypropylene mesh in the vagina has been reported to be significantly different than that in the abdominal wall musculature [21, 139]. Thus, testing of the present strategy in more relevant model systems must be performed to demonstrate utility in these applications. Additionally, the present study used only one concentration of IL-4 and only investigated 40 bilayers of IL-4 loaded coating. Further studies will be necessary to determine the ideal number of coating layers and optimal time of release in vivo. Ideally, the smallest dose of IL-4 and shortest time of release should be identified to reduce the potential for systemic effects of IL-4 release.

Finally, the mechanism by which shifts in macrophage phenotype drives improved implant integration have yet to be identified. While it is logical that the presence of a chronically activated M1 macrophage population at the tissue-implant interface would lead to tissue degradation or encapsulation in the long term, it is unclear how M2 macrophages affect the tissue remodeling process and whether M1 macrophages play any essential role in the early remodeling phase (i.e. phagocytosis, activation of local cell populations, production of chemotactic signals). It is likely that both M1 and M2 macrophages play important roles in tissue remodeling, and that the timing of the phenotypic switch will prove an essential factor in determining the degree of success.

3.4 CONCLUSIONS

The released IL-4 from LbL coated meshes can promote macrophage polarization towards an M2 phenotype *in-vivo*. In addition, the effects of the local released IL-4 from LbL coated meshes on macrophage polarization extend up to 50 µm of distance from the mesh surface. Interestingly, the assessment of different macrophage subpopulations showed distinct susceptibility to IL-4 and components of the coating. Gene expression analyses using tissues from explanted meshes showed that the IL-4 eluting mesh group was associated with higher expression of M2 macrophage-related genes and MMPs, but lower expression in M1 macrophage-related genes and CTGF, compared to other groups. Shifting the macrophage response towards an M2-like phenotype led to decreased fibrotic capsule deposition surrounding mesh fibers but also changes in collagen composition, suggesting improved mesh integration into the host tissue and the potential for reduction in downstream complications. Finally, these results are strong evidence to

support our hypothesis that early-stage macrophage polarization at the tissue-implant interface towards an M2 phenotype would mitigate the foreign body reaction and hence promote better integration of non-degradable biomaterials into the host tissue in the long term. While the present study focused only upon polypropylene mesh commonly used for soft tissue reconstruction, the methods and findings presented can likely be extended to include other material types and applications.

4.0 AIM III: ELUCIDATE THE EFFECTS OF AGING IN THE HOST RESPONSE AGAINST BIOMATERIALS TO DESIGN A CONTEXTUAL DELIVERY REGIMEN

4.1 INTRODUCTION

While temporal and spatial control of macrophage polarization towards an M1 or M2 phenotype can now be achieved in multiple ways [140-142], the ability to effectively promote the desired phenotypic profile is likely predicated upon an in-depth, context- and tissue-dependent understanding of how host factors affect the response to biomaterials. A number of recent studies have highlighted the importance of the implantation site and/or the pathologic state of the tissue into which a biomaterial is implanted. For example, polyether–polyurethane sponge implants evoked distinct responses when placed in intraperitoneal versus subcutaneous locations [143] and polypropylene mesh implanted abdominally was shown to evoke a reduced inflammatory response compared to those implanted vaginally [139], demonstrating differences in immune cell activity based upon implant location. Intraperitoneal implants in diabetic rats were associated with increases in inflammatory factors as compared to non-diabetic animals [144] and increased fibrosis was observed in lupus-prone mouse models [145], demonstrating the effects of underlying pathology on the host response. Another recent study showed differences in the host response to adhesive materials in animal models of colitis and colon cancer [146], demonstrating that the observed host response was not only due to implant material composition, but also the

pre-implantation state and cellular composition of the tissue of interest. Of note, the authors were able to use the information gleaned from these studies to create improved context- and disease-dependent materials for these applications. Thus, it has been suggested that the ideas of "biocompatibility," the host macrophage reaction, and ideal material requirements and modification strategies may need to be revisited on a disease, tissue, and even patient-by-patient basis [147].

Aging is an unavoidable process known to affect multiple aspects of the immune system in both humans and animals [148]. While the effects of aging upon the adaptive immune system are increasingly well described, the phenotypic and functional changes within the innate immune system with aging are less clear. However, immunosenescence, dysregulation of macrophage function and polarization, and delayed resolution of acute immune responses in aged individuals have all been reported [68-70]. Therefore, it is logical that aging would also have effects upon the host response to implantable materials. However, studies examining the effects of aging upon the host response to implants and the implications of this response for long-term integration and function have not been performed. Thus, there is a clear need to elucidate the impacts of aging upon the host response in order to develop implantable materials which more effectively address the needs of an increasingly aged population.

By 2050, the number of individuals over the age of 65 is expected to increase by 71% to nearly 2 billion worldwide, with the number of US citizens over the age of 65 surpassing 20% by 2030 [149]. As a result, there is an increasing demand for implantable medical devices intended to treat age-related disorders. Despite the increasing usage of implantable medical devices in aged patient populations, the impacts of aging upon the host response have never been investigated in-depth. The literature which does exist on the topic largely hypothesizes the

potential impacts of aging upon the host response [150] based upon the known effects of aging on the immune system and upon wound healing, though a small number of relevant studies have recently been performed [151-154]. In one study, Sicari et al. demonstrated that increased source animal age of tissue derived biomaterials, such as decellularized ECM constructs, reduced the number of M2 polarized macrophages and lead to a poor outcome of tissue remodeling compared to young host-derived biomaterials [151]. Olivares-Navarrette et al. showed that titanium implants with varying roughness and surface energy yielded lower bone-to-implant contact, neovascularization, and bone formation in aged rats [152]. Finally, in vitro analyses of senescent macrophages induced by extended culture demonstrated deficits in phagocytosis and cytokine release in response to titanium dioxide particles and polystyrene materials, suggesting macrophage function may be compromised in the aged host response [153, 154].

The purpose of the present study is two-fold. We first aimed to evaluate the early host macrophage response and downstream integration following placement of polypropylene mesh in young (8-week-old) versus aged (18-month-old) mice. The host response against polypropylene mesh in aged mice resulted in delayed cell recruitment, significant differences in macrophage surface marker expression and a highly shifted pro-inflammatory (M1) response at early stages, associated with an unresolved host response in the long-term, compared to young adult mice. Therefore, the second part of the study contemplates the development of a sequential delivery regimen to restore the delayed recruitment and shift the highly inflammatory response of macrophages in old mice towards an M2-like phenotype, using MCP-1 and IL-4, respectively.

4.2 METHODS

4.2.1 Materials

C57BL/6 female mice, 8 – 10 weeks old and 18 months old were obtained from the National Institute on Aging Mouse Colony. A polypropylene mesh, Gynemesh® PS (Ethicon, Somerville, NJ) was used. Bovine serum albumin (BSA) and histologic staining materials were purchased from Sigma Aldrich (St. Louis, MO). Rabbit anti-mouse arginase (Arg-1), inducible nitric oxide synthase (iNOS), CD68 and anti-rabbit, anti-rat, anti-goat Alexa-fluor (donkey) secondary antibodies were purchased from Abcam (Cambridge, MA). Rabbit anti-mouse iNOS, CD68, CD11b and goat anti-mouse CD68 were purchased from Santa Cruz (Dallas, TX). Rabbit anti-mouse iNOS (ab3523) and Rabbit anti-mouse Arginase (ab91279) were purchased from Abcam (Cambridge, MA). Rat anti-mouse F4/80 was purchased from ABD Serotec (Raleigh, NC). Anti-rat Alexa-fluor 488 (donkey) and anti-rabbit Alexa-fluor 488 (donkey) were purchased from Thermo Fisher, Invitrogen (Pittsburgh, PA). DAPI was purchased from Thermo Fisher Scientific (Pittsburgh, PA). Qiagen RNEasy Mini Prep Kits were purchased from Fisher Scientific (Pittsburgh, PA). High Capacity RNA-to-cDNA kits, Taqman gene expression assays, and Taqman Gene Expression Master Mix was purchased from Thermo Fisher, Invitrogen (Pittsburgh, PA). Vybrant Phagocytosis Kit was purchased from Thermo Fisher, Invitrogen (Pittsburgh, PA). Sulfanilamide, phosphoric acid and N-1-napthylethylenediamine were purchased from Sigma-Aldrich (St. Louis, MO).

4.2.2 Mouse implantation model

An implantation model using C57BL/6 female mice, 8 – 10 weeks old and 18 months were used following proper housing and treatment procedures approved by the Institutional Animal Care and Use Committee (IACUC) of the University of Pittsburgh. NIH guidelines for the care and use of laboratory animals (NIH Publication #85-23 Rev. 1985) were observed. A power analysis was performed to determine that 5 animals per group was required to maintain a statistical power of at least 80%, based on previous studies using the same model [155].

A midline incision was made and a subcutaneous pocket was created in the abdomen of each mouse in order to implant a 1 cm^2 piece of polypropylene mesh. 3-0 polycaprolactone sutures were used to close the incision, then 0.5 mg/kg of Baytril and 0.2 mg/kg of Buprenex were administered for 3 days as antibiotic and analgesic, respectively. Buprenorphine (Buprenex), an opioid analgesic, has been studied and shown not to exert any effects nor alterations in the immunological response, both acutely and chronically administered [112, 113]. After 3, 7, 14 or 90 days, mice were euthanized and skin/mesh/muscle complex tissues were harvested and fixed for 72 hours in neutral buffered formalin. Finally, fixed tissues were paraffin embedded and cross-sections of 7 μm were used for histological studies.

4.2.3 Histologic staining and evaluation

Paraffin embedded tissue cross-sections were used for H&E, Alcian Blue, Masson's Trichrome and Picro Sirius Red staining. H&E, Alcian Blue and Masson's Trichrome stained tissue sections were imaged on a Nikon Eclipse E600 microscope (Tokyo, Japan) at 10X, 20X, and 40X

respectively. Picro Sirius Red stained tissue sections were imaged at 20X on a Nikon Eclipse TE2000-E (Tokyo, Japan), equipped with circularly polarized light.

ImageJ (version 1.48, NIH) equipped with a color deconvolution plug-in (version 1.5) was used to quantify glycosaminoglycans and collagen capsule surrounding mesh fibers at 3, 7, 14 and 90 days (3 different single fibers per sample, N = 7 each group) in images taken from histological tissue sections stained with Alcian Blue and Masson's Trichrome, respectively. In addition, the mean capsule thickness (including both the cellular reaction at the immediate implant surface and the surrounding collagen capsule) was calculated as the mean of apical, basal, and lateral measurements taken perpendicular to the surface of the mesh fiber in Masson's Trichrome stained tissue sections.

A custom-designed algorithm (Mathworks MathLab, version R2015a. Natick, MA) was used to evaluate quantitatively the distribution of collagen fiber sizes surrounding mesh fibers at 90 days (3 different single fibers per sample, N = 7 each group) in images taken from histological tissue sections stained with Picro Sirius Red.

4.2.4 Immunolabeling and evaluation of macrophage populations

Paraffin embedded tissue sections were deparaffinized and hydrated in a series of xylene/alcohol/water. Incubation with proteinase K (1X) for 10 minutes at 37ºC and/or boiling in citric acid buffer (pH=6) for 20 minutes were performed to retrieve antigens. Slides were washed twice in TBST (25 mM Tris buffer + 0.1% tween 20). Then, a 5% donkey serum + 2% BSA + 0.1% tween 20 + 0.1% triton X-100 solution was used as blocking agent (2 hours, RT). Table 4 lists the antibodies and concentrations used in the present study.

Table 4. Primary and secondary antibody combinations and dilutions used to perform fluorescent co-immunolabeling on tissue cross sections of 8-week and 18-month mice implanted with polypropylene mesh for 3, 7 and 14 days.

Labeling	**1ºAb**	**1ºAb**	**2ºAb Alexa 594**	**2ºAb Alexa (488)**
$F4/80^+$ $CD68^+$	1:50 (rat F4/80)	1:150 (rabbit CD68)	1:100 (anti-rat)	1:200 (anti-rabbit)
$F4/80^+$ $CD11b^+$	1:50 (rat F4/80)	1:100 (goat CD11b)	1:200 (anti-goat)	1:100 (anti-rat)
$CD11b^+$ $CD68^+$	1:150 (goat CD11b)	1:150 (rabbit CD68)	1:200 (anti-goat)	1:200 (anti-rabbit)
$iNOS^+$ $CD68^+$	1:100 (rabbit iNOS)	1:150 (goat CD68)	1:200 (anti-rabbit)	1:200 (anti-goat)
Arg-1^+ $CD68^+$	1:150 (rabbit Arg-1)	1:150 (goat CD68)	1:400 (anti-goat)	1:200 (anti-goat)

All primary antibodies were incubated overnight at 4ºC in blocking buffer. Secondary antibodies were incubated for 40 minutes at RT. Vectashield with DAPI mounting media (Vector laboratories, Burlingame, CA) was used to stain nuclei and mount. Images of centered single fibers were taken on a Nikon Eclipse E600 microscope equipped with epi-fluorescence at 40X. Cell counting using ImageJ (version 1.48, NIH) was performed to identify and quantify macrophage populations from cells surrounding single centered mesh fibers (3 different single fibers, N = 7 each group).

4.2.5 Harvest, culture and polarization of bone marrow-derived macrophages

Bone marrow-derived macrophages were harvested from 8-10 week and 18-month-old C57BL/6 mice. Briefly, femur and tibiae were harvested and separated from muscle and connective tissue. Bones were cut at either end to expose bone marrow. Sterile syringe and needles were used to flush out bone marrow using macrophage differentiation media (DMEM, 10% FBS, 10% L-929

Supernatant, 1% PenStrep, 2% NEAA, 1% HEPES, 0.2% β-2 mercaptoethanol). Bone marrow lysate was reconstituted in media and filtered through a sterile cell filter. Cells were cultured for 7 days in media to differentiate them into macrophages. Following 7 days of differentiation culture, macrophages were treated polarizing regimens. Naïve macrophage (M0) controls were treated with basal media for 24 hours. M1 (20 ng/mL IFN-γ and 100 ng/mL LPS) and M2 (20 ng/mL IL-4) polarizing cytokines were used to create pro-inflammatory and anti-inflammatory/regulatory macrophages respectively.

4.2.6 Immunolabeling analysis

Cells were fixed with 2% paraformaldehyde (PFA) for 30 minutes then washed in 1X PBS. Cells were blocked using 2% donkey serum, 1% bovine serum albumin (BSA), 0.1% Triton X-100, 0.1% Tween-20 for 1 hour at room temperature. Primary antibodies were diluted in this blocking buffer as follows and incubated overnight at 4 °C. Cells were washed in 1X PBS then incubated in fluorescently-labeled secondary antibodies for 1 hour at room temperature. Cell nuclei were counterstained with DAPI. Table 5 lists the antibodies and concentrations used in the present study. Images were taken in an array of 3 × 3 images per each well using a Carl Zeiss Observer.Z1 microscope and then the intensity of staining was analyzed using Cell Profiler Image Analysis Software (Broad Institute, Cambridge, MA) using the same number of cells for all tested conditions.

Table 5. Primary and secondary antibody dilutions used to perform indirect fluorescent antibody labeling of in vitro bone marrow-derived macrophage cultures.

Labeling	1º Antibody	2º Antibody
iNOS	1:100 (rabbit iNOS)	1:200 (donkey anti-rabbit)
Arginase-1	1:200 (rabbit arginase)	1:200 (donkey anti-rabbit)

4.2.7 Gene expression analysis

Following treatments, macrophages were harvested for RNA using Qiagen RNEasy MiniPrep RNA Isolation Columns following standard protocol. RNA was quantified using a NanoDrop Spectrophotometer. cDNA templates were created using Invitrogen High Capacity RNA-to-cDNA kits. Taqman Gene Expression Assays were performed for the following markers: iNOS, IL-1β, IL-12β, TNF-α, IL-10, Arg, Fizz1, MRC1, PPARγ.

4.2.8 Nitric oxide assay

Following treatments, supernatant from macrophages were collected. Nitric oxide content was assayed using a Greiss Reagent system. Sulfanilamide (1% in 5% phosphoric acid) was added to supernatants for 10 minutes. Then, 0.1% N-1-napthylethylenediamine in water was added to the mixture for an additional 10 minutes. The absorbance at 540 nm was measured using a spectrophotometer.

4.2.9 Phagocytosis assay

Following treatments, cells were assayed for phagocytic ability using Vybrant Phagocytosis Assay Kit. Cells were incubated in FITC-labeled dead *e. coli* particles for 2 hours in the cell culture incubator. Following thorough washing, the cells were fixed with 2% PFA for 30 minutes then washed with 1X PBS. Cell nuclei were counterstained with DAPI. Images were taken in an array of 3 × 3 images per each well using a Carl Zeiss Observer.Z1 microscope and then the FITC fluorescence intensity of staining was analyzed using Cell Profiler Image Analysis Software using the same number of cells for all tested conditions.

4.2.10 Plasma treatment and Layer by Layer coating of polypropylene meshes

Polypropylene (PP) meshes were cleaned using a 1:1 acetone:isopropanol mixture and then air dried prior to irradiation with 15 seconds of argon plasma at 600W, an argon gas flow of 35 mL/min and a steady state pressure of 250 mTorr (50 mTorr initial pressure) using an Ion 40 Gas Plasma System (PVA Tepla America, Inc). Maleic anhydride powder (1.5 gr) was placed into a glass plate inside of the machine chamber. 1 cm^2 pieces of PP mesh were then placed around the plate to a distance of 8.5 cm. After an initial pressure of 50 mTorr was reached, 30 seconds of maleic anhydride plasma treatment was performed at 600W, an argon gas flow of 35 mL/min and a steady state pressure of 250 mTorr. Finally, PP meshes were rinsed for 30 minutes with milli-Q water and then boiled for 20 minutes in fresh milli-Q water.

Coating was adapted to a customized automated dipping instrument (8-position SILAR coating system, PTL-SC-6A. MTI Corporation, Richmond, CA). Mesh coating was equivalent, only requiring longer washing times to remove the polymer excess, due to the absence of air

drying. Meshes were dipped in chitosan (2 mg/mL in 0.5% acetic acid) for 10 minutes at RT, then washed 3 times (1-minute each) in milli-Q water. Next, meshes were dipped in a dermatan sulfate solution (2mg/mL in water) for 10 minutes at room temperature. Meshes were washed again in milli-Q water and air-dried. This cycle was repeated until a core coating of 10 bilayers ($PP^{-}[CH/DS]_{10}$) was achieved. After coating, meshes were lyophilized and stored at 4°C.

4.2.11 MCP-1 and IL-4 loading and release assays

Similarly to IL-4, dermatan sulfate (2 mg/mL) was incubated overnight at 4ºC to MCP-1 (0.75 and 1.5 µg/mL) prior coating. For sequential regimens, both MCP-1 (0.75 µg/mL) and IL-4 (1.5 µg/mL) were added to dermatan sulfate (2 mg/mL) and incubated overnight at 4ºC. Then, polypropylene meshes with a 10-bilayer core coating were further coated with 20 bilayers containing MCP-1. For sequential delivery, core-coated meshes were further coated with 20 bilayers containing IL-4 and then coated with 20 additional bilayers containing both MCP-1 and IL-4. After coating, IL-4 loaded meshes were lyophilized and stored at -20°C. All mesh materials were then terminally sterilized using ethylene oxide.

Immunolabeling was used to qualitatively demonstrate the loading and distribution of MCP-1 throughout the coating. MCP-1 eluting meshes and controls were immersed in a 1% BSA solution to block non-specific adsorption of antibodies (1h, RT). Washing was performed in between each step by dipping the meshes 4 times in 0.05% Tween 20. Then meshes were immersed and incubated in a solution of anti-murine MCP-1 (from rabbit) as primary antibody (1:100 in 0.1% BSA, 2 hours, RT). Meshes were then immersed in a solution of anti-rabbit-Alexa Fluor 546 as a secondary antibody (1:100 in 0.1% BSA, 30 min, RT). Mesh fluorescence was observed under confocal microscopy (Leica DMI4000 B, Buffalo Grove, IL), in which an

excitation/emission of 480/520 nm was used to observe the mesh autofluorescence (green) and 561/572 nm to observe the specific fluorescence due to the loaded MCP-1 (red).

Loading efficiency and release assays were performed following manufacturer instructions of the Peprotech MCP-1 ELISA kit. First, 1 cm^2 pieces of MCP-1 eluting (20 bilayers) and coated (no cytokine) meshes were immersed into 400 µL of a solution 0.05 units/mL chondroitinase ABC and 0.05 units/mL chitosanase in 1X PBS. Incubation was performed to multiple time points at 37°C, after which 400 µL of solution were aliquoted and stored at -80°C until the end of the experiment. After collection, replacement with fresh solution was performed to continue the release assay. To perform the ELISA assays, 100 µL aliquots were used from each sample at each time point.

4.2.12 Statistical analysis

Comparisons of means were performed by either unpaired t-test (two-tailed), one-way or two-way analysis of variance (ANOVA), using at least $p < 0.05$ as statistical significance criteria followed by Tukey's test to compare groups and Sidak's test to compare time points. Shapiro-Wilk was used to test normality. All statistical tests were performed on GraphPad Prism V7 (La Jolla California, USA).

4.3 RESULTS AND DISCUSSION

4.3.1 Histomorphologic evaluation of the early host response

The overall histomorphologic appearance of the early host response to the implanted mesh materials in H&E stained sections was largely similar in 8-week-old and 18-month-old mice (Figure 21); however, the results suggested slower migration of mononuclear cells to the mesh surface in the 18-month-old group. Briefly, at 3 days, the site of remodeling was characterized by provisional matrix deposition and early invasion of the site by predominantly mononuclear cells with a small number of neutrophils remaining. Of note, though the number of cells within the site of remodeling was found to be quantitatively similar at the 3 day time point, there was an increased proportion of cells closer to the implant surface in the 8-week-old group as compared to the 18-month-old group. However, fewer cells were observed at the surface of the implant than were observed in the area distant from the immediate surface in either group. By 7 days, additional neomatrix deposition with little to no organization was observed accompanied by angiogenesis in the peri-implant area. The response at 7 days was predominated by mononuclear cells in the area immediately surrounding the mesh, with spindle shaped cells observed more distantly within the newly deposited matrix. The distribution of cells within the 20X images were similar for both 8-week and 18-month-old mice, though both a qualitative and quantitative decrease in cell density were noted for the 18-month-old group as compared to the 8-week-old group. The formation of multinucleated giant cells at the mesh surface was observed in both groups at the 7 day time point and persisted throughout the remainder of the study. By 14 days, additional matrix deposition was observed, with a small degree of organization of the newly deposited matrix around the apical and basal aspects of the individual fibers. The number of

vessels within the site of remodeling was observed to decrease, though the remaining vessels were more mature than was observed at 7 days. The response immediately surrounding the mesh was predominated by mononuclear cells with an increased proportion of spindle shaped cells observed within remodeling site as compared to the 7 day time point. The qualitative and quantitative distribution of cells within the site of remodeling was similar for both groups at the 14 day time point.

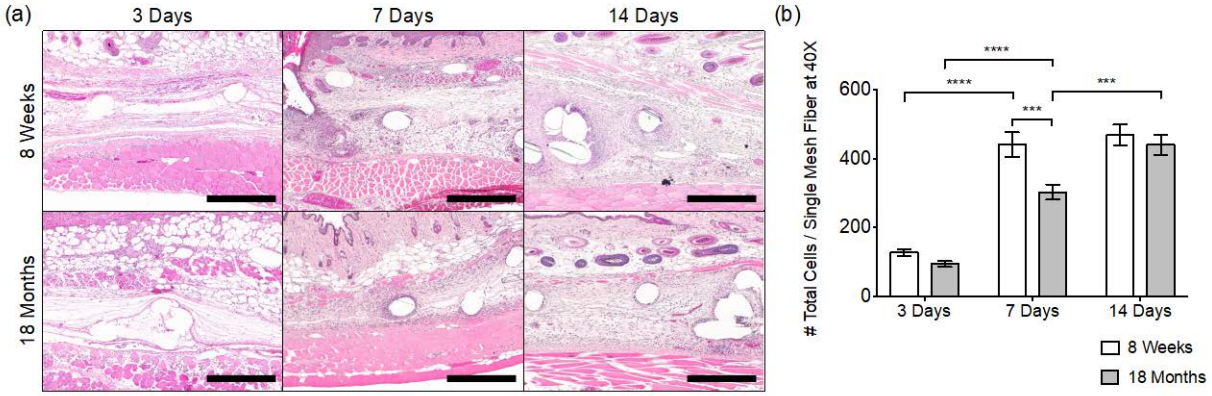

Figure 21. (a) Images of H&E stained tissue cross sections at 10X and (b) total cell counts (DAPI) surrounding single mesh fibers in 40X images at 3, 7 and 14 days. Scale bars represent 200 µm. Bars represent the mean ± SEM. Statistical significance as (***) $p < 0.001$ and (****) $p < 0.0001$. All other differences are non-significant. N = 7

4.3.2 Characterization of macrophage populations in the early host response

Macrophages and newly recruited monocytes were detected at the implanted mesh surface by immunostaining with commonly described surface markers: F4/80, CD68, and CD11b (Figure

22a). The number of F4/80^{+} single-positive cells peaked at 7 days in both the 8 and 18-month-old mice, consistent with cell recruitment, however there were significantly fewer F4/80^{+} cells present in the 18-month-old mice at 3 days (Figure 22b). The number of CD68^{+} cells remained consistent in the 8-week-old mice, but peaked at 7 days in the 18-month-old mice. In addition, there were significantly fewer CD68^{+} cells present in the 18-month-old mice at 3 and 14 days. Very few cells expressed CD11b at the 3 day time point, however the CD11b^{+} cells peaked in both the 8 and 18-month-old mice at 7 days.

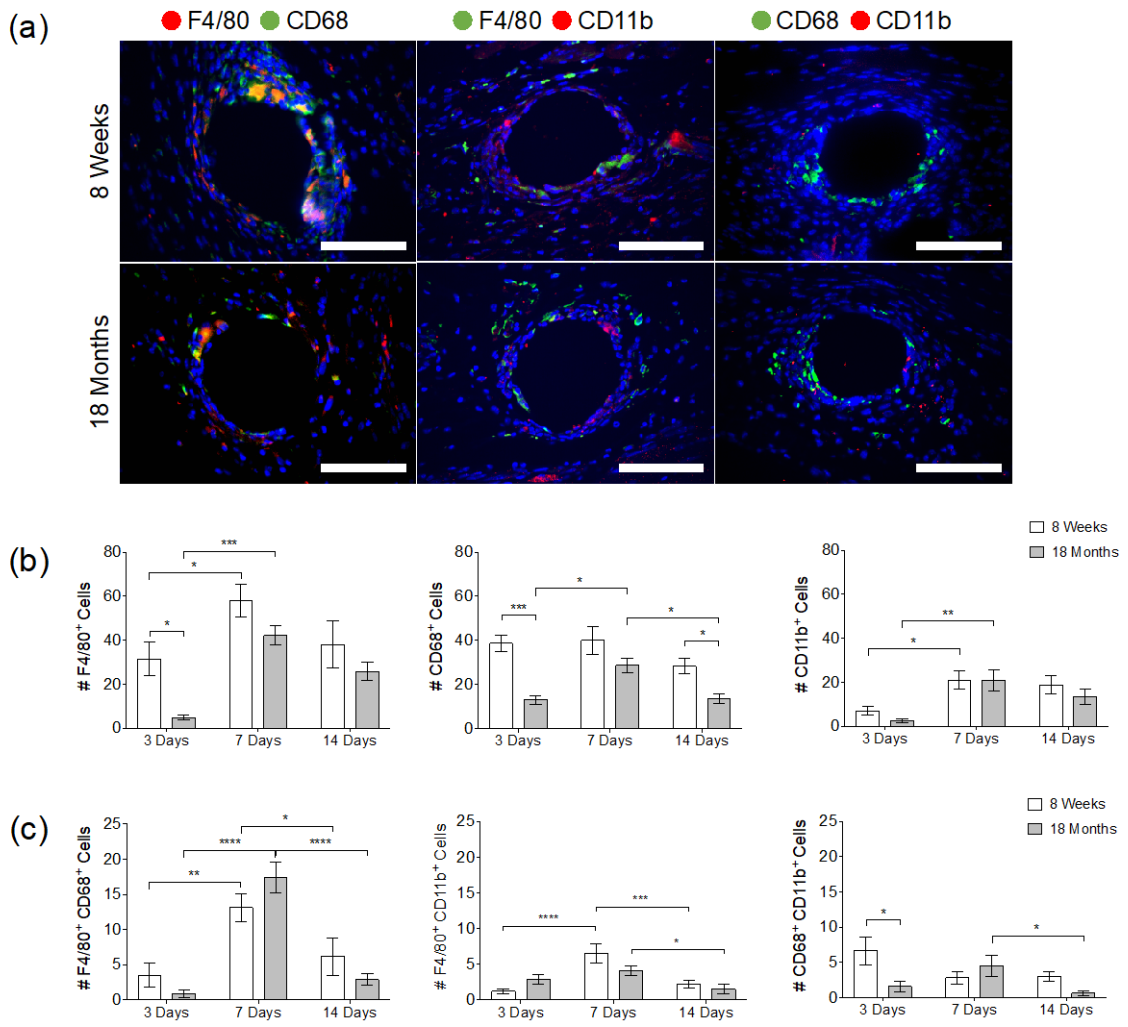

Figure 22. (a) Fluorescence microscopy images of F4/80 CD68, F4/80 CD11b and CD68 CD11b co-immunolabeled tissue cross sections at a single mesh fiber at 7 days. DAPI was used to stain cell nuclei. Scale bars represent 50 µm. Cell counts of (b) $F4/80^+$, $CD68^+$ and $CD11b^+$ cells and (c) $F4/80^+$ $CD68^+$, $F4/80^+$ $CD11b^+$ and $CD68^+$ $CD11b^+$ cells surrounding single mesh fibers at 3, 7 and 14 days. Bars represent the mean ± SEM. Statistical significance as (*) $p < 0.05$, (**) $p < 0.01$, (***) $p < 0.001$ and (****) $p < 0.0001$. All other differences are non-significant. N = 7

Few differences were observed between the two age groups in the double-labeled macrophages (Figure 22c). The number of $F4/80^+$ $CD68^+$ cells peaked at 7 days in both groups,

and represented the greatest co-expression of macrophage markers at all time points, while very little co-expression was observed in the other groups. The number of $F4/80^+$ $CD11b^+$ cells increased at 7 days in 8-week-old mice, but was unchanged in the 18-month-old mice. The number of $CD68^+$ $CD11b^+$ macrophages was significantly decreased in 18-month-old animals compared to 8-week-old mice at 3 days. While the number of $CD68^+$ $CD11b^+$ macrophages did not change in 8-week-old animals, there was a decrease in the 18-month-old from 7 to 14 days.

Distinct macrophage populations identified as tissue-resident versus circulating with unique phenotypes and functions are widely identified in the literature. Each of these populations likely plays a distinct role in tissue homeostasis and the response to injury and pathogen on a tissue by tissue basis. In the liver, several studies have identified differential roles for $CD68^+$ tissue-resident Kupffer cells and $CD11b^+$ infiltrating bone marrow derived macrophages in pathogen clearance and tumor cell destruction, respectively [156-158]. A number of recent studies have now described shifts in the proportions of tissue-resident versus circulating cells occurring within individual tissues with age and with important implications for the host response and outcomes following injury. For example, aging of cardiac muscle leads to progressive replacement of embryonic macrophages with bone marrow derived macrophages [157]. The infiltrating macrophages were found to have a pro-fibrotic gene signature, leading to impaired tissue regeneration that could be reversed by inhibiting monocyte recruitment [159-161].

In the present study, $CD68^+$ cells remained unchanged temporally in the 8-week-old mice, suggesting the possibility of a local cell origin as opposed to recruitment from bone marrow. Furthermore, this $CD68^+$ population co-localized with arginase-1 and was significantly decreased at the earliest time point in the 18-month-old animals. While the exact origin of these

cells remains unclear, the recruitment and polarization of this population likely represents a key event which drives the downstream host response. A recent study showed that a reservoir of peritoneal cavity macrophages exists which can rapidly infiltrate injured organs in response to cell death signals [162]. This infiltration was found to occur rapidly (2-3 days post-injury) across the mesothelial lining of the peritoneum and into deeper tissue locations. Of significant interest, this population also assumed an alternatively activated M2-like phenotype upon arrival at the injury site. While the full set of mechanisms by which these cells are able to rapidly infiltrate tissues outside of the peritoneal cavity is unknown, the study demonstrated that the migration was dependent upon CD44, the receptor for hyaluronan. While the role of changes in the local tissue microenvironment were not investigated in depth in the present study, a reduction in the presence or production of glycosaminoglycan constituents, including hyaluronan, at early time points in the host response could have led to a reduction in the recruitment of early responding cells and/or changes in their polarization profile.

4.3.3 *In vitro* assessment of macrophage polarization and function

In order to determine whether there were inherent genetic or functional differences in the ability of macrophages to polarize in aged mice, bone marrow-derived macrophages were harvested from 8-week-old and 18-month-old C57BL/6 mice. Bone marrow derived macrophages were treated using protocols for M1 (IFN-γ/LPS) and M2 (IL-4) as described above to determine their ability to polarize to these established phenotypes. Macrophage phenotype was assessed using indirect fluorescent antibody labeling for classical M1 (iNOS) and M2 (Arg-1) markers. Labeling showed that IFN-γ/LPS treatment resulted in significant increases in iNOS labeling in both 8-week-old and 18-month-old macrophages compared to both M0 (naïve, untreated) and

M2 controls (Figure 23a). There was a significant increase in iNOS staining in macrophages harvested from 18-month-old as compared to 8-week-old mice in the IFN-γ/LPS treatment group. There were no differences in iNOS expression in M0 baseline or M2 treated macrophages from 8-week-old and 18-month-old sources. IL-4 treatment resulted in a significant increase in Arg-1 labeling while IFN-γ/LPS treatment resulted in no significant difference (Figure 23b). There were no significant differences in Arg-1 labeling between 8-week-old and 18-month-old macrophages with any treatment regimen.

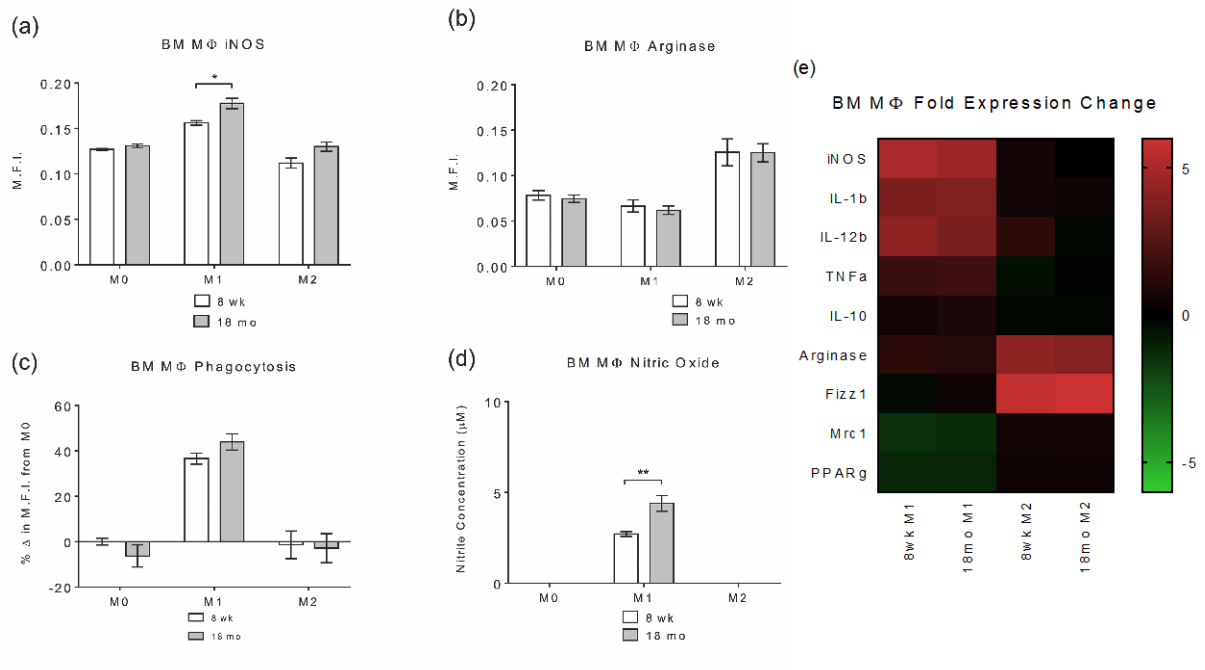

Figure 23. Image analysis of (a) iNOS and (b) Arginase-1 of macrophages treated with media (M0), IFN-γ/LPS (M1) or IL-4 (M2) for 24 hours, isolated from 8-week and 18-month old C57BL/6 mice. Representative images are shown in Figure S5. (c) Phagocytosis function using Vybrant FITC-labeled E. Coli particles incubated on treated macrophages for 2 hours. Representative images are shown in Figure S5. (d) Nitric oxide production using Greiss reagent system on supernatants from treated macrophages. (e) Taqman gene expression assays assessing the gene expression of pro- and anti-inflammatory gene targets. Bars represent the mean ± SEM. Statistical significance as (*) $p < 0.05$ and (**) $p < 0.01$. All other differences are non-significant. N = 5

Macrophage functionality was assessed using phagocytosis assays and nitric oxide production as these are classical markers of macrophage activation. Phagocytosis was assessed using Vybrant FITC-labeled *e. coli* particles and subsequent mean fluorescent intensity determination as an approximation of the amount of particles phagocytosed (Figure 23c). Results showed that IFN-γ/LPS treatment in both 8-week-old and 18-month-old macrophages resulted in a significant increase in phagocytic particle uptake compared to M0 and M2 controls. There was

no significant difference between 8-week-old and 18-month-old macrophage phagocytosis following any of the treatment regiments, suggesting that there are no intrinsic deficiencies in phagocytic functionality with aging. Nitric oxide production was assessed using the Greiss reagent system on supernatants following treatment (Figure 23d). Assays showed that 8-week-old and 18-month-old macrophages exhibited a significant increase in supernatant nitrite concentration with IFN-γ/LPS treatment compared to M0 and M2 treatment groups. There was also a significant increase in nitric oxide production from 8-week-old to 18-month-old macrophages in the IFN-γ/LPS treatment group. However, both the 8-week-old and 18-month-old macrophage retained the ability to produce nitric oxide in response to inflammatory signals.

Macrophage gene expression was determined using Taqman gene expression assays on common genes involved in the murine inflammatory process (iNOS, IL-1b, IL-12b, TNFa, IL-10, Arg-1, Fizz1, Mrc1, and PPARγ). Gene expression analysis showed that treatment of 8-week-old and 18-month-old bone marrow-derived macrophages with IFN-γ/LPS or IL-4 resulted in gene expression patterns which are indicative of M1 and M2 polarization, respectively (Figure 23e). No differences in gene expression were observed between macrophages harvested from 8-week-old and 18-month-old mice following either IFN-γ/LPS or IL-4 treatment. These findings illustrate that the ability of both 8-week-old and 18-month-old macrophages to polarize towards M1 and M2 phenotypes remain intact, complementing previously published literature in the field [70].

4.3.4 *In vivo* macrophage polarization profile in the early host response

Macrophage polarization to an M1 or M2 state was evaluated in vivo using inducible nitric oxide synthase (iNOS) or arginase-1 (Arg-1) expression respectively (Figure 24a). Arg-1 expression

was induced significantly at 7 days in the 8-week-old mice, but remained unchanged in 18-month-old mice, suggesting a deficit in M2 polarization in aged mice (Figure 24b). At 14 days post-implantation, Arg-1 expression in the 8-week-old group returned to basal levels similar to the 18-month-old mice. Interestingly, co-labeling Arg-1 with CD68 revealed that $CD68^+$ cells accounted for the vast majority of Arg-1 expressing cells at all time points. On the other hand, iNOS expression was induced significantly at 7 days in the 18-month-old mice, but remained unchanged in the 8-week-old mice (Figure 24c, d**),** demonstrating an M1 profile in the aged cells. While both 8-week and 18-month-old mice showed reduced iNOS expression at 14 days, the 18-month-old cells retained a higher iNOS expression compared to 8-week-old. Co-labeling of iNOS with CD68 accounted for very few of the $iNOS^+$ cells, suggesting that another cell type is responsible for iNOS expression. The total cell percentage of M1/M2 macrophage polarization is included in Figure 25.

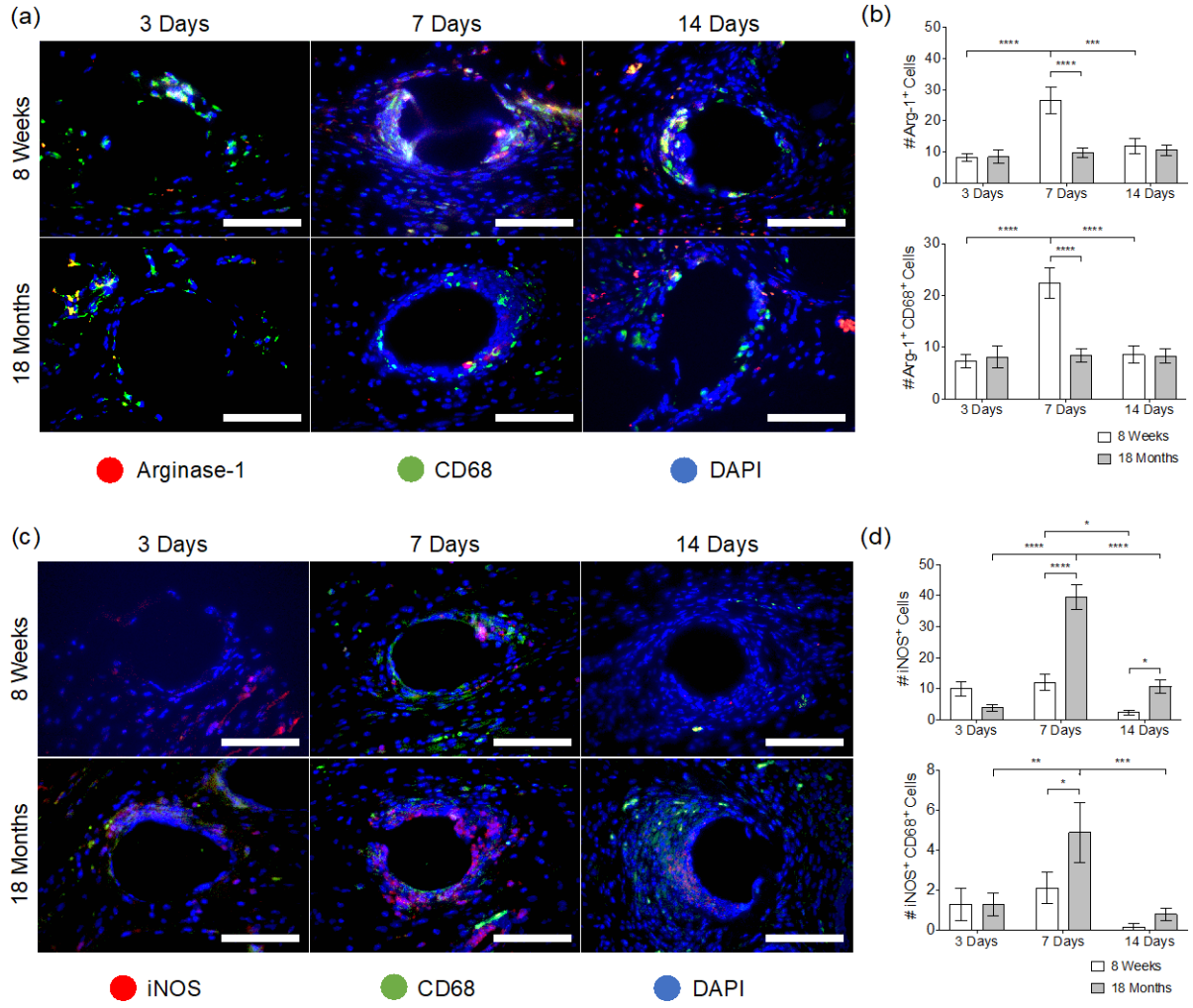

Figure 24. Fluorescence microscopy images of (a) Arginase-1 (red) CD68 (green) co-immunolabeling, and (b) iNOS (red) CD68 (green) co-immunolabeling at a single mesh fiber at 3, 7 and 14 days. DAPI was used to stain cell nuclei. Scale bars represent 50 µm. Cell count image analysis of (c) Arg-1$^+$, Arg-1$^+$ CD68$^+$ cells and (d) iNOS$^+$, iNOS$^+$ CD68$^+$ cells at 3, 7 and 14 days. Bars represent the mean ± SEM. Statistical significance as (*) $p < 0.05$, (**) $p < 0.01$, (***) $p < 0.001$ and (****) $p < 0.0001$. All other differences are non-significant. N = 7

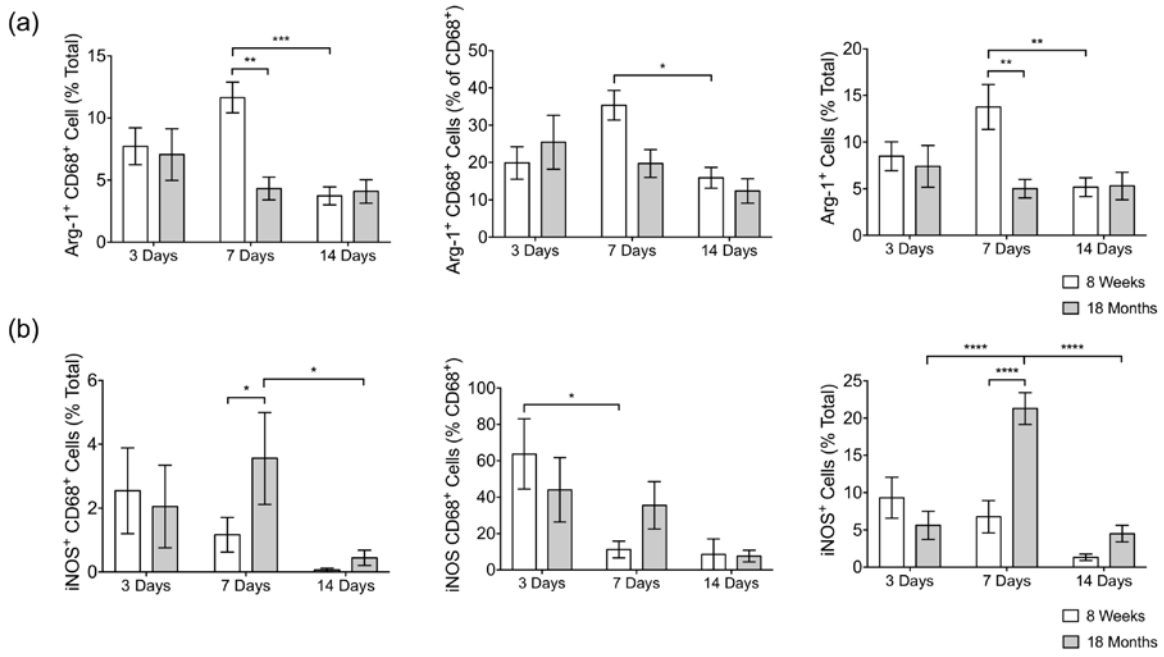

Figure 25. Percentage of (a) Arg-1$^+$, Arg-1$^+$ CD68$^+$ cells and (b) iNOS$^+$, iNOS$^+$ CD68$^+$ cells surrounding single mesh fibers of tissue cross sections from 8-week and 18-month mice implanted with a 1 cm^2 piece of polypropylene mesh for 3, 7 and 14 days. Bars represent the mean ± SEM. Statistical significance as (*) $p < 0.05$, (**) $p < 0.01$, (***) $p < 0.001$ and (****) $p < 0.0001$, using two-way ANOVA with Tukey's (groups) and Sidak's (days) tests. All other differences are non-significant. N = 7

In the present study, bone marrow derived macrophages harvested from 8-week-old and 18-month-old mice were subjected to standard M1 and M2 polarization regimes. The results demonstrate that both 8-week-old and 18-month-old macrophages retained the ability to polarize towards M1 and M2 phenotypes, and were functionally intact. Few differences between polarized macrophages harvested from the bone marrow of 8-week-old and 18-month-old mice were noted; however, the expression of iNOS and production of NO were found to be higher in 18-month-old mice as compared to 8-week-old mice. These results correlate well with the finding of larger numbers of recruited iNOS$^+$ cells present within the remodeling site of implants

in 18-month-old animals. This cell population was found to be largely separate from the Arg-1 expressing $CD68^+$ population in both 8-week-old and 18-month-old mice, suggesting the possibility of multiple, distinct macrophage populations participating in the host response.

4.3.5 *In vivo* effects of the aged microenvironment upon the host response

As the above results suggest that local tissue cues could have effects on the profile and functionality of macrophages in the host response, the glycosaminoglycan (GAG) composition of the local microenvironment was evaluated by means of an Alcian Blue histological staining. GAG composition was evaluated in the present study as GAGs represent an important structural component of the tissue extracellular matrix, with key roles in regulating macrophage polarization both acting as a substrate for early infiltrating macrophage populations and by sequestering signaling molecules [93, 162]. The presence of GAGs (blue) was detected in both implanted mice groups (Figure 26a, b), with no differences observed at 3, 14, and 90 days. Interestingly, at 7 days, the 18-month-old group had significantly less GAG deposition, corresponding temporally with the observed changes in macrophage recruitment and polarization.

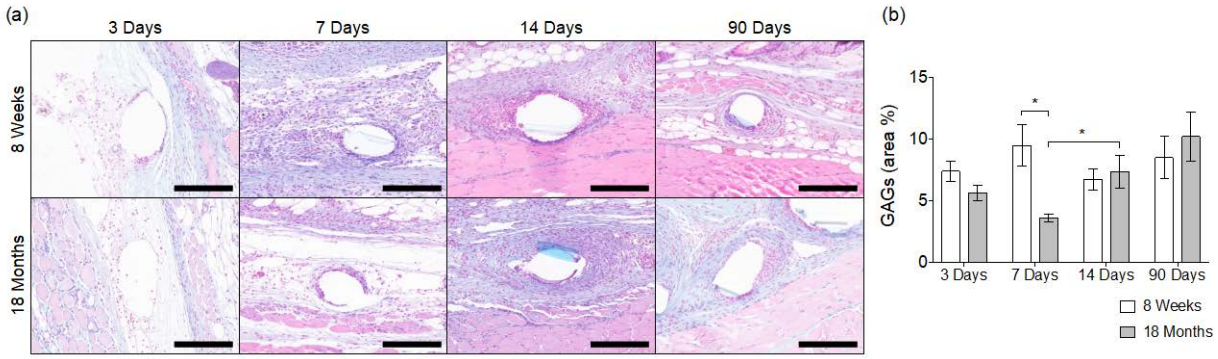

Figure 26. (a) Images of Alcian Blue stained tissue cross sections (GAGs in blue) and (b) image analysis of GAG deposition as percentage of total inflammatory tissue area (excluding skin and muscle) surrounding single mesh fibers at 20X of tissue cross sections from 8-week and 18-month mice implanted with a 1 cm^2 piece of polypropylene mesh for 3, 7, 14 and 90 days. Scale bars represent 100 µm. Bars represent the mean ± SEM. Statistical significance as (*) $p < 0.05$. All other differences are non-significant. N = 7

4.3.6 Long-term *in vivo* evaluation of fibrotic capsule deposition

Fibrotic capsule deposition and composition were used as metrics to determine the impact of aging on the host response against polypropylene mesh in the long term (90 days). The capsule was defined as the distance between the implant surface and the outer aspect of the dense collagenous matrix surrounding the mesh fibers (Figure 27a, black arrow), inclusive of the cell layer adjacent to the surface and within the capsule (Figure 27a, green arrow). Quantitative analysis revealed no difference in the area or thickness of the collagenous portion between the 8-week and 18-month-old implanted mice (Figure 27b, c). Further assessment of the composition of the fibrotic capsule revealed no differences in the capsule composition between the two age groups (Figure 27e, f). However, 18-month-old mice were observed to have a significant

increase in both the thickness of the cell layer and total number of cells at the mesh fiber surface at 90 days (Figure 27c, d), suggesting an unresolved host response to the implanted mesh.

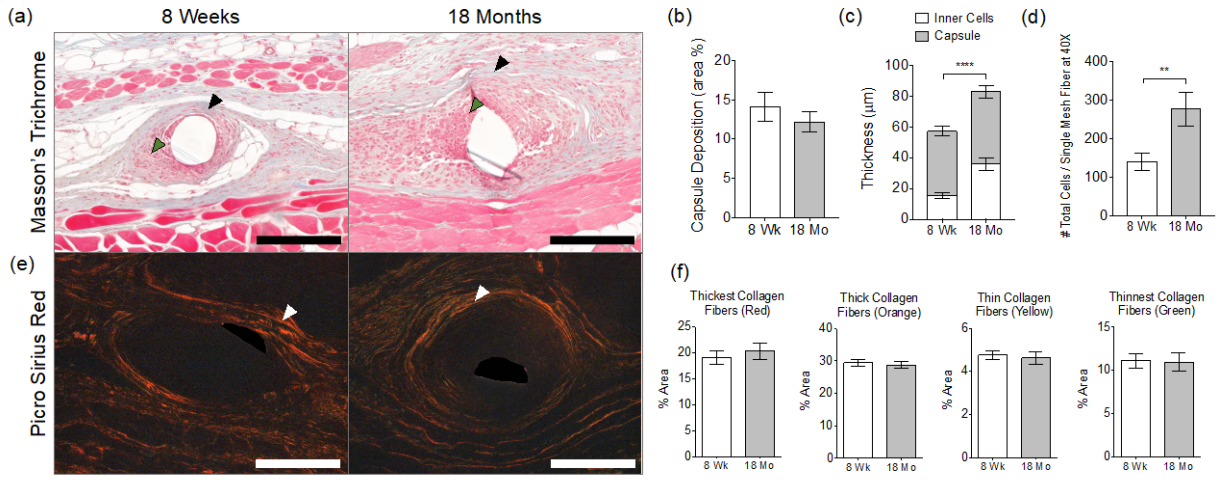

Figure 27. (a) Masson's Trichrome stained tissue sections of 8-week and 18-month mice at 90 days. Black and green arrowheads indicate the collagenous portion of the capsule and cellular reaction surrounding single mesh fibers, respectively. Scale bars represent 200 µm. (b) Image analysis of capsule deposition as percentage from the area of inflammatory tissue (excluding skin and muscle), (c) Thickness of capsule, inner cells and total thickness; and (d) total number of cells, surrounding single mesh fibers. (e) Picro Sirius Red stained tissue sections of 8-week and 18-month mice at 90 days. White arrowheads indicate the capsule surrounding single mesh fibers. (f) Image analysis of collagen capsule composition surrounding single mesh fibers, of samples stained with Picro Sirius Red. Scale bars represent 100 µm. Bars represent the mean ± SEM. Statistical significance as (**) $p < 0.01$ and (****) $p < 0.0001$. All other differences are non-significant. N = 7

The findings of delayed, dysregulated, and unresolved host responses in the present study correlate well with observations of dysregulated inflammation and delayed resolution of inflammatory responses to pathogen and in wound healing [148]. For example, a study of punch biopsies from healthy human subjects between the ages of 19-96 years old post wounding

showed that the macrophage response in aged subjects peaked at 84 days as opposed to 7 days in younger subjects [163]. The delayed infiltration of macrophages in wound healing has been associated with poor re-epithelialization, reduced angiogenesis, deficits in collagen deposition, and decreased wound strength [164]. Altered immune responses to wounding or pathogens in aged individuals have largely been attributed to altered function of the adaptive immune system, however multiple studies have noted the impacts of aging upon the innate immune compartment [68-70]. The studies which have observed immune dysfunction in aged macrophage populations have largely been performed using tissue-derived macrophages while the function of macrophages derived from the bone marrow has been shown to remain largely intact in multiple studies [69, 70], suggesting that age-related changes in the local tissue microenvironment may play a role in the observed dysfunction [165, 166].

In summary, the findings of the present study suggest that the host macrophage response to polypropylene mesh implants is delayed, dysregulated, and unresolved in aged animals as compared to young. Specifically, it was observed that there was a deficit in early responding macrophage populations in 18-month-old mice as compared to 8-week-old at 3 days and retarded recruitment of additional macrophage populations at 7 days. The population which was present at the 7 day time point was found to express significantly less Arg-1 and significantly more iNOS in 18-month-old animals as compared to 8-week-old, suggesting a more M1-like pro-inflammatory profile. Our studies and others have shown the 7-14 day post implantation time frame to be significantly predictive of downstream outcomes, with higher numbers of M2 polarized cells and higher ratios of M2:M1 cells as indicators of improved integration and remodeling [32, 67, 100, 155]. Thus, this finding indicates the potential for poor downstream integration and remodeling in 18-month-old animals. Similarly, shifting the response towards an

M2 phenotype via IL-4 delivery may present limitations in aged subject due to the delayed recruitment of macrophages, as the release of IL-4 was designed to be taken up by macrophages in the first two weeks, not being able to reverse the highly inflammatory M1 response, or lead to unexpected effects due to other cells taking up the IL-4. Therefore, we have developed a sequential delivery regimen for old mice that restores the delayed macrophage recruitment and reverses the highly inflammatory macrophage response towards an M2-like phenotype, using MCP-1 and IL-4, respectively. To do so, we have first done a study to evaluate the loading, release profile and bioactivity of MCP-1, and then explore the sequential delivery capabilities of the multilayered coating.

4.3.7 MCP-1 bioactivity, dosing and release assays

As similar to IL-4 loading, MCP-1 can be incorporated into the mesh coating by previous incubation with Dermatan Sulfate, and that the length of release and amount of MCP-1 is also dependent on the number of coating bilayers. To increase initial cell recruitment, a release no longer than a week was intended for MCP-1. We have estimated that the same 20-bilayers used to obtain up to a week of release of IL-4, will also be similar to MCP-1. Release assays confirmed that the release of MCP-1 using 20-bilayers (coating solution containing 1.5 μg/mL of MCP-1) of coating was consistent to approximately 8 days of release (Figure 28c), but higher amounts of cytokine than 20-bilayers of IL-4 (Figure 5). Confocal microscopy confirms that MCP-1 is uniformly distributed through the entire surface of the mesh (Figure 28a).

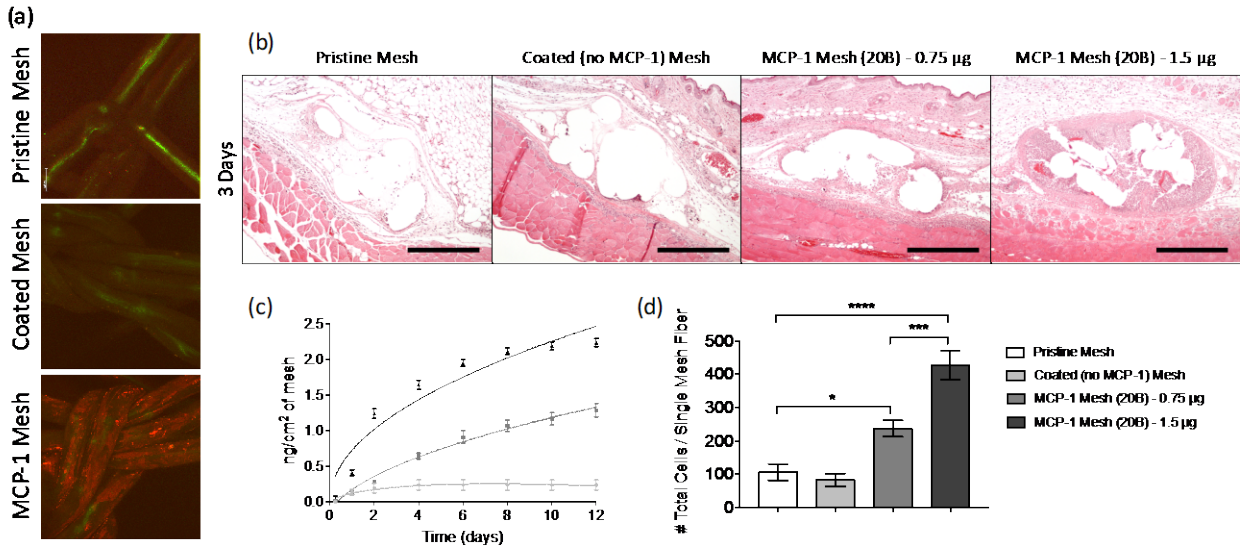

Figure 28. (a) Confocal microscopy images of MCP-1 immunolabeled (red) polypropylene fibers (green) of pristine (i), coated [no cytokine] (ii) and MCP-1 loaded [20B] (iii) mesh. Scale bars represent 100 µm. (b) H&E stained tissue sections at 10X from mice implanted with a 1 cm^2 piece of pristine, coated (no cytokine), MCP-1 (0.75 and 1.5 µg/mL in coating solutions, 20B) at 3 days post-implantation. Scale bars represent 200 µm. (c) Cumulative release of MCP-1 (nanograms) versus time (days) from 1 cm^2 pieces of coated mesh loaded with 0.75 and 1.5 µg/mL of MCP-1 (20B). Coated (no cytokine) mesh was used as a control. Points represent the mean ± SEM. (d) Image analysis of total cells (DAPI) surrounding single mesh fibers of tissue cross sections of mice implanted with MCP-1 eluting meshes and controls, 3 days post-implantation. Bars represent the mean ± SEM. Statistical significance as (*) $p < 0.05$, (***) $p < 0.001$ and (****) $p < 0.0001$, using two-way ANOVA with Tukey's tests. All other differences are non-significant

When MCP-1 (20B) eluting meshes were implanted subcutaneously into young adult mice, histological assessment three days post-implantation showed a highly exacerbated and localized cell recruitment but also signs of inflammation and mesh erosion in H&E stained tissue cross sections, confirming that MCP-1 is bioactive after loading and mesh sterilization (Figure 28b, d). Dose of MCP-1 was adjusted by decreasing the amount of MCP-1 in the coating solution

to 0.75 μg/mL (a half), and release assays confirmed that the dose of MCP-1 was reduced nearly a half, and preserving the same length of release (Figure 28c). This suggests that the released amount of MCP-1 is proportional to the amount of MCP-1 in the coating solution. Implantation of meshes containing half the amount of MCP-1 were also capable of increasing cell recruitment compared to coated (no cytokine) and pristine meshes, but also lower than the eluting mesh containing higher amount of MCP-1, with no signs of mesh erosion (Figure 28b, d). Therefore, the following studies will use MCP-1 meshes with 20 bilayers where the coating solutions contain 0.75 μg/mL of MCP-1.

4.3.8 Sequential release of MCP-1 and IL-4

A sequential delivery regimen of MCP-1 and IL-4 will be used in old mice to restore the delayed macrophage recruitment and shift the highly inflammatory response towards an M2 phenotype, respectively. The multilayered nature of the coating was used to provide first concomitant release of both MCP-1 and IL-4 in the 20 external layers, then followed by single release of IL-4 in the 20 internal layers of the coating (excluding core coating). ELISA assays corroborated that the release profile of IL-4 was similar when released from both single IL-4 and sequential IL-4/MCP-1 eluting meshes (Figure 29a). Similarly, MCP-1 release profile in both single MCP-1 and sequential IL-4/MCP-1 eluting meshes were not significantly different (Figure 29b). Sequential released was then observed by an initial concomitant release of MCP-1 and IL-4 but followed by release of IL-4 only (Figure 29c), releasing nearly 80% of the total dose of MCP-1 in eight days, and 80% of IL-4 by approximately 12 days (Figure 29d).

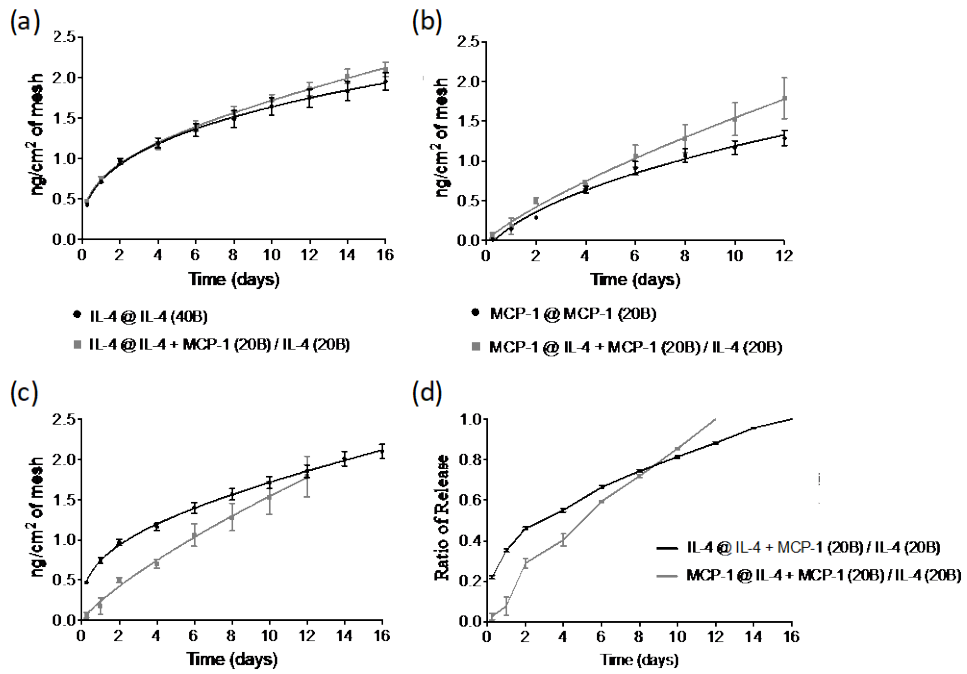

Figure 29. (a) Cumulative release of IL-4 (nanograms) versus time (days) from eluting meshes containing 40 bilayers of IL-4 (black curve) and 20 bilayers of MCP-1/IL-4 plus 20 bilayers of IL-4 (gray curve). (b) Cumulative release of MCP-1 (nanograms) versus time (days) from eluting meshes containing 20 bilayers of MCP-1 (black curve) and 20 bilayers of MCP-1/IL-4 plus 20 bilayers of IL-4 (gray curve). (c) Cumulative release of MCP-1 (gray curve) and IL-4 (black curve) versus time (days) from eluting meshes containing 20 bilayers of MCP-1/IL-4 plus 20 bilayers of IL-4. (d) Ratio of released MCP-1 and IL-4 (nanograms) versus time (days) from eluting meshes containing 20 bilayers of MCP-1/IL-4 plus 20 bilayers of IL-4. Points represent the mean ± SEM

4.3.9 Mesh implantation studies of single and sequential delivery regimens in aged and young mice

Efficacies of single and sequential delivery regimens of IL-4 and MCP-1 were evaluated by implanting eluting meshes containing each or both cytokines in aged (18 month-old) and young adult (8 week-old) mice. Histological assessments by H&E staining and DAPI cell counting

analysis (Figure 30) at 3 days post-implantation showed increased cell recruitment in all eluting meshes containing MCP-1 in both young and aged mice, with the exception of coated (no cytokine) mesh in old mice that resulted in a highly exacerbated recruitment of cells highly localized around the mesh fibers (Figure 30a).

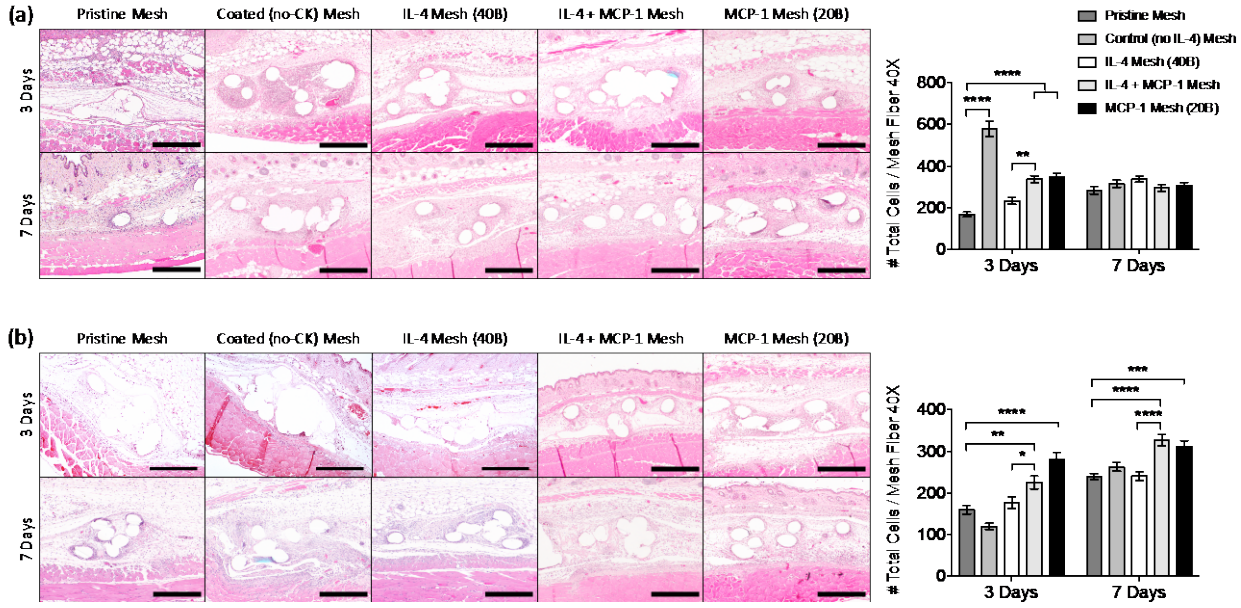

Figure 30. Images of H&E stained tissue cross sections (10X) and total cell counts (DAPI) surrounding single mesh fibers (40X) at 3 and 7 days from (a) old and (b) young mice implanted with a 1 cm^2 piece of pristine, coated (no cytokine), single and sequential MCP-1 and IL-4 eluting meshes. Scale bars represent 200 µm. Bars represent the mean ± SEM. Statistical significance as (*) $p < 0.05$, (**) $p < 0.01$, (***) $p < 0.001$ and (****) $p < 0.0001$, using two-way ANOVA with Tukey's tests. All other differences are non-significant

At 7 days, cell recruitment was similar in all aged mouse groups, but still increased for young mice, suggesting that the effects of MCP-1 last longer in younger mice. Of note, the exacerbated cell infiltration observed in the coated (no cytokine) aged mice group diminished to similar levels observed in other groups. Interestingly, the degree of cell recruitment observed in

any of the eluting meshes containing MCP-1 was not that extensive as the one observed in the coating containing no cytokines, suggesting that cells other than macrophages and the aged microenvironment play an important role in this response. A study performed by Lohmann et al. [167], has shown that glycosaminoglycan-based hydrogels sequester inflammatory chemokines such as MCP-1, IL-8 and MIP-1β, from chronic wounds fluids. It may be possible that the coating also captures the inflammatory chemokines from the aged microenvironment, but instead of sequestering and diluting the cytokines in the hydrogel bulk, the coating concentrates all the inflammatory cytokines in the surface of the mesh biomaterial, enhancing cell infiltration. This would also be consistent with results at 7 days, where the coating has been mostly degraded and therefore both cytokine sequestering and cell recruitment have diminished. This would not be the case for young mice, where the microenvironment is not as inflammatory as in aged mice.

4.3.10 Effects of single and sequential delivery regimens on macrophage polarization at the early-stages of the host response

Co-immunolabeling of histological tissue sections was performed to assess the effects of each single and sequential delivery regimens on macrophage ($F4/80^+$) recruitment and polarization towards M2 ($Arg\text{-}1^+$ $F4/80^+$, Figure 31) and M1 ($iNOS^+$ $F4/80^+$, Figure 32) macrophages. Quantification revealed that all eluting coated meshes containing MCP-1 were capable of initially increasing $F4/80^+$ macrophage recruitment in both aged and young adult mice, but persisted in aged mice by 7 days, while increased macrophage recruitment in young mice was no longer present (Figure 33). Even though coated (no cytokine) mesh elicited a highly exacerbated recruitment of cells, this was not correlated to $F4/80^+$ macrophage recruitment, suggesting that

cells other than F4/80^{+} macrophages participate in this response influenced by the aged microenvironment.

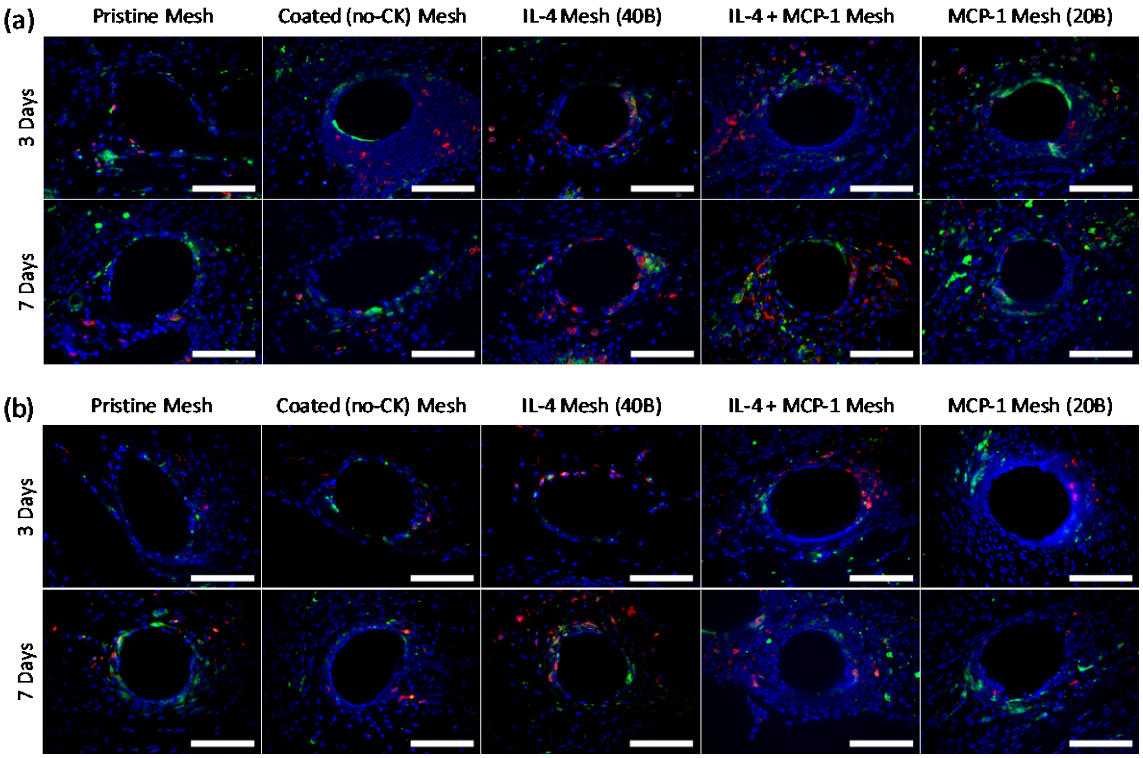

Figure 31. Fluorescence microscopy images of arginase-1 (red) and F4/80 (green) co-immunolabelled tissue sections from (a) old and (b) young mice implanted with a 1 cm^2 piece of pristine, coated (no cytokine), single and sequential MCP-1 and IL-4 eluting meshes, 3 and 7 days post-implantation. DAPI was used to stain cell nuclei. Scale bars represent 50 µm

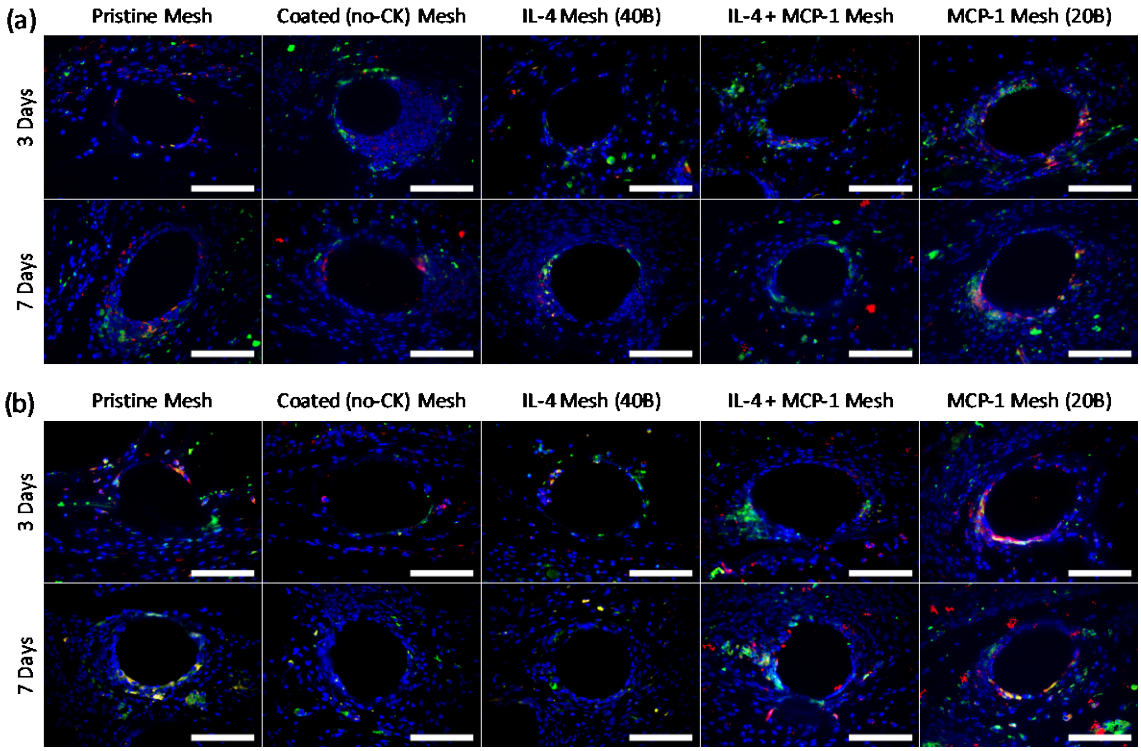

Figure 32. Fluorescence microscopy images of iNOS (red) and F4/80 (green) co-immunolabelled tissue sections from (a) old and (b) young mice implanted with a 1 cm^2 piece of pristine, coated (no cytokine), single and sequential MCP-1 and IL-4 eluting meshes, 3 and 7 days post-implantation. DAPI was used to stain cell nuclei. Scale bars represent 50 µm

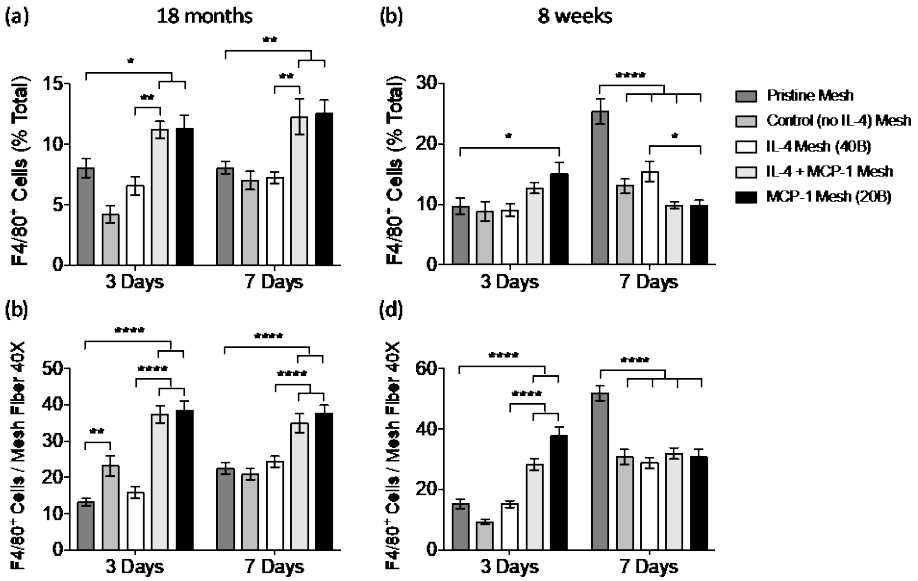

Figure 33. Image analysis of F4/80$^+$ macrophages as percentages of total cells (a, b) and number (c, d) surrounding single mesh fibers of tissue cross sections from (a, c) old and (b, d) young mice implanted with a 1 cm^2 piece of pristine, coated (no cytokine), single and sequential MCP-1 and IL-4 eluting meshes, 3 and 7 days post-implantation. Bars represent the mean ± SEM (N = 8). Statistical significance as (*) $p < 0.05$, (**) $p < 0.01$, (***) $p < 0.001$ and (****) $p < 0.0001$, using two-way ANOVA with Tukey's (groups) and Sidak's (days) tests. All other differences are non-significant

On the other hand, the host response to IL-4, sequential delivery of IL-4/MCP-1 and coating components was well distinct in aged versus young implanted mice. To reveal and quantify M2 macrophages, F4/80$^+$ macrophages have been evaluated in co-labeling with Arg-1. Results have shown that old mice implanted with IL-4 eluting coatings did not have a significant higher percent of M2 (Arg-1$^+$ F4/80$^+$) macrophages, compared to the pristine mesh group. However, the percentage of M2 macrophages in the sequential MCP-1/IL-4 group was significantly increased and consistently increased for both 3 and 7 days, compared to all groups with no IL-4 (Figure 34). Therefore, while single delivery of IL-4 was not enough to counteract the high inflammatory response present in old mice, the sequential delivery regimen of IL-4 and

MCP-1 was capable of restoring recruitment and shift the macrophage response towards an M2-like phenotype. Contrarily, sequential delivery regimens in young mice were not as effective as IL-4 alone promoting an M2-like response. Young mice implanted with MCP-1/IL-4 eluting mesh showed an initial increase in the percentage of M2 macrophages at 3 days, but dramatically decreased to similarly low percentages found in all groups other than IL-4 at 7 days. Therefore, IL-4 eluting mesh was the most effective regimen shifting the response towards an M2 phenotype, in young mice.

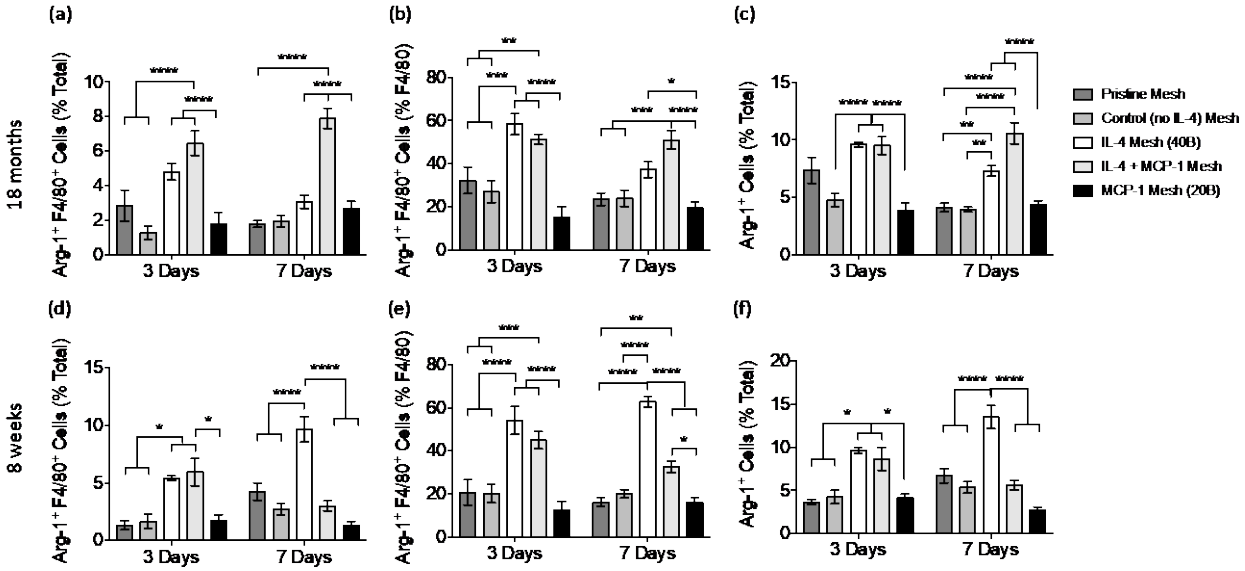

Figure 34. Image analysis of Arg-1$^+$ F4/80$^+$ macrophages as percentages of (a, d) total cells and (b, e) F4/80$^+$ macrophages, as well as (c, f) total percentage of Arg-1$^+$cells, surrounding single mesh fibers of tissue cross sections from (a - c) old and (d - f) young mice implanted with a 1 cm^2 piece of pristine, coated (no cytokine), single and sequential MCP-1 and IL-4 eluting meshes, 3 and 7 days post-implantation. Bars represent the mean ± SEM (N = 8). Statistical significance as (*) $p < 0.05$, (**) $p < 0.01$, (***) $p < 0.001$ and (****) $p < 0.0001$, using two-way ANOVA with Tukey's (groups) and Sidak's (days) tests. All other differences are non-significant

To reveal and quantify M1 macrophages, $F4/80^+$ macrophages have been evaluated in co-labeling with iNOS. Results also reveal some differences between old and young animals. In old animals, mice implanted with both pristine or MCP-1 eluting meshes presented the highest percentages of M1 ($iNOS^+$ $F4/80^+$) macrophages compared to all other groups (Figure 35). Percentage of M1 macrophages in these two groups was similar in both 3 and 7 days. In young mice, the percentage of M1 macrophages was similar for all groups at 3 days, and then at 7 days the pristine mesh group presented the highest percentage of M1 macrophages, in contrast to mice implanted with MCP-1, that did not elicit higher percentages of M1 macrophages. This suggest that MCP-1 only affects macrophage recruitment, but does not have effects on macrophage polarization, and it is consistent with other studies done on MCP-1. Polarization towards M1 macrophages is mainly due to an inflammatory response against the polypropylene biomaterial, and increased percentage of M1 macrophages found in old mice implanted with MCP-1 are likely a consequence of the high percentage of $F4/80^+$ macrophages recruited to the surface of the biomaterial, that become M1 macrophages due to the highly inflammatory environment of aged mice.

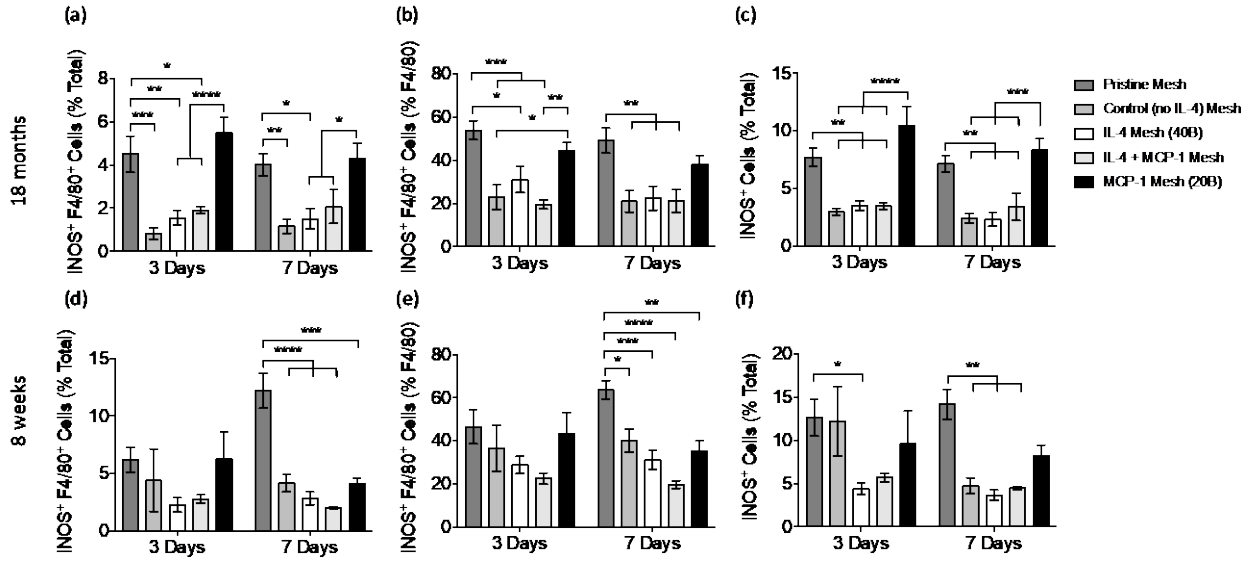

Figure 35. Image analysis of iNOS$^+$ F4/80$^+$ macrophages as percentages of (a, d) total cells and (b, e) F4/80$^+$ macrophages, as well as (c, f) total percentage of iNOS$^+$cells, surrounding single mesh fibers of tissue cross sections from (a - c) old and (d - f) young mice implanted with a 1 cm^2 piece of pristine, coated (no cytokine), single and sequential MCP-1 and IL-4 eluting meshes, 3 and 7 days post-implantation. Bars represent the mean ± SEM (N = 8). Statistical significance as (*) $p < 0.05$, (**) $p < 0.01$, (***) $p < 0.001$ and (****) $p < 0.0001$, using two-way ANOVA with Tukey's (groups) and Sidak's (days) tests. All other differences are non-significant

4.3.11 Effects of single and sequential delivery regimens in the host response in the long-term

The effects of macrophage recruitment and polarization via single and sequential delivery regimens in the long term have been evaluated by means of capsule deposition assessment 90 days post-implantation. Histological tissue sections have been stained with Masson's Trichrome to reveal the presence, morphology and distribution of the fibrotic capsule surrounding the surgical mesh implant. First of all, all mice implanted with MCP-1 meshes showed higher

capsule density than all other groups, but similar capsule area to mice implanted with pristine meshes (Figure 36).

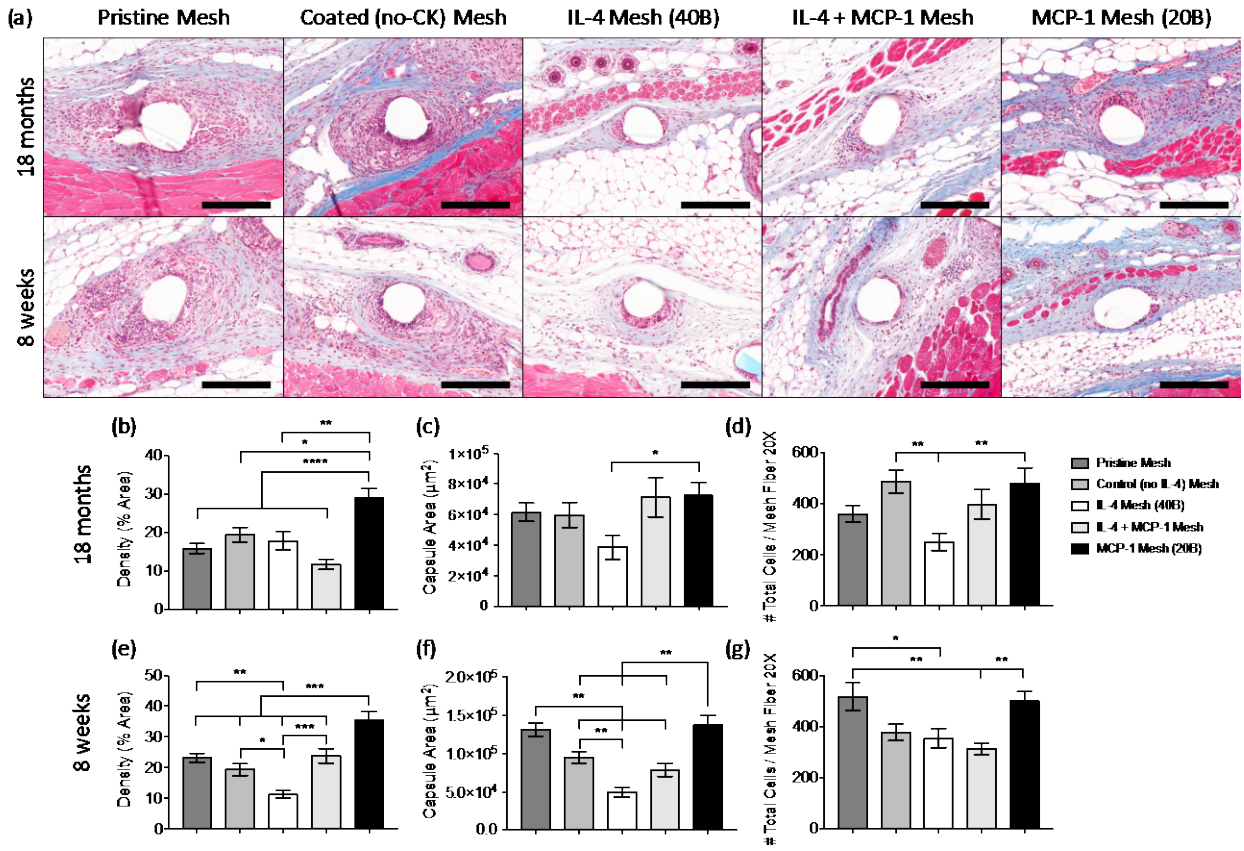

Figure 36. (a) Masson's Trichrome stained tissue sections of old and young mice implanted with a 1 cm^2 piece of pristine, coated (no cytokine), single and sequential MCP-1 and IL-4 eluting meshes, 90 days post-implantation. (b) Image analysis of capsule density (area %; b, e), capsule area (μm^2; c, f) and total cell number (d, g) on single mesh fibers (20X) from aged (b – d) and young (e - g) mice. Bars represent the mean ± SEM. Statistical significance as (*) $p < 0.05$, (**) $p < 0.01$, (***) $p < 0.001$ and (****) $p < 0.0001$, using two-way ANOVA with Tukey's test. All other differences are non-significant

In old mice, implantation of IL-4 eluting mesh was not associated with a reduction in collagen density, but presented diminished capsule area, compared to all other groups. On the other hand, MCP-1/IL-4 group showed less dense capsules compared to all other mesh groups, but no significant differences in capsule area. In young mice, only mice implanted with IL-4 eluting mesh exhibited both decreased density and thickness of the capsule, while the sequential regimen of MCP-1 and IL-4 was capable of decreasing capsule thickness.

In previous studies, it has been suggested that the host response to polypropylene mesh in aged animals is still not resolved by 90 days, revealed by the significantly higher number of cells surrounding the implant (Figure 27d). To evaluate if this response is still unresolved in the presence of single and sequential delivery regimens, we have quantified the number of cells and compared to young mice as well. Results show that mice implanted with MCP-1 eluting mesh have similar cell numbers to the pristine mesh groups in both old and young mice (Figure 36d, g). In aged mice, only IL-4 presented a significant reduction in the number of cells, compared to the pristine mesh group. A reduction in the number of cells was also observed in young mice implanted with both IL-4 and MCP-1/IL-4 eluting meshes, compared to pristine meshes.

4.4 CONCLUSIONS

Taken together, the results of the present work suggest that there are significant differences between the host response to materials in young and aged animals. These differences could not be accounted for by age-related accumulation of cell-intrinsic defects alone, and it is likely that the local tissue microenvironment also plays a large role in dictating the host response regardless of material composition. The present study used only a limited set of surface markers and makes

inferences about the origin of cells based upon these markers. Further study is necessary to determine the specific origin of the cells which participate in the host response in young and old animals as well as to clearly determine their in vivo phenotype and functional profile. However, it is clear that there are differences in the host response between young and aged animals, and that a better understanding of these differences will help to design materials and strategies which that more effectively modulate the host immune response in aged individuals.

It has been demonstrated that the multilayered nature of layer by layer coatings can be used to provide both concomitant and sequential delivery of MCP-1 and IL-4. The concentration of cytokine in the coating solution is proportional to the amount released in vitro, while the number of layers influences both the amount and length of release. In vivo implantation of eluting meshes revealed that the effects of MCP-1 promoting cell and macrophage recruitment are preserved in both old and young animals, restoring the delayed recruitment in the host response of aged mice. However, the host response in presence of IL-4, sequential delivery of IL-4/MCP-1 and coating components was well distinct in old versus young implanted mice. While single delivery of IL-4 was not enough to counteract the high inflammatory response present in old mice, the sequential delivery regimen of IL-4 and MCP-1 was capable of restoring recruitment and shift the macrophage response towards an M2-like phenotype, associated to decreased capsule deposition in the long term. Contrarily, sequential delivery regimens in young mice were not as effective as IL-4 alone promoting an M2-like response, but still capable of reducing inflammatory macrophages and capsule deposition. In addition, the exacerbated cell recruitment in aged mice implanted with coated (no cytokine) mesh was not correlated to an increase in recruited F4/80^{+} macrophages nor effects on polarization, suggesting that other cells influenced by the aged microenvironment may play an important role promoting this response.

These results raise important questions about the design and performance of biomaterials-based therapies and devices often intended to treat elderly patients and demonstrates that a proper understanding of patient- and context-dependent biological responses have the potential to improve outcomes in aged individuals.

5.0 DISSERTATION SYNOPSIS

The work presented in this dissertation exploits macrophage modulation as an approach to mitigate the foreign body reaction and promote better integration of implanted biomaterials into the host tissue, using a multilayered eluting coating for single and sequential delivery of cytokines that preserve the architecture and functionality of surgical mesh implants. Modulation of macrophage are mainly focused to facilitate an M1 to M2 transition, or modify macrophage recruitment. This strategy is innovative and has the potential to outperform current approaches, as it is focused on the positive aspects of the immune system, instead of avoiding the immune response. In addition, the impact of aging on the host response against biomaterials was elucidated and used to develop improved and contextual delivery regimens, exploiting the sequential delivery capabilities of the coating to deliver multiple cytokines. The major findings for each aim are outlined below.

5.1 MAJOR FINDINGS

5.1.1 Aim I

To develop a conformal eluting coating for localized and transient delivery of IL-4 that preserves both the architecture and structural properties of polypropylene surgical mesh implants.

- Surface characterization confirmed that a uniform and conformal coating was done, containing both Chitosan and Dermatan Sulfate.
- The coating can be uniformly loaded with IL-4 through the entire surface of the mesh.
- Release assays showed that the amount of IL-4 and length of release are dependent on the number of coating bilayers containing IL-4.
- The coating procedure and ETO sterilization did not alter the bioactivity of IL-4, being capable of polarizing bone marrow-derived macrophages in vitro.
- The mesh coating seems to enhance and/or protect the bioactivity of IL-4.
- The coating preserved both the architecture and structural properties of the surgical meshes.

5.1.2 Aim II

To study the effects of the released IL-4 and the coating components on the host response at early stages and in the long term, in a murine implantation model. The host response was studied using histological assessments, macrophage characterization and gene expression analysis.

- The release of IL-4 in mesh implanted mice increased polarization of macrophages towards an M2 phenotype in all macrophage populations evaluated.
- The effects of the released IL-4 were localized up to 50 μm of distance from the mesh surface.
- $F4/80^+$, $CD68^+$ and $CD11b^+$ macrophages showed distinct susceptibility to IL-4 and components of the coating.
- The coating components were associated to a decrease in $F4/80^+$ macrophages and a reduction in M1 macrophages in both $F4/80^+$ and $CD68^+$ macrophage populations.

- Mice implanted with IL-4 mesh presented upregulation in M2-like macrophage genes, downregulation in M1-like macrophage genes and increased MMP activity.
- Shifts towards an M2-like macrophage response in the IL-4 group were associated to decreased thickness and deposition of fibrotic capsule. Also, changes in capsule composition were observed, in which the thinnest collagen fibers predominated, compared to all other groups.
- Even though the presence of the coating was associated to diminished percentage of M1 macrophages, it was not capable of shifting the macrophage response towards an M2 phenotype, and was not associated to changes in capsule deposition and composition.

5.1.3 Aim III

To determine the impact of aging in the host response against biomaterials, regarding cellular response, macrophage regulation and implant integration into the host tissue.

- The host response against polypropylene mesh in old animals presented delayed recruitment of cells and macrophages, compared to young animals.
- Old mice presented changes in surface marker expression of macrophages participating in the host response.
- The macrophage response in old animals was found to be highly shifted to an M1 phenotype, compared to young animals.
- In the long term (90 days), old mice presented unresolved inflammation, but no changes in deposition and composition of fibrotic capsule.
- The differences observed between young and old mice could not be accounted for by age-related accumulation of cell-intrinsic defects alone, suggesting that the local tissue

microenvironment also plays a large role in dictating the host response regardless of material composition.

5.1.4 Sub-Aim III

To develop a sequential delivery regimen of MCP-1 and IL-4, to restore the delayed macrophage recruitment and reverse the highly inflammatory M1 response found in old animals, respectively. Single and sequential delivery regiments were evaluated in both old and young mice regarding cellular response, macrophage regulation and implant integration into the host tissue.

- MCP-1 was uniformly loaded through the entire surface of the mesh, and released in bioactive form to increase cell recruitment in vivo.
- The multilayered nature of the layer by layer coating can be used to provide both concomitant and sequential delivery of MCP-1 and IL-4.
- The changes in the concentration of cytokine in the coating solutions are directly proportional to the amount released in vitro, with no changes in length of release.
- Implantation of eluting meshes revealed that the effects of MCP-1 promoting cell and macrophage recruitment are preserved in both old and young animals, restoring the delayed recruitment in the host response of aged mice.
- The host response to single and sequential delivery regimens was well distinct in old versus young animals:
    1) While single delivery of IL-4 was not enough to counteract the high inflammatory response present in old mice, the sequential delivery regimen of IL-4 and MCP-1 was capable of restoring recruitment and shift the macrophage response towards an M2-like phenotype, associated to decreased capsule deposition in the long term.

2) Sequential delivery regimens of MCP-1 and IL-4 in young mice were not as effective as IL-4 alone promoting an M2-like macrophage response, but still capable of reducing pro-inflammatory M1 macrophages and capsule deposition.

- The exacerbated cell recruitment in aged mice implanted with coated (no cytokine) mesh was not correlated to an increase in recruited $F4/80^{+}$ macrophages nor effects on polarization, suggesting that other cells influenced by the aged microenvironment may play an important role promoting this response.

5.2 LIMITATIONS AND FUTURE DIRECTIONS

Release assays were used to study the release of cytokines in vitro and as an estimate for release in vivo; however, it is currently unknown whether coating degradation and release of MCP-1 and IL-4 in vivo occurs in a similar manner. The implantation studies and results regarding the effects of cytokines at early stages of the host response seem to suggest that the length of cytokine release is shorter - with IL-4 lasting less than 14 days and MCP-1 less than 7 days, in which the effects of these cytokines are not present. Further studies will be performed using fluorescently tagged cytokines on live imaging systems to determine the release of cytokines in vivo. Similarly, we have investigated the effects of only 40 bilayers of IL-4 (2 ng/cm^2 of mesh) and 20 bilayers of MCP-1 (1 - 2 ng/cm^2 of mesh) on the host response against mesh, so further regimens will be evaluated based on in vivo release studies.

To evaluate the feasibility of our approach, we have performed a subcutaneous implantation of surgical mesh in a mouse model, due to the immunological similarities with human, but also robustness and reliability of the surgical procedure. However, it presents limited

clinical relevance compared to transabdominal and transvaginal surgeries performed for pelvic organ prolapse. These surgical procedures are more complex and use bigger pieces of mesh, which are sutured in multiple tissue structures to hold the implant in place, being able to stand uniaxial tensile forces in the vaginal cavity. This mechanical component is not present in our model, as small pieces of mesh are lying flat in the abdomen after subcutaneous implantation, so the only factor playing a major role in our study is the host response against the mesh biomaterial. It is also likely that our subcutaneous procedure does not recapitulate entirely the biological structure and properties of the vaginal tissue, as the host response to polypropylene mesh in the vagina has been reported to be significantly different than that in the abdominal wall musculature [21, 139]. Consequently, a more clinically relevant model is currently under study using an abdominal sacrocolpopexy surgical procedure in rabbits.

Study of macrophage populations was limited to the use of three common markers - F4/80, CD68 and CD11b. Similarly, the identification of M1 and M2 macrophages was limited to the use of iNOS and Arg-1, respectively. Although results were clear and conclusive suggesting shifts in macrophage polarization, additional macrophage characterization of cells from explanted tissues are currently being performed using flow cytometry analysis, capable of identifying multiple surface markers in a single cell. Gene expression assays were performed to evaluate more exhaustively the early phenotypic changes promoted by IL-4 and the coating components. Further protein studies will be performed in future studies to reveal the downstream activation cascades of these genes, as the expression of some genes are not necessarily correlated with protein expression.

Quantification through image analysis to study the host response and macrophage characterization was often performed in the area of single fibers rather than knots, in order to

normalize the host response to the same surface area of mesh in our analysis. Surface area normalization in mesh knots is difficult due to the complex variety of shapes, including but not limited to number of fibers, distance between fibers and fused fibers. Recent published studies have demonstrated that density (and hence area) of the mesh is a local driver of the host macrophage response, where increased mesh density is associated with a denser cellular response [21, 22]. While investigation of the differences in the host response between fibers and knots was beyond the scope of the present study, it will be important to evaluate the effects of the cytokine eluting meshes in knots to illustrate cytokine effects in the presence of high density and complex geometry of the implant.

Deposition, thickness and composition of the capsule, as well as total cell number were the only assessments done to study the long-term outcomes of the host response against eluting mesh. A few foreign body giant cells (FBGC) were observed at the tissue-biomaterial interface on each group; however, quantification and comparison are not reliable due to the reduced number of FBGC on each image field (from zero to three cells per field). Presence of mesh shrinking is another common parameter evaluated in surgical mesh implantation studies, which is a reduction in size of the implant and believed to be a consequence of scar tissue formation around the mesh implant due to stress shielding. We are unable to perform this assessment due to the reduced size of the implant, and because the mesh is implanted in a flat subcutaneous pocket with no sutures, and hence the mechanical contribution to this response is minimal and well distinct to the tensile forces experienced in the vaginal cavity. In abdominal and transvaginal implantation of mesh, sutures are placed to hold the mesh in position, where mainly uniaxial tensile forces are exerted into mesh and playing a more important role in the host response against mesh.

5.3 CONCLUSIONS

The results of this study have shown that modulation of macrophage recruitment and polarization is a promising approach to improve implant integration into the host tissue, rather than only mitigating the foreign body reaction. The present work demonstrates in a similar way to previous studies that an increased M2 to M1 ratio is associated with better remodeling outcomes, and in this particular case to an improved resolution of the host response against biomaterials.

In addition, implantation studies on aged animals have shown that the impact of aging in the host response against biomaterials is significant, resulting in delayed recruitment, macrophage imbalances and impaired resolution of the host response in the long term. The improved performance of our contextual and sequential delivery regimen in old animals demonstrates that a proper understanding of the biological context is instrumental for the clinical success of biomaterial-based approaches in aged individuals. The well distinct host response to single and sequential delivery regimens in old versus young animals suggests that the aged microenvironment is playing an important role in these altered responses.

Finally, the multilayered eluting coating technology has demonstrated to be an ideal platform to provide localized, controlled and sequential delivery of proteins, preserving the architecture and functionality of implanted biomaterials. While the present study focused on polypropylene mesh commonly used for pelvic organ prolapse, the methods and findings presented can likely be extended to include other material types and applications.

BIBLIOGRAPHY

[1] Z. Jallah, R. Liang, A. Feola, W. Barone, S. Palcsey, S.D. Abramowitch, N. Yoshimura, P. Moalli, The impact of prolapse mesh on vaginal smooth muscle structure and function, BJOG (2015).

[2] A.H. MacLennan, A.W. Taylor, D.H. Wilson, D. Wilson, The prevalence of pelvic floor disorders and their relationship to gender, age, parity and mode of delivery, BJOG 107(12) (2000) 1460-70.

[3] J. Mant, R. Painter, M. Vessey, Epidemiology of genital prolapse: observations from the Oxford Family Planning Association Study, Br J Obstet Gynaecol 104(5) (1997) 579-85.

[4] S.E. Swift, The distribution of pelvic organ support in a population of female subjects seen for routine gynecologic health care, Am J Obstet Gynecol 183(2) (2000) 277-85.

[5] A.M. Weber, H.E. Richter, Pelvic organ prolapse, Obstet Gynecol 106(3) (2005) 615-34.

[6] J.E. Jelovsek, C. Maher, M.D. Barber, Pelvic organ prolapse, Lancet 369(9566) (2007) 1027-38.

[7] J.O. DeLancey, Anatomy and biomechanics of genital prolapse, Clin Obstet Gynecol 36(4) (1993) 897-909.

[8] J.O. DeLancey, The anatomy of the pelvic floor, Curr Opin Obstet Gynecol 6(4) (1994) 313-6.

[9] G.B. Diwadkar, M.D. Barber, B. Feiner, C. Maher, J.E. Jelovsek, Complication and reoperation rates after apical vaginal prolapse surgical repair: a systematic review, Obstet Gynecol 113(2 Pt 1) (2009) 367-73.

[10] P. Dallenbach, To mesh or not to mesh: a review of pelvic organ reconstructive surgery, Int J Womens Health 7 (2015) 331-43.

[11] C. Cheon, C. Maher, Economics of pelvic organ prolapse surgery, Int Urogynecol J 24(11) (2013) 1873-6.

[12] D.R. Ellington, H.E. Richter, Indications, contraindications, and complications of mesh in surgical treatment of pelvic organ prolapse, Clin Obstet Gynecol 56(2) (2013) 276-88.

[13] C. Bower, J.S. Roth, Economics of abdominal wall reconstruction, Surg Clin North Am 93(5) (2013) 1241-53.

[14] L.L. Subak, L.E. Waetjen, S. van den Eeden, D.H. Thom, E. Vittinghoff, J.S. Brown, Cost of pelvic organ prolapse surgery in the United States, Obstet Gynecol 98(4) (2001) 646-51.

[15] J.M. Wu, A.F. Hundley, R.G. Fulton, E.R. Myers, Forecasting the prevalence of pelvic floor disorders in U.S. Women: 2010 to 2050, Obstet Gynecol 114(6) (2009) 1278-83.

[16] M. Murphy, A. Holzberg, H. van Raalte, N. Kohli, H.B. Goldman, V. Lucente, N. Pelvic Surgeons, Time to rethink: an evidence-based response from pelvic surgeons to the FDA Safety Communication: "UPDATE on Serious Complications Associated with Transvaginal Placement of Surgical Mesh for Pelvic Organ Prolapse", Int Urogynecol J 23(1) (2012) 5-9.

[17] P. Collinet, F. Belot, P. Debodinance, E. Ha Duc, J.P. Lucot, M. Cosson, Transvaginal mesh technique for pelvic organ prolapse repair: mesh exposure management and risk factors, Int Urogynecol J Pelvic Floor Dysfunct 17(4) (2006) 315-20.

[18] R.U. Margulies, C. Lewicky-Gaupp, D.E. Fenner, E.J. McGuire, J.Q. Clemens, J.O. Delancey, Complications requiring reoperation following vaginal mesh kit procedures for prolapse, Am J Obstet Gynecol 199(6) (2008) 678 e1-4.

[19] E.J. Stanford, A. Cassidenti, M.D. Moen, Traditional native tissue versus mesh-augmented pelvic organ prolapse repairs: providing an accurate interpretation of current literature, Int Urogynecol J 23(1) (2012) 19-28.

[20] S.J. Pulliam, T.R. Ferzandi, L.S. Hota, E.A. Elkadry, P.L. Rosenblatt, Use of synthetic mesh in pelvic reconstructive surgery: a survey of attitudes and practice patterns of urogynecologists, Int Urogynecol J Pelvic Floor Dysfunct 18(12) (2007) 1405-8.

[21] B.N. Brown, D. Mani, A.L. Nolfi, R. Liang, S. Abramowitch, P.A. Moalli, Characterization of the host inflammatory response following implantation of prolapse mesh in rhesus macaque, Am J Obstet Gynecol (2015).

[22] A.L. Nolfi, B.N. Brown, R. Liang, S.L. Palcsey, M.J. Bonidie, S.D. Abramowitch, P.A. Moalli, Host response to synthetic mesh in women with mesh complications, Am J Obstet Gynecol (2016).

[23] F.A. Ganj, O.A. Ibeanu, A. Bedestani, T.E. Nolan, R.R. Chesson, Complications of transvaginal monofilament polypropylene mesh in pelvic organ prolapse repair, Int Urogynecol J Pelvic Floor Dysfunct 20(8) (2009) 919-25.

[24] B. Feiner, J.E. Jelovsek, C. Maher, Efficacy and safety of transvaginal mesh kits in the treatment of prolapse of the vaginal apex: a systematic review, BJOG 116(1) (2009) 15-24.

[25] C.M. Maher, B. Feiner, K. Baessler, C.M. Glazener, Surgical management of pelvic organ prolapse in women: the updated summary version Cochrane review, Int Urogynecol J 22(11) (2011) 1445-57.

[26] L.C. Skoczylas, L.C. Turner, L. Wang, D.G. Winger, J.P. Shepherd, Changes in prolapse surgery trends relative to FDA notifications regarding vaginal mesh, Int Urogynecol J 25(4) (2014) 471-7.

[27] R. Liang, K. Knight, S. Abramowitch, P.A. Moalli, Exploring the basic science of prolapse meshes, Curr Opin Obstet Gynecol 28(5) (2016) 413-9.

[28] R. Liang, S. Abramowitch, K. Knight, S. Palcsey, A. Nolfi, A. Feola, S. Stein, P.A. Moalli, Vaginal degeneration following implantation of synthetic mesh with increased stiffness, BJOG 120(2) (2013) 233-43.

[29] W.R. Barone, P.A. Moalli, S.D. Abramowitch, Textile properties of synthetic prolapse mesh in response to uniaxial loading, Am J Obstet Gynecol 215(3) (2016) 326 e1-9.

[30] J.M. Anderson, A. Rodriguez, D.T. Chang, Foreign body reaction to biomaterials, Seminars in immunology 20(2) (2008) 86-100.

[31] R. Liang, W. Zong, S. Palcsey, S. Abramowitch, P.A. Moalli, Impact of prolapse meshes on the metabolism of vaginal extracellular matrix in rhesus macaque, Am J Obstet Gynecol 212(2) (2015) 174 e1-7.

[32] B.N. Brown, R. Londono, S. Tottey, L. Zhang, K.A. Kukla, M.T. Wolf, K.A. Daly, J.E. Reing, S.F. Badylak, Macrophage phenotype as a predictor of constructive remodeling following the implantation of biologically derived surgical mesh materials, Acta Biomater 8(3) (2012) 978-87.

[33] B.N. Brown, B.D. Ratner, S.B. Goodman, S. Amar, S.F. Badylak, Macrophage polarization: an opportunity for improved outcomes in biomaterials and regenerative medicine, Biomaterials 33(15) (2012) 3792-802.

[34] B.N. Brown, B.M. Sicari, S.F. Badylak, Rethinking regenerative medicine: a macrophage-centered approach, Frontiers in immunology 5 (2014) 510.

[35] D.M. Mosser, J.P. Edwards, Exploring the full spectrum of macrophage activation, Nature reviews. Immunology 8(12) (2008) 958-69.

[36] J. Xue, S.V. Schmidt, J. Sander, A. Draffehn, W. Krebs, I. Quester, D. De Nardo, T.D. Gohel, M. Emde, L. Schmidleithner, H. Ganesan, A. Nino-Castro, M.R. Mallmann, L. Labzin, H. Theis, M. Kraut, M. Beyer, E. Latz, T.C. Freeman, T. Ulas, J.L. Schultze, Transcriptome-based network analysis reveals a spectrum model of human macrophage activation, Immunity 40(2) (2014) 274-88.

[37] B.N. Brown, S.F. Badylak, Expanded applications, shifting paradigms and an improved understanding of host-biomaterial interactions, Acta Biomater 9(2) (2013) 4948-55.

[38] M.T. Wolf, C.L. Dearth, C.A. Ranallo, S.T. LoPresti, L.E. Carey, K.A. Daly, B.N. Brown, S.F. Badylak, Macrophage polarization in response to ECM coated polypropylene mesh, Biomaterials 35(25) (2014) 6838-49.

[39] A. Darehzereshki, M. Goldfarb, J. Zehetner, A. Moazzez, J.C. Lipham, R.J. Mason, N. Katkhouda, Biologic versus nonbiologic mesh in ventral hernia repair: a systematic review and meta-analysis, World J Surg 38(1) (2014) 40-50.

[40] X. Jia, C. Glazener, G. Mowatt, G. MacLennan, C. Bain, C. Fraser, J. Burr, Efficacy and safety of using mesh or grafts in surgery for anterior and/or posterior vaginal wall prolapse: systematic review and meta-analysis, BJOG 115(11) (2008) 1350-61.

[41] G. Gigliobianco, S.R. Regueros, N.I. Osman, J. Bissoli, A.J. Bullock, C.R. Chapple, S. MacNeil, Biomaterials for pelvic floor reconstructive surgery: how can we do better?, Biomed Res Int 2015 (2015) 968087.

[42] J.M. Anderson, K. Defife, A. McNally, T. Collier, C. Jenney, Monocyte, macrophage and foreign body giant cell interactions with molecularly engineered surfaces, J Mater Sci Mater Med 10(10/11) (1999) 579-88.

[43] J.A. Jones, A.K. McNally, D.T. Chang, L.A. Qin, H. Meyerson, E. Colton, I.L. Kwon, T. Matsuda, J.M. Anderson, Matrix metalloproteinases and their inhibitors in the foreign body reaction on biomaterials, J Biomed Mater Res A 84(1) (2008) 158-66.

[44] K.M. DeFife, M.S. Shive, K.M. Hagen, D.L. Clapper, J.M. Anderson, Effects of photochemically immobilized polymer coatings on protein adsorption, cell adhesion, and the foreign body reaction to silicone rubber, J Biomed Mater Res 44(3) (1999) 298-307.

[45] Y. Ikada, Surface modification of polymers for medical applications, Biomaterials 15(10) (1994) 725-36.

[46] S. Darzi, I. Urbankova, K. Su, J. White, C. Lo, D. Alexander, J.A. Werkmeister, C.E. Gargett, J. Deprest, Tissue response to collagen containing polypropylene meshes in an ovine vaginal repair model, Acta Biomater 39 (2016) 114-123.

[47] D.P. Poppas, J.J. Sung, C.M. Magro, J. Chen, J.P. Toyohara, B.J. Ramshaw, D. Felsen, Hydrogel coated mesh decreases tissue reaction resulting from polypropylene mesh implant: implication in hernia repair, Hernia 20(4) (2016) 623-32.

[48] L.M. Pierce, J.R. Asarias, P.T. Nguyen, J.R. Mings, A.P. Gehrich, Inflammatory cytokine and matrix metalloproteinase expression induced by collagen-coated and uncoated polypropylene meshes in a rat model, Am J Obstet Gynecol 205(1) (2011) 82 e1-9.

[49] R.T. Siniscalchi, M. Melo, P.C. Palma, I.M. Dal Fabbro, C. Vidal Bde, C.L. Riccetto, Highly purified collagen coating enhances tissue adherence and integration properties of monofilament polypropylene meshes, Int Urogynecol J 24(10) (2013) 1747-54.

[50] Y. Altinel, E. Ozturk, G. Ozkaya, E.U. Akyildiz, Y. Ulcay, H. Ozguc, The effect of a chitosan coating on the adhesive potential and tensile strength of polypropylene meshes, Hernia 16(6) (2012) 709-14.

[51] N. Udpa, S.R. Iyer, R. Rajoria, K.E. Breyer, H. Valentine, B. Singh, S.P. McDonough, B.N. Brown, L.J. Bonassar, Y. Gao, Effects of chitosan coatings on polypropylene mesh for implantation in a rat abdominal wall model, Tissue Eng Part A 19(23-24) (2013) 2713-23.

[52] S.T. Jayanth, A. Pulimood, D. Abraham, A. Rajaram, M.J. Paul, A. Nair, A randomized controlled experimental study comparing chitosan coated polypropylene mesh and Proceed mesh for abdominal wall defect closure, Ann Med Surg (Lond) 4(4) (2015) 388-94.

[53] M. Cervigni, F. Natale, C. La Penna, M. Saltari, A. Padoa, M. Agostini, Collagen-coated polypropylene mesh in vaginal prolapse surgery: an observational study, Eur J Obstet Gynecol Reprod Biol 156(2) (2011) 223-7.

[54] W. He, G.C. McConnell, T.M. Schneider, R.V. Bellamkonda, A novel anti-inflammatory surface for neural electrodes, Advanced Materials 19(21) (2007) 3529-3533.

[55] C.J. Brandt, D. Kammer, A. Fiebeler, U. Klinge, Beneficial effects of hydrocortisone or spironolactone coating on foreign body response to mesh biomaterial in a mouse model, J Biomed Mater Res A 99(3) (2011) 335-43.

[56] M. Keeney, H. Waters, K. Barcay, X. Jiang, Z. Yao, J. Pajarinen, K. Egashira, S.B. Goodman, F. Yang, Mutant MCP-1 protein delivery from layer-by-layer coatings on orthopedic implants to modulate inflammatory response, Biomaterials 34(38) (2013) 10287-95.

[57] X. Jiang, T. Sato, Z. Yao, M. Keeney, J. Pajarinen, T.H. Lin, F. Loi, K. Egashira, S. Goodman, F. Yang, Local delivery of mutant CCL2 protein-reduced orthopaedic implant wear particle-induced osteolysis and inflammation in vivo, Journal of orthopaedic research : official publication of the Orthopaedic Research Society 34(1) (2016) 58-64.

[58] E.M. Hetrick, H.L. Prichard, B. Klitzman, M.H. Schoenfisch, Reduced foreign body response at nitric oxide-releasing subcutaneous implants, Biomaterials 28(31) (2007) 4571-80.

[59] S.P. Nichols, A. Koh, N.L. Brown, M.B. Rose, B. Sun, D.L. Slomberg, D.A. Riccio, B. Klitzman, M.H. Schoenfisch, The effect of nitric oxide surface flux on the foreign body response to subcutaneous implants, Biomaterials 33(27) (2012) 6305-12.

[60] S. Chen, J.A. Jones, Y. Xu, H.Y. Low, J.M. Anderson, K.W. Leong, Characterization of topographical effects on macrophage behavior in a foreign body response model, Biomaterials 31(13) (2010) 3479-91.

[61] S. Lee, J. Choi, S. Shin, Y.M. Im, J. Song, S.S. Kang, T.H. Nam, T.J. Webster, S.H. Kim, D. Khang, Analysis on migration and activation of live macrophages on transparent flat and nanostructured titanium, Acta Biomater 7(5) (2011) 2337-44.

[62] Q.L. Ma, L.Z. Zhao, R.R. Liu, B.Q. Jin, W. Song, Y. Wang, Y.S. Zhang, L.H. Chen, Y.M. Zhang, Improved implant osseointegration of a nanostructured titanium surface via mediation of macrophage polarization, Biomaterials 35(37) (2014) 9853-9867.

[63] D.M. Faulk, R. Londono, M.T. Wolf, C.A. Ranallo, C.A. Carruthers, J.D. Wildemann, C.L. Dearth, S.F. Badylak, ECM hydrogel coating mitigates the chronic inflammatory response to polypropylene mesh, Biomaterials 35(30) (2014) 8585-95.

[64] M.T. Wolf, C.A. Carruthers, C.L. Dearth, P.M. Crapo, A. Huber, O.A. Burnsed, R. Londono, S.A. Johnson, K.A. Daly, E.C. Stahl, J.M. Freund, C.J. Medberry, L.E. Carey, A. Nieponice, N.J. Amoroso, S.F. Badylak, Polypropylene surgical mesh coated with extracellular matrix mitigates the host foreign body response, J Biomed Mater Res A 102(1) (2014) 234-46.

[65] N. Mokarram, A. Merchant, V. Mukhatyar, G. Patel, R.V. Bellamkonda, Effect of modulating macrophage phenotype on peripheral nerve repair, Biomaterials 33(34) (2012) 8793-801.

[66] T. Sato, J. Pajarinen, A. Behn, X. Jiang, T.H. Lin, F. Loi, Z. Yao, K. Egashira, F. Yang, S.B. Goodman, The Effect of Local IL-4 Delivery or CCL2 Blockade on Implant Fixation and Bone Structural Properties in a Mouse Model of Wear Particle Induced Osteolysis, J Biomed Mater Res A (2016).

[67] K.L. Spiller, S. Nassiri, C.E. Witherel, R.R. Anfang, J. Ng, K.R. Nakazawa, T. Yu, G. Vunjak-Novakovic, Sequential delivery of immunomodulatory cytokines to facilitate the M1-to-M2 transition of macrophages and enhance vascularization of bone scaffolds, Biomaterials 37 (2015) 194-207.

[68] C. Sebastián, J. Lloberas, A. Celada, Molecular and Cellular Aspects of Macrophage Aging, in: T. Fulop, C. Franceschi, K. Hirokawa, G. Pawelec (Eds.), Handbook on Immunosenescence, Springer Netherlands2009, pp. 919-945.

[69] E. Linehan, Y. Dombrowski, R. Snoddy, P.G. Fallon, A. Kissenpfennig, D.C. Fitzgerald, Aging impairs peritoneal but not bone marrow-derived macrophage phagocytosis, Aging cell 13(4) (2014) 699-708.

[70] S. Mahbub, C.R. Deburghgraeve, E.J. Kovacs, Advanced age impairs macrophage polarization, J Interferon Cytokine Res 32(1) (2012) 18-26.

[71] S.B. Orenstein, E.R. Saberski, D.L. Kreutzer, Y.W. Novitsky, Comparative analysis of histopathologic effects of synthetic meshes based on material, weight, and pore size in mice, J Surg Res 176(2) (2012) 423-9.

[72] R.K. Huffaker, T.W. Muir, A. Rao, S.S. Baumann, T.J. Kuehl, L.M. Pierce, Histologic response of porcine collagen-coated and uncoated polypropylene grafts in a rabbit vagina model, Am J Obstet Gynecol 198(5) (2008) 582 e1-7.

[73] L. Liu, G. Chen, T. Chao, B.D. Ratner, E.H. Sage, S. Jiang, Reduced foreign body reaction to implanted biomaterials by surface treatment with oriented osteopontin, J Biomater Sci Polym Ed 19(6) (2008) 821-35.

[74] K. Junge, R. Rosch, U. Klinge, M. Saklak, B. Klosterhalfen, C. Peiper, V. Schumpelick, Titanium coating of a polypropylene mesh for hernia repair: effect on biocompatibilty, Hernia 9(2) (2005) 115-9.

[75] S. Huerta, A. Varshney, P.M. Patel, H.G. Mayo, E.H. Livingston, Biological Mesh Implants for Abdominal Hernia Repair: US Food and Drug Administration Approval Process and Systematic Review of Its Efficacy, JAMA Surg 151(4) (2016) 374-81.

[76] Y. Fei, J. Li, W. Tian, [Application of biological mesh for reconstruction of pelvic floor in patients with perineal hernia], Zhongguo Xiu Fu Chong Jian Wai Ke Za Zhi 28(10) (2014) 1270-2.

[77] G. Peppas, I.D. Gkegkes, M.C. Makris, M.E. Falagas, Biological mesh in hernia repair, abdominal wall defects, and reconstruction and treatment of pelvic organ prolapse: a review of the clinical evidence, Am Surg 76(11) (2010) 1290-9.

[78] G. El-Gazzaz, H.H. Erem, E. Aytac, L. Salcedo, L. Stocchi, R.P. Kiran, Risk of infection and hernia recurrence for patients undergoing ventral hernia repair with non-absorbable or biological mesh during open bowel procedures, Tech Coloproctol 17(3) (2013) 315-20.

[79] J. Borges, J.F. Mano, Molecular interactions driving the layer-by-layer assembly of multilayers, Chem Rev 114(18) (2014) 8883-942.

[80] H. Ai, S.A. Jones, Y.M. Lvov, Biomedical applications of electrostatic layer-by-layer nano-assembly of polymers, enzymes, and nanoparticles, Cell Biochem Biophys 39(1) (2003) 23-43.

[81] M. Macdonald, N.M. Rodriguez, R. Smith, P.T. Hammond, Release of a model protein from biodegradable self assembled films for surface delivery applications, J Control Release 131(3) (2008) 228-34.

[82] M.L. Macdonald, N.M. Rodriguez, N.J. Shah, P.T. Hammond, Characterization of tunable FGF-2 releasing polyelectrolyte multilayers, Biomacromolecules 11(8) (2010) 2053-9.

[83] N.J. Shah, M.N. Hyder, J.S. Moskowitz, M.A. Quadir, S.W. Morton, H.J. Seeherman, R.F. Padera, M. Spector, P.T. Hammond, Surface-mediated bone tissue morphogenesis from tunable nanolayered implant coatings, Sci Transl Med 5(191) (2013) 191ra83.

[84] N.J. Shah, M.N. Hyder, M.A. Quadir, N.M. Dorval Courchesne, H.J. Seeherman, M. Nevins, M. Spector, P.T. Hammond, Adaptive growth factor delivery from a polyelectrolyte coating promotes synergistic bone tissue repair and reconstruction, Proc Natl Acad Sci U S A 111(35) (2014) 12847-52.

[85] N.J. Shah, M.L. Macdonald, Y.M. Beben, R.F. Padera, R.E. Samuel, P.T. Hammond, Tunable dual growth factor delivery from polyelectrolyte multilayer films, Biomaterials 32(26) (2011) 6183-93.

[86] U. Klinge, B. Klosterhalfen, V. Birkenhauer, K. Junge, J. Conze, V. Schumpelick, Impact of polymer pore size on the interface scar formation in a rat model, J Surg Res 103(2) (2002) 208-14.

[87] N. Aumsuwan, S.H. Ye, W.R. Wagner, M.W. Urban, Covalent attachment of multilayers on poly(tetrafluoroethylene) surfaces, Langmuir 27(17) (2011) 11106-10.

[88] B.M. Sicari, J.L. Dziki, B.F. Siu, C.J. Medberry, C.L. Dearth, S.F. Badylak, The promotion of a constructive macrophage phenotype by solubilized extracellular matrix, Biomaterials 35(30) (2014) 8605-12.

[89] K.A. Jones, A. Feola, L. Meyn, S.D. Abramowitch, P.A. Moalli, Tensile properties of commonly used prolapse meshes, Int Urogynecol J Pelvic Floor Dysfunct 20(7) (2009) 847-53.

[90] S.K. Shukla, A.K. Mishra, O.A. Arotiba, B.B. Mamba, Chitosan-based nanomaterials: a state-of-the-art review, Int J Biol Macromol 59 (2013) 46-58.

[91] M. Kong, X.G. Chen, K. Xing, H.J. Park, Antimicrobial properties of chitosan and mode of action: a state of the art review, Int J Food Microbiol 144(1) (2010) 51-63.

[92] C.G. Lee, C.A. Da Silva, C.S. Dela Cruz, F. Ahangari, B. Ma, M.J. Kang, C.H. He, S. Takyar, J.A. Elias, Role of chitin and chitinase/chitinase-like proteins in inflammation, tissue remodeling, and injury, Annu Rev Physiol 73 (2011) 479-501.

[93] E. den Dekker, S. Grefte, T. Huijs, G.B. ten Dam, E.M. Versteeg, L.C. van den Berk, B.A. Bladergroen, T.H. van Kuppevelt, C.G. Figdor, R. Torensma, Monocyte cell surface glycosaminoglycans positively modulate IL-4-induced differentiation toward dendritic cells, J Immunol 180(6) (2008) 3680-8.

[94] R.J. Miron, D.D. Bosshardt, OsteoMacs: Key players around bone biomaterials, Biomaterials 82 (2016) 1-19.

[95] M. Barbeck, A. Motta, C. Migliaresi, R. Sader, C.J. Kirkpatrick, S. Ghanaati, Heterogeneity of biomaterial-induced multinucleated giant cells: Possible importance for the regeneration process?, J Biomed Mater Res A 104(2) (2016) 413-8.

[96] J.M. Anderson, J.A. Jones, Phenotypic dichotomies in the foreign body reaction, Biomaterials 28(34) (2007) 5114-20.

[97] J.D. Bryers, C.M. Giachelli, B.D. Ratner, Engineering biomaterials to integrate and heal: the biocompatibility paradigm shifts, Biotechnology and bioengineering 109(8) (2012) 1898-911.

[98] P.J. Murray, T.A. Wynn, Protective and pathogenic functions of macrophage subsets, Nature reviews. Immunology 11(11) (2011) 723-37.

[99] C.D. Mills, M1 and M2 Macrophages: Oracles of Health and Disease, Critical reviews in immunology 32(6) (2012) 463-88.

[100] B.N. Brown, J.E. Valentin, A.M. Stewart-Akers, G.P. McCabe, S.F. Badylak, Macrophage phenotype and remodeling outcomes in response to biologic scaffolds with and without a cellular component, Biomaterials 30(8) (2009) 1482-91.

[101] B.V. Fearing, M.E. Van Dyke, In vitro response of macrophage polarization to a keratin biomaterial, Acta Biomater 10(7) (2014) 3136-44.

[102] R. Guo, A.R. Merkel, J.A. Sterling, J.M. Davidson, S.A. Guelcher, Substrate modulus of 3D-printed scaffolds regulates the regenerative response in subcutaneous implants through the macrophage phenotype and Wnt signaling, Biomaterials 73 (2015) 85-95.

[103] L.R. Madden, D.J. Mortisen, E.M. Sussman, S.K. Dupras, J.A. Fugate, J.L. Cuy, K.D. Hauch, M.A. Laflamme, C.E. Murry, B.D. Ratner, Proangiogenic scaffolds as functional templates for cardiac tissue engineering, Proc Natl Acad Sci U S A 107(34) (2010) 15211-6.

[104] E.M. Sussman, M.C. Halpin, J. Muster, R.T. Moon, B.D. Ratner, Porous implants modulate healing and induce shifts in local macrophage polarization in the foreign body reaction, Ann Biomed Eng 42(7) (2014) 1508-16.

[105] A.R. Reeves, K.L. Spiller, D.O. Freytes, G. Vunjak-Novakovic, D.L. Kaplan, Controlled release of cytokines using silk-biomaterials for macrophage polarization, Biomaterials 73 (2015) 272-83.

[106] J. Pajarinen, Y. Tamaki, J.K. Antonios, T.H. Lin, T. Sato, Z. Yao, M. Takagi, Y.T. Konttinen, S.B. Goodman, Modulation of mouse macrophage polarization in vitro using IL-4 delivery by osmotic pumps, J Biomed Mater Res A 103(4) (2015) 1339-45.

[107] S.B. Goodman, Wear particles, periprosthetic osteolysis and the immune system, Biomaterials 28(34) (2007) 5044-8.

[108] E. Jamsen, V.P. Kouri, J. Olkkonen, A. Cor, S.B. Goodman, Y.T. Konttinen, J. Pajarinen, Characterization of macrophage polarizing cytokines in the aseptic loosening of total hip replacements, Journal of orthopaedic research : official publication of the Orthopaedic Research Society 32(9) (2014) 1241-6.

[109] T.H. Lin, S. Kao, T. Sato, J. Pajarinen, R. Zhang, F. Loi, S.B. Goodman, Z. Yao, Exposure of polyethylene particles induces interferon-gamma expression in a natural

killer T lymphocyte and dendritic cell coculture system in vitro: a preliminary study, J Biomed Mater Res A 103(1) (2015) 71-5.

[110] J. Pajarinen, E. Jamsen, Y.T. Konttinen, S.B. Goodman, Innate immune reactions in septic and aseptic osteolysis around hip implants, Journal of long-term effects of medical implants 24(4) (2014) 283-96.

[111] T.H. Lin, J. Pajarinen, T. Sato, F. Loi, C. Fan, L.A. Cordova, A. Nabeshima, E. Gibon, R. Zhang, Z. Yao, S.B. Goodman, NF-kappaB decoy oligodeoxynucleotide mitigates wear particle-associated bone loss in the murine continuous infusion model, Acta Biomater (2016).

[112] P. Sacerdote, Opioids and the immune system, Palliat Med 20 Suppl 1 (2006) s9-15.

[113] C. Martucci, A.E. Panerai, P. Sacerdote, Chronic fentanyl or buprenorphine infusion in the mouse: similar analgesic profile but different effects on immune responses, Pain 110(1-2) (2004) 385-92.

[114] C. Porta, E. Riboldi, A. Ippolito, A. Sica, Molecular and epigenetic basis of macrophage polarized activation, Seminars in immunology 27(4) (2015) 237-48.

[115] D. Tugal, X. Liao, M.K. Jain, Transcriptional control of macrophage polarization, Arterioscler Thromb Vasc Biol 33(6) (2013) 1135-44.

[116] T. Lawrence, G. Natoli, Transcriptional regulation of macrophage polarization: enabling diversity with identity, Nature reviews. Immunology 11(11) (2011) 750-61.

[117] M.J. Smith, G.L. Koch, Differential expression of murine macrophage surface glycoprotein antigens in intracellular membranes, J Cell Sci 87 (Pt 1) (1987) 113-9.

[118] C.L. Holness, R. Da Silva, J. Fawcett, S. Gordon, D. Simmons, Macrosialin, a mouse macrophage-restricted glycoprotein, is a member of the lamp/lgp family, Journal of Biological Chemistry 268(13) (1993) 9661-9666.

[119] R.P. da Silva, S. Gordon, Phagocytosis stimulates alternative glycosylation of macrosialin (mouse CD68), a macrophage-specific endosomal protein, Biochem J 338 (Pt 3) (1999) 687-94.

[120] E.L. Gautier, T. Shay, J. Miller, M. Greter, C. Jakubzick, S. Ivanov, J. Helft, A. Chow, K.G. Elpek, S. Gordonov, Gene-expression profiles and transcriptional regulatory pathways that underlie the identity and diversity of mouse tissue macrophages, Nature immunology 13(11) (2012) 1118-1128.

[121] S.K. Nadkarni, M.C. Pierce, B.H. Park, J.F. de Boer, P. Whittaker, B.E. Bouma, J.E. Bressner, E. Halpern, S.L. Houser, G.J. Tearney, Measurement of collagen and smooth muscle cell content in atherosclerotic plaques using polarization-sensitive optical coherence tomography, J Am Coll Cardiol 49(13) (2007) 1474-81.

[122] N. Jetten, N. Roumans, M.J. Gijbels, A. Romano, M.J. Post, M.P. de Winther, R.R. van der Hulst, S. Xanthoulea, Wound administration of M2-polarized macrophages does not improve murine cutaneous healing responses, PLoS One 9(7) (2014) e102994.

[123] T.A. Wynn, A. Chawla, J.W. Pollard, Macrophage biology in development, homeostasis and disease, Nature 496(7446) (2013) 445-55.

[124] Y.C. Liu, X.B. Zou, Y.F. Chai, Y.M. Yao, Macrophage polarization in inflammatory diseases, Int J Biol Sci 10(5) (2014) 520-9.

[125] S.R. Meyers, M.W. Grinstaff, Biocompatible and bioactive surface modifications for prolonged in vivo efficacy, Chem Rev 112(3) (2012) 1615-32.

[126] P.H. van Bilsen, E.R. Popa, L.A. Brouwer, J. Vincent, C.E. Taylor, L.F. de Leij, M. Hendriks, M.J. van Luyn, Ongoing foreign body reaction to subcutaneous implanted (heparin) modified Dacron in rats, J Biomed Mater Res A 68(3) (2004) 423-7.

[127] A.P. Khandwekar, D.P. Patil, A.A. Hardikar, Y.S. Shouche, M. Doble, In vivo modulation of foreign body response on polyurethane by surface entrapment technique, J Biomed Mater Res A 95(2) (2010) 413-23.

[128] A.K. McNally, J.M. Anderson, Interleukin-4 induces foreign body giant cells from human monocytes/macrophages. Differential lymphokine regulation of macrophage fusion leads to morphological variants of multinucleated giant cells, Am J Pathol 147(5) (1995) 1487-99.

[129] R.C. Smith, M. Riollano, A. Leung, P.T. Hammond, Layer-by-layer platform technology for small-molecule delivery, Angew Chem Int Ed Engl 48(47) (2009) 8974-7.

[130] D. Choi, J. Hong, Layer-by-layer assembly of multilayer films for controlled drug release, Arch Pharm Res 37(1) (2014) 79-87.

[131] I.G. Luzina, A.D. Keegan, N.M. Heller, G.A. Rook, T. Shea-Donohue, S.P. Atamas, Regulation of inflammation by interleukin-4: a review of "alternatives", Journal of leukocyte biology 92(4) (2012) 753-64.

[132] I.G. Luzina, V. Lockatell, N.W. Todd, K. Highsmith, A.D. Keegan, J.D. Hasday, S.P. Atamas, Alternatively spliced variants of interleukin-4 promote inflammation differentially, Journal of leukocyte biology 89(5) (2011) 763-70.

[133] P.J. Murray, T.A. Wynn, Obstacles and opportunities for understanding macrophage polarization, Journal of leukocyte biology 89(4) (2011) 557-63.

[134] M. Rath, I. Muller, P. Kropf, E.I. Closs, M. Munder, Metabolism via Arginase or Nitric Oxide Synthase: Two Competing Arginine Pathways in Macrophages, Frontiers in immunology 5 (2014) 532.

[135] T.A. Wynn, K.M. Vannella, Macrophages in Tissue Repair, Regeneration, and Fibrosis, Immunity 44(3) (2016) 450-62.

[136] L. Barron, T.A. Wynn, Fibrosis is regulated by Th2 and Th17 responses and by dynamic interactions between fibroblasts and macrophages, Am J Physiol Gastrointest Liver Physiol 300(5) (2011) G723-8.

[137] D.J. Holt, L.M. Chamberlain, D.W. Grainger, Cell-cell signaling in co-cultures of macrophages and fibroblasts, Biomaterials 31(36) (2010) 9382-94.

[138] D.J. Holt, D.W. Grainger, Multinucleated giant cells from fibroblast cultures, Biomaterials 32(16) (2011) 3977-87.

[139] L.M. Pierce, A. Rao, S.S. Baumann, J.E. Glassberg, T.J. Kuehl, T.W. Muir, Long-term histologic response to synthetic and biologic graft materials implanted in the vagina and abdomen of a rabbit model, Am J Obstet Gynecol 200(5) (2009) 546 e1-8.

[140] M.M. Alvarez, J.C. Liu, G. Trujillo-de Santiago, B.H. Cha, A. Vishwakarma, A.M. Ghaemmaghami, A. Khademhosseini, Delivery strategies to control inflammatory response: Modulating M1-M2 polarization in tissue engineering applications, J Control Release (2016).

[141] R. Garash, A. Bajpai, B.M. Marcinkiewicz, K.L. Spiller, Drug delivery strategies to control macrophages for tissue repair and regeneration, Experimental biology and medicine 241(10) (2016) 1054-63.

[142] A. Vishwakarma, N.S. Bhise, M.B. Evangelista, J. Rouwkema, M.R. Dokmeci, A.M. Ghaemmaghami, N.E. Vrana, A. Khademhosseini, Engineering Immunomodulatory Biomaterials To Tune the Inflammatory Response, Trends in biotechnology 34(6) (2016) 470-82.

[143] J.B. Mendes, P.P. Campos, M.A. Ferreira, Y.S. Bakhle, S.P. Andrade, Host response to sponge implants differs between subcutaneous and intraperitoneal sites in mice, Journal of biomedical materials research. Part B, Applied biomaterials 83(2) (2007) 408-15.

[144] T. Oviedo-Socarras, A.C. Vasconcelos, I.X. Barbosa, N.B. Pereira, P.P. Campos, S.P. Andrade, Diabetes alters inflammation, angiogenesis, and fibrogenesis in intraperitoneal implants in rats, Microvascular research 93 (2014) 23-9.

[145] P.P. Campos, A.C. Vasconcelos, M.A. Ferreira, S.P. Andrade, Alterations in the dynamics of inflammation, proliferation and apoptosis in subcutaneous implants of lupus-prone mice, Histology and histopathology 26(4) (2011) 433-42.

[146] N. Oliva, M. Carcole, M. Beckerman, S. Seliktar, A. Hayward, J. Stanley, N.M. Parry, E.R. Edelman, N. Artzi, Regulation of dendrimer/dextran material performance by altered tissue microenvironment in inflammation and neoplasia, Science translational medicine 7(272) (2015) 272ra11.

[147] B.D. Ratner, Healing with medical implants: The body battles back, Science translational medicine 7(272) (2015) 272fs4.

[148] E.C. Stahl, B.N. Brown, Cell Therapy Strategies to Combat Immunosenescence, Organogenesis 11(4) (2015) 159-72.

[149] V.A.V. Jennifer M Ortman, Howard Hogan, An Aging Nation: The Older Population in the United States, US Census Bureau (2014).

[150] A.N.A. Rao, M.N.; Grainger, D.W., Aging and the Host Response to Implanted Biomaterials, in: S.F. Badylak (Ed.), Host Response to Biomaterials: The Impact of Host Response on Biomaterial Selection, Elsevier, London, 2015.

[151] B.M. Sicari, S.A. Johnson, B.F. Siu, P.M. Crapo, K.A. Daly, H. Jiang, C.J. Medberry, S. Tottey, N.J. Turner, S.F. Badylak, The effect of source animal age upon the in vivo remodeling characteristics of an extracellular matrix scaffold, Biomaterials 33(22) (2012) 5524-33.

[152] R. Olivares-Navarrete, A.L. Raines, S.L. Hyzy, J.H. Park, D.L. Hutton, D.L. Cochran, B.D. Boyan, Z. Schwartz, Osteoblast maturation and new bone formation in response to titanium implant surface features are reduced with age, Journal of bone and mineral research : the official journal of the American Society for Bone and Mineral Research 27(8) (2012) 1773-83.

[153] D.J. Holt, D.W. Grainger, Senescence and quiescence induced compromised function in cultured macrophages, Biomaterials 33(30) (2012) 7497-507.

[154] M.E. Bruno, M. Sittner, R.L. Cabrini, M.B. Guglielmotti, D.G. Olmedo, D.R. Tasat, In vitro age dependent response of macrophages to micro and nano titanium dioxide particles, Journal of biomedical materials research. Part A 103(2) (2015) 471-8.

[155] D. Hachim, S.T. LoPresti, C.C. Yates, B.N. Brown, Shifts in macrophage phenotype at the biomaterial interface via IL-4 eluting coatings are associated with improved implant integration, Biomaterials 112 (2016) 95-107.

[156] M. Kinoshita, T. Uchida, A. Sato, M. Nakashima, H. Nakashima, S. Shono, Y. Habu, H. Miyazaki, S. Hiroi, S. Seki, Characterization of two F4/80-positive Kupffer cell subsets by their function and phenotype in mice, Journal of hepatology 53(5) (2010) 903-10.

[157] K. Molawi, Y. Wolf, P.K. Kandalla, J. Favret, N. Hagemeyer, K. Frenzel, A.R. Pinto, K. Klapproth, S. Henri, B. Malissen, H.R. Rodewald, N.A. Rosenthal, M. Bajenoff, M. Prinz, S. Jung, M.H. Sieweke, Progressive replacement of embryo-derived cardiac macrophages with age, The Journal of experimental medicine 211(11) (2014) 2151-8.

[158] M. Ikarashi, H. Nakashima, M. Kinoshita, A. Sato, M. Nakashima, H. Miyazaki, K. Nishiyama, J. Yamamoto, S. Seki, Distinct development and functions of resident and recruited liver Kupffer cells/macrophages, Journal of leukocyte biology 94(6) (2013) 1325-36.

[159] A.R. Pinto, J.W. Godwin, A. Chandran, L. Hersey, A. Ilinykh, R. Debuque, L. Wang, N.A. Rosenthal, Age-related changes in tissue macrophages precede cardiac functional impairment, Aging (Albany NY) 6(5) (2014) 399-413.

[160] S. Epelman, K.J. Lavine, A.E. Beaudin, D.K. Sojka, J.A. Carrero, B. Calderon, T. Brija, E.L. Gautier, S. Ivanov, A.T. Satpathy, J.D. Schilling, R. Schwendener, I. Sergin, B. Razani, E.C. Forsberg, W.M. Yokoyama, E.R. Unanue, M. Colonna, G.J. Randolph, D.L. Mann, Embryonic and adult-derived resident cardiac macrophages are maintained through distinct mechanisms at steady state and during inflammation, Immunity 40(1) (2014) 91-104.

[161] K.J. Lavine, S. Epelman, K. Uchida, K.J. Weber, C.G. Nichols, J.D. Schilling, D.M. Ornitz, G.J. Randolph, D.L. Mann, Distinct macrophage lineages contribute to disparate patterns of cardiac recovery and remodeling in the neonatal and adult heart, Proc Natl Acad Sci U S A 111(45) (2014) 16029-34.

[162] J. Wang, P. Kubes, A Reservoir of Mature Cavity Macrophages that Can Rapidly Invade Visceral Organs to Affect Tissue Repair, Cell 165(3) (2016) 668-78.

[163] G.S. Ashcroft, M.A. Horan, M.W. Ferguson, Aging alters the inflammatory and endothelial cell adhesion molecule profiles during human cutaneous wound healing, Laboratory investigation; a journal of technical methods and pathology 78(1) (1998) 47-58.

[164] G.S. Ashcroft, S.J. Mills, J.J. Ashworth, Ageing and wound healing, Biogerontology 3(6) (2002) 337-45.

[165] R.D. Stout, J. Suttles, Immunosenescence and macrophage functional plasticity: dysregulation of macrophage function by age-associated microenvironmental changes, Immunological reviews 205 (2005) 60-71.

[166] C.R. Gomez, V. Nomellini, D.E. Faunce, E.J. Kovacs, Innate immunity and aging, Experimental gerontology 43(8) (2008) 718-28.

[167] N. Lohmann, L. Schirmer, P. Atallah, E. Wandel, R.A. Ferrer, C. Werner, J.C. Simon, S. Franz, U. Freudenberg, Glycosaminoglycan-based hydrogels capture inflammatory chemokines and rescue defective wound healing in mice, Sci Transl Med 9(386) (2017).